MULTIBODY COMPUTATIONAL BIOMECHANICAL MODEL

OF THE UPPER BODY

by

SARAH REBECCA DUBOWSKY

A Dissertation submitted to the

Graduate School – New Brunswick

Rutgers, The State University of New Jersey

In partial fulfillment of the requirements

For the degree of

Doctor of Philosophy

Graduate Program in Biomedical Engineering

and

The Graduate School of Biomedical Sciences

University of Medicine and Dentistry of New Jersey

Written under the direction of

Noshir A. Langrana

And approved by

_____

_____

_____

_____

New Brunswick, New Jersey

May, 2008

ABSTRACT OF THE DISSERTATION

Multibody Computational Biomechanical Model of the Upper Body

By SARAH REBECCA DUBOWSKY

Dissertation Director:

Dr. Noshir A. Langrana

In the US alone, more than 10,000 spinal cord injuries (SCI) are reported each year. Those who use a manual wheelchair (WC) depend upon their upper limbs to provide a means of locomotion during completion of their activities of daily living. As a result of greater than normal usage of the upper limbs, shoulder pain and pathology is common among manual wheelchair users (MWUs). The use of a patient-specific computational biomechanical model of WC propulsion may help guide rehabilitation that may improve clinical instruction and patient performance. The focus of the work will be two-fold: 1.) experimentally investigate the simultaneous kinematics, kinetics, and electromyography (EMG) throughout WC propulsion, and 2.) computationally, use these data for the creation and validation of a computational model examining resulting shoulder joint forces.

  1.) <u>Experimentally</u>: An integrated data collection and analysis of kinematics, kinetics, and EMG data allow for the comparison of differences in WC

propulsion between able-bodied and persons with paraplegia. Resulting muscle activity differences may be responsible for the observed kinematic and kinetic disparities between the two groups. The high incidence of shoulder pain in MWUs may be the result of such differences.

2.) <u>Computational</u>: When prescribing a WC, the use of a computational model may aide in determining an axle placement in which shoulder joint forces are at a minimum. Created from the information collected above, a patient-specific model was used to calculate the magnitude of shoulder joint forces throughout propulsion. In addition, results from a parametric study, determine the effect of axle placement on the magnitude of these forces. The overall goal is to find an ideal axle placement that minimizes the magnitude of these forces throughout propulsion.

In summary, the current patient-specific computational model can serve as a rehabilitative guide in WC prescription. With its ability to identify varying magnitudes of compressive loads in different axle positions, clinicians can target the resulting axle positions that minimize shoulder joint forces as an ideal set-up when prescribing a WC. In turn, minimizing joint forces from injury onset may prolong a MWU's pain-free propulsion and quality of life.

ACKNOWLEDGEMENTS

iv

wisdom and positive encouragement; thank you to those who have struggled and succeeded right along with me, sharing in our joy and pain; and thank you to those who will follow me, for your admiration and for always believing in me, which believe it or not, led *me* to believe in me. And lastly, a very special thank you to the engineers at AnyBody, the professors at Aalborg University (in particular John Rasmussen), and to the Danish people; my month abroad was a wonderful experience and I can't wait for the opportunity to go back.

DEDICATION

I would of course like to thank my parents, Roger and Jane, for instilling in me the virtue of hard work and the desire to learn, and for never letting me leave the house without assuring them that I would always "do my best." It is that motto that I live with today. In that sense, I would also like to thank my big brother Shaun, for setting that invisible bar so high so that in following him, even if I ever fell short there was no way I would ever fail. What is that old saying, shoot for the moon, if you miss, you will still land among the stars? To this day, I am still, and will always be, in awe of my brother. Thank you, Shaun, for making growing up fun.

In addition, I would like to thank my extended family. In particular Lauren, my sister-in-law who, I swear, had I not met through my brother, I would most surely have found anyway; it's like we have been friends forever, and she has always been an amazing confidante and friend. Along those lines I would also like to thank my father-in-law Hy, for his words of wisdom as someone who has gone through the process before.

And of course, to my husband, Eric. Where would I be had I not found my soul mate and best friend? It has been a long trip, but never once did you give up on me. With the good, comes the bad. You have shared in my excitement from my first conference and poster presentation to my first publication, and you have also been my shoulder to cry on and the sounding board to take my frustration out on. You believed in me when I didn't believe in myself. I hope every day that I can return the favor of unending support, understanding, and love that you give to me.

Table of Contents

LIST OF FIGURES

LIST OF TABLES

CHAPTER 1

INTRODUCTION

Shoulder Anatomy and Biomechanics

The shoulder complex has multiple degrees of freedom resulting from the following joints: the glenohumeral (GH) joint, the acromioclavicular (AC) joint, the sternoclavicular (SC) joint, and the scapulothoracic articulation (Figure 1-1). The glenohumeral joint is a shallow ball-and-socket joint between the head of the humerus and the glenoid cavity of the scapula; the acromioclavicular joint is formed by the acromial end of the clavicle and the acromion of the scapula, and the sternoclavicular joint is formed by the sternal end of the clavicle and the manubrium of the sternum. The scapulothoracic articulation is formed by the skeletal muscles that support and position the scapula; there is no direct bone or ligamentous connection between the body of the scapula and the thorax, and the scapula is usually constrained to glide on the thorax [1]. In addition to the joints and articulating surfaces defining the shoulder complex, the upper limb has additional joints such as the elbow joint, radioulnar joint, and wrist joint. The upper limb joints, coupled with the upper body motion in the neck and spine total 31 degrees of freedom in the upper body complex (Table 1-1).

The musculature involved in movement of the shoulder complex is very complicated and intricate. As a result, current research efforts are focused primarily on the muscles analyzed via surface EMG during the data collection phase of the experimental efforts [2]. These muscles include the anterior and posterior deltoids,

trapezius, pectoralis major, and biceps and triceps. Investigated muscles are shown

below in Figure 1-2, and a summary of their actions are shown in Table 1-2.

The role of the shoulder joint complex in an individual with a spinal cord

injury essentially becomes that of the hip joint in an able-bodied individual, and is

responsible for locomotion by means of wheelchair propulsion. Unlike the hip joint

complex in standard gait analysis, there are no standard activities for the arm, due in

part to the fact that the large range of motion of the arm results in a variety of motion

patterns to achieve a specific goal [3]. In MWs with paraplegia, the shoulder joint

complex maintains a large range of motion, but takes on the greater physical burden of

cyclic propulsion. The act of wheelchair propulsion itself is commonly divided into

two phases: the contact and recovery phases. During the contact phase the path of the

hand is confined to the push rim, however during recovery, the arm is unconfined in

its path back towards wheel contact. The length of these two phases, in addition to

cadence, upper arm kinematics, kinetics, muscle firing patterns, wheelchair axle

placement, recovery patterns, and stroke frequency are all specific to individuals, and

can vary dramatically between persons.

Figure 1-1: Shoulder joint complex [4]
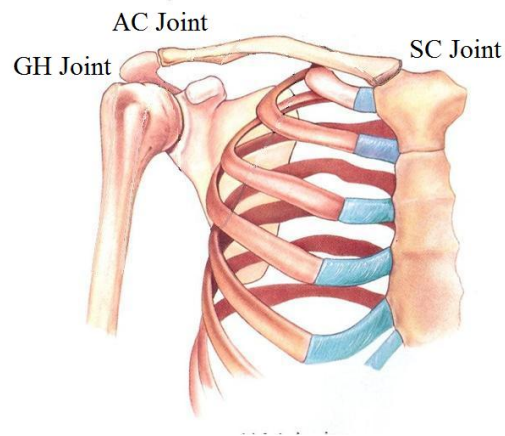
Figure 1-2: Muscles of the shoulder joint complex [4]
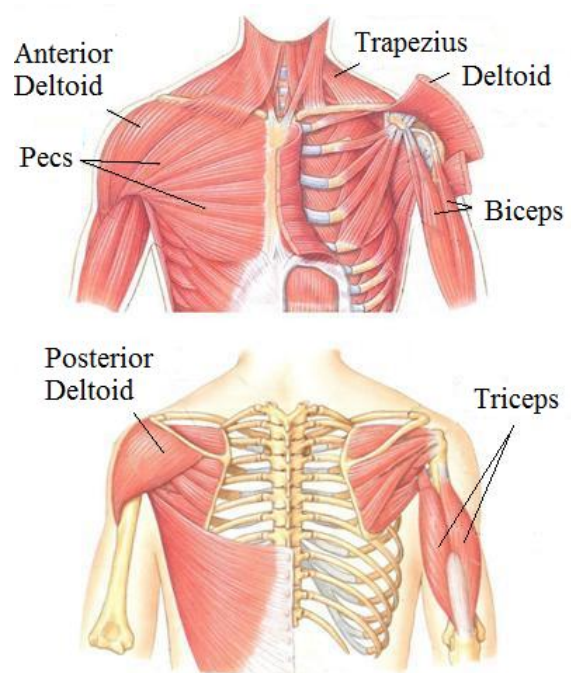
Table 1-1: Joint movement in the upper limb

Joint	Degrees Of Freedom	Motion
GH Joint	3	1.) Flexion / Extension 2.) Abduction / Adduction 3.) Internal / External Rotation
AC Joint	3	1.) Upward / Downward Rotation 2.) Winging 3.) Tipping
SC Joint	3	1.) Elevation / Depression 2.) Protraction / Retraction 3.) Axial Rotation
Elbow Joint	1	1.) Flexion / Extension
Radioulnar Joint	1	1.) Pronation / Supination
Wrist Joint	2	1.) Flexion / Extension 2.) Abduction / Adduction
Neck Joint	2	1.) Flexion / Extension 2.) Rotation
Spine	3	1.) Flexion / Extension 2.) Lateral Bending 3.) Rotation

Table 1-2: Muscle movements in the shoulder complex

Muscle	Action
Anterior Deltoid	Flexion / Abduction at the shoulder joint
Posterior Deltoid	Extension / Abduction at the shoulder joint
Trapezius	Elevate / Retract / Depress / Rotate scapula upward Elevate clavicle Extend neck
Pectoralis Major	Flexion / Adduction / Medial Rotation at the shoulder joint
Biceps	Flexes elbow Supinates forearm Flexes shoulder
Triceps	Extends elbow

Clinical Complications in the Shoulder

Complications associated with a spinal cord injury are usually categorized as either primary or secondary complications. Primary complications are those associated with the actual trauma of the initial spinal cord injury itself; secondary complications are those indirectly resulting from a spinal cord injury. Many common secondary complications that can develop immediately or even years after an initial spinal cord injury include obesity, diabetes, cardiovascular disease, and shoulder pain, in specific, pain resulting from overuse injuries of the shoulder complex. Commonly reported musculoskeletal pain may be due to impingement, instability, decreased range of motion, and tendonitis. Pathology is often associated with such pain, and Lal [5] and Mercer, et al. [6] have reported evidence of degenerative changes or abnormalities in the shoulder ranging in incidence from 72% to 97% of the studied sample of individuals with spinal cord injury. It is no wonder then, that the reported prevalence of shoulder pain in MWUs is so high (31% - 73%) [7-16].

These clinical issues translate into societal issues as shoulder pain can become debilitating and MWUs struggle with activities of daily living, leading to a decrease in independence and quality of life. When addressing working capabilities after injury, shoulder pain has even been described as so debilitating that it is worse than the loss of function from a spinal cord injury itself [17].

Problem Description

In the United States alone, more than 10,000 spinal cord injuries are reported each year. This population depends upon their upper limbs to provide a means of locomotion during completion of their activities of daily living. As a result of greater than normal usage of the upper limbs, proper propulsion mechanics are paramount in preventing injuries and maintaining comfort during locomotion. During the rehabilitation process following a spinal cord injury, an individual is prescribed a wheelchair. However, during rehabilitation minimal time is spent instructing the patient on proper propulsion techniques. Most patients are left on their own to discover how to propel the chair.

Researchers have studied the biomechanical factors and underlying musculature involved during standard wheelchair propulsion [18-20], and it is thought that prolonged wheelchair use and transfers as well as pressure relief techniques may cause the high frequency of upper limb cumulative trauma and strain injuries in spinal cord injury [21]. The prevalence of these symptoms correlates to the duration since injury; in the first five years post-injury, 12% of patients experienced shoulder pain, especially during transfers, and this percentage grows to 100% sixteen years post-injury [12]. These studies illustrate the importance of good muscular strength, muscular endurance, proper biomechanics, and suitable wheelchair set-up in maintaining the integrity of the musculoskeletal system of wheelchair users as they perform their activities of daily living [10, 16, 18-26]. By minimizing the stress placed on the upper body with a correct wheelchair set-up, in particular with an

appropriate axle placement, an individual may prevent such trauma as glenohumeral joint impingement [23, 24, 26], and prolong a pain-free independent propulsion and thus, quality of life. When pain is resolved, MWUs tend to participate more in community activities and have a better quality of life.

The major aim of this research project is to determine first, if differences in the simultaneous analysis of kinematics, kinetics, and EMG exist between two populations (able-bodied and persons with paraplegia), and subsequently, if a computational biomechanical model of the upper limbs can enhance wheelchair prescription leading to rehabilitation for individuals with paraplegia by minimizing shoulder joint forces.

Existing Research on Experimentally Collected Kinematics, Kinetics, and EMG

The kinematics, kinetics, and EMG activity throughout wheelchair propulsion have each been investigated individually [27-30]. Roux investigated the use of a kinematical model to describe the motion of the joints in the upper limb in order to study the influence of repetition on kinematics, although there was no incorporation of kinetics and EMG in the investigation [27, 30]. Robertson, focusing solely on push rim kinetics, characterized differences between non-wheelchair and wheelchair users regarding point of force application and net joint forces and moments [29]. Mulroy explored the fine-wire muscle activity of twelve shoulder muscles of persons with paraplegia, and found two synergies of shoulder muscle function during wheelchair propulsion, but there was no simultaneous investigation into propulsion kinematics or

push rim force profiles [28]. Other investigators, focused on quantifying joint forces and moments in the shoulder complex by coupling kinematics and kinetics data, have provided insight into recommendations for maintaining glenohumeral joint integrity, however EMG has been neglected in these analyses [29, 31-34]. Point of force application on the hand and the mechanical efficiency of various propulsion techniques have been investigated from the coupling of these parameters as well [21, 27, 35]. EMG and kinematics have been coupled together for a variety of investigations including EMG use to estimate shoulder and elbow kinematics in predicting joint moments, analysis of adaptations in kinematics and muscle activity in the initial phase of learning hand rim wheelchair propulsion, and in reporting the muscle activities in propulsion and recovery phases of wheelchair propulsion [36-38]. None of these investigations though, look at the entire picture of kinematics, kinetics, and EMG. Research of the literature tends to show that studies couple only two of the three aforementioned parameters for analysis, however to our knowledge there are few that compare all three parameters *together* [20].

An investigation by Kulig, et al., which focused on shoulder joint kinetics and kinematics during the push phase of wheelchair propulsion, concluded that to determine the true demands on the shoulder during wheelchair propulsion, "the effects of kinematics, kinetics, and EMG need to be considered together" [32]. While there exists multiple studies that compare a combination of participant kinematics, kinetics, and EMG, to our knowledge there are few that compare all three parameters together [20]. The possible linkage between the kinetics, kinematics, and EMG data of able-

bodied participants and individuals with paraplegia during wheelchair propulsion is new and emerging. The relationship of the variables between these two cohorts may shed light onto why the prevalence of shoulder pain in MWUs is so high [7-16].

Existing Shoulder Models

The complexity of the shoulder coupled with its multiple degrees of freedom has historically presented modeling problems. To this point, very few shoulder models exist, and none have the flexibility to be made patient-specific. Extended research has produced five main models for the shoulder, however the current focus will be primarily on the Swedish and Dutch Shoulder Models, as they are the most commonly referenced in literature [39, 40]. It is important to note that neither the Swedish nor Dutch shoulder models, nor any of the shoulder models that will be mentioned in the following section, is patient-specific to the extent that the current model is, and none have been used clinically as a method for a potentially preventative wheelchair set-up and rehabilitation.

Swedish Shoulder Model

One of the first biomechanical shoulder models to be constructed, Karlsson and Peterson's "Swedish" shoulder model is capable of predicting static muscle and joint forces under different upper limb positions and load situations [39]. Constructed based on cadaver morphological measurements by Hogfors, et al. [41], shoulder muscle properties from a study by Karlsson and Jarvholm [42], and anthropometrics

data from literature [43], the model corresponds to a young male person. The model is
used to analyze static load sharing between muscles (modeled as strings), bones
(modeled as rigid bodies), and ligaments. Construction in the model is limited to the
scapula, clavicle, humerus, and 23 associated muscles to drive the motion of the
shoulder. To solve for the indeterminacy at the shoulder, an optimization technique is
employed to calculate the musculoskeletal forces in the shoulder by minimizing the
sum of squared muscle stresses as an objective function (1-1):

$$\min \sum \left(\frac{F_i}{A_i} \right)^2 \tag{1-1}$$

Where F_i is the muscle force, A_i is the cross-sectional area of the muscle, subject to the
following constraints:

$$[a][F] = [-P] \tag{1-2}$$

$$F_{i\min} \leq F_i \leq F_{i\max} \tag{1-3}$$

The first constraint (1-2) is the equilibrium equation (force and moment) for the
humerus (inclusive of the entire arm), and the second constraint (1-3) is the limit for
each internal force; $F_{i\min} = 0$ (muscles can only pull, not push) and $F_{i\max} = kA_i$, where k
is a constant from literature [44] which depends on the maximum tension in the
muscles.

Realizable results were obtained, however there are some restrictions in this
model that should be noted. First, the objective function (1-1) is used only to
minimize the total sum of muscle forces to be 'as low as possible,' so the ligament
forces are not included in this analysis; consequently, the coracohumeral ligament is

considered totally passive which in reality is not true [39]. Similarly, the capsular ligament is not represented in the model, another inaccuracy. Second, the model is only representative of the scapula, clavicle, and humerus; together, the humerus and lower arm are considered to be a rigid body (although it should be noted that future work did focus on incorporating other shoulder bones and muscles into the computer model). However, no equilibrium equations have been formulated for the elbow joint which is problematic when considering the muscle forces of the biceps and triceps, both of which cross this joint. Third, there is no constraint on the direction of the glenohumeral contact force in the current model; current results would indicate subluxation in a healthy shoulder when compared to literature, which is unreasonable given the movements performed. Last, this is only a static analysis representative of one particular subject; the model is not patient-specific and not representative of dynamic movement.

Dutch Shoulder Model

Van der Helm constructed a model of the shoulder mechanism from which the overall goal was to gain insight into the function of morphological structures [40]. Constructed to reflect the right shoulder of a "more or less median cadaver [40]," all morphological data used in the model were obtained from a cadaver study by Veeger, et al., van der Helm, et al., and van der Helm and Veenbaas [45-47]. The model consisted of the thorax, clavicle, scapula, and humerus (later expanded to include the radius and ulna), three joints, three extracapsular ligaments, and 20 associated

muscles. The result was a model with six degrees of freedom – three at the humerus, and three at the shoulder girdle (2 degrees of freedom at the sternoclavicular joint – the axial rotation of the clavicle was ignored due to the fact that it could not be measured – and 1 degree of freedom at the acromioclavicular joint).

Modeling the shoulder mechanism was attained by a finite element method specially developed for multi-degree-of-freedom spatial mechanisms with flexible bodies [40]. Kinematics within the model was expressed via a Lagrangian approach for several different static positions throughout 180º of humeral abduction. Corresponding muscle and joint forces were calculated via inverse dynamics with one of the four optimization criteria used in the model, and shown below, where F is the muscle force, and $PCSA$ is the physiological cross sectional area of the muscle [40]:

i. Minimization of the sum of quadratic muscle forces

    a. $\min \sum F^2$ (1-4)

ii. Minimization of the sum of quadratic muscle stresses (similar to the Swedish shoulder model)

    a. $\min \sum \left(\dfrac{F}{PCSA} \right)^2$ (1-5)

iii. Minimization of the sum of quadratic muscle forces, normalized to the maximal muscle force $F_i max$ which is a function of PCSA and length of the muscle

    a. $\min \sum \left(\dfrac{F_i}{F_i \max} \right)^2$ (1-6)

iv. Minimization of the maximal muscle stress in the entire mechanism

a. $\min\max\left(\dfrac{F_1}{PCSA_1},\dfrac{F_2}{PCSA_2},....,\dfrac{F_i}{PCSA_i},....,\dfrac{F_N}{PCSA_N}\right)$ \hfill (1-7)

Additional constraints in the analysis included: 1.) resultant force vector of the humerus must point to the glenoid cavity (to avoid dislocation), 2.) muscles can only pull, not push, and 3.) the force exerted by a muscle element cannot exceed the muscle strength.

Results for the above optimization criteria were analyzed: criteria (i.) gives incorrect results because it does not account for muscle PCSA; criteria (ii.) is limited by the fact that muscle elements with a large moment arm are favored mathematically; criteria (iii.) is limited by the fact that muscle optimum length is unknown in vivo; and criteria (iv.) is numerically unstable at extremely high muscle stresses. Authors prefer criteria (ii.), however results from (ii.)-(iv.) demonstrate few differences. Overall, results from the shoulder model were encouraging, and further study utilizing the model has been done on the following: standardization of arm motions [48], goal-directed arm motions [49], and manual wheelchair propulsion [50].

Current limitations on the model include the following: 1.) the medial border of the scapula is always attached to the thorax which does not allow for scapular winging (which may not be accurately representative of physiological movements); 2.) the analysis is only on static postures throughout glenohumeral abduction; and 3.) the model was created from a "more or less median cadaver [40]," however its validation against EMG data from both literature and that which was experimentally collected

may not be representative of the cadaver's morphology, impacting the overall accuracy of the model. It has been acknowledged that small changes in morphological inputs have drastic changes in muscle force outputs [45, 51], stressing the need for patient-specificity for accurate results.

Other Shoulder Models

Following the development of the Dutch Shoulder Model, Charlton and Johnson created the Newcastle Model. The model was visualized using the commercially available software, SIMM, and joint and muscle forces were calculated using custom routines in MATLAB. The load sharing problem among the muscles was solved using the least-squares method [52, 53], according to the following equation:

$$V(F_i) = \sum_i \left(\frac{F_i}{PCSA_i} \right)^2 \qquad (1\text{-}8)$$

GH joint force component results compared favorably with findings from the Dutch [40] and Swedish [39] shoulder models. However, caution should be taken when further investigating the output values from the Newcastle model as it is not validated against anything other than previous computational model outputs. This lack of validation questions the accuracy of the model, a point that the authors acknowledge with the statement "This is of course not a particularly accurate model of the GH joint [54]."

The CHARM Project (Comprehensive Human Animation Resource Model), initiated by the European Commission, was a long term research project to reconstruct the human body in 3-dimensional form using medical images from the Visible Human Male (VHM) Data Set provided by the U.S. National Library of Medicine. Its aim has been to develop a comprehensive human animation resource database to allow for the modeling and simulation of the human musculoskeletal system. The overall goal of the project is a finite element simulation of muscular contraction and soft tissue deformation. There are some acknowledged limitations of the model, including the fact that muscles with broad attachments have not been divided into multiple fibers to accurately represent the distribution of force vectors, the SC and AC joints each have only two degrees of freedom [55] , and the current model is only a kinematic dynamic representation with no inverse dynamics applications to calculate resulting joint and muscle forces throughout a defined movement.

Lastly, in 1999, Garner and Pandy developed a kinematic model of the arm, again created from the National Library of Medicine's VHM dataset. The initial model was unilateral and included seven bones (clavicle, scapula, humerus, radius, ulna, carpal bones, and hand), seven joints whose structure was based on anatomic descriptions from literature, and had 13 degrees of freedom [56]. Two years later, the model was further elaborated with the addition of 26 upper body muscles represented as 42 muscle bundles [57], with the path of each muscle bundle modeled using a novel approach called the obstacle-set method [58]. The model used a two-step optimization iterative solving technique to minimize the difference between the calculated and

measured values of net muscle torque. As with the previously discussed models, there are a number of acknowledged limitations: the model is not dynamic; the muscles in the upper limb need to be further segmented; the model is not patient-specific; and the sole means of model validation – comparing results from literature to the calculated results from the current model – is neither thorough nor accurate.

AnyBody Modeling System (AnyBody Technology A/S, Aalborg, Denmark)

Modeling in AnyBody is done by text-based input via a special modeling language called AnyScript. AnyScript is a declarative, object-oriented language similar to Java or C++ for the development of multibody dynamics models of the musculoskeletal system. This is a modeling *system*, meaning that users have the option of either constructing a musculoskeletal model from scratch, or modifying an existing model, or a combination of both. It is this property that makes AnyBody so attractive for patient-specific modeling; a physiologically realizable upper-limb model can be constructed, and C-style patient-specific "include" statements can be used to drive the model for unique outputs. Furthermore, this system is efficient enough to allow for the "ergonomic design optimization [59]" of models, which enables pre- and post- intervention analyses to be performed.

The idea of optimization is based on the assumption that forces between different shoulder muscles are distributed consistently in similar tasks. Load distribution criteria, as investigated by several different authors [60], has commonly been found to be in the form of:

$$G(F) = \sum_{i=1}^{n} \left(\frac{f_i^{(m)}}{N_i} \right)^p \qquad (1\text{-}9)$$

Where G is the objective function of the recruitment strategy, m denotes the components of F that are muscle forces ($f^{(M)}$) while the remainder of F is unknown joint reactions, N_i are normalization functions depending on the muscle physiology and load conditions (muscle PCSA, strain, and strain rate), and the power p can be varied to produce objective functions with different properties. The popular choices, p=1..3, fail to produce physiologically realistic muscle forces under some conditions *unless* additional constraints are imposed on the problem. This occurs most often when the external load on the body is increased towards the physiological maximum; at this point, increased muscle forces must balance the increased load [60]. However, when the external load reaches its physiological maximum, criteria with lower values of p will unrealistically predict some muscles being loaded above their physiological strength.

A systematic study was performed by Challis and Kerwin to test 15 different choices of N_i and p [61]. Challis and Kerwin concluded that the best results were obtained with very large values of p (p=100) and the normalization N_i equal to the maximum force a muscle can exert under the given conditions:

$$N_i = F_{\max,i}^{(m)}(L_i, v_i) \qquad (1\text{-}10)$$

Such that the fraction in equation (1-9) becomes the relative activation of muscle i. An objective function of degree 100 would be very difficult to handle numerically, but

it is evident that for increasing values of p and using equations (1-9) and (1-10), the

objective function approaches:

$$\min_{i} \max \left(\frac{F_i^{(m)}}{F_{max,i}^{(m)}(L_i, v_i)} \right) \tag{1-11}$$

Where the muscle strength, $F^{(m)}_{max\,i}$, depends on the current state of the muscle in

terms of length, L_i, and contraction speed, v_i. To determine $F^{(m)}_{max\,i}$ in each situation, a

Hill muscle model is used. It takes the force/velocity and force/length relations into

account and it has been modified to take the length change of the muscle due to tendon

compliance into account [62]. Coupled with the following equations, we now have an

optimization problem that enables us to determine the muscle and joint forces:

$$C f = d \tag{1-12}$$

$$\frac{f_i(M)}{N_i} \leq \beta, i \in \{1,...,n(M)\} \tag{1-13}$$

$$f_i(M) \geq 0, i \in \{1,...n(M)\} \tag{1-14}$$

Equation (1-12) is the dynamic equilibrium equation, which acts as a constraint in the

optimization problem; C is the coefficient-matrix for the unknown forces, and d

contains all known applied loads and inertia forces. The constraints in equation (1-13)

ensure that the only way to reduce the objective criterion, β, is to simultaneously

reduce all the relative muscle forces. The non-negativity constraints on the muscle

forces (1-14), state that muscles can only pull, not push [63]. Assuming that muscle

fatigue and activity – as defined by the fraction in equation 1-11 above – are

proportional, this min/max criterion delays fatigue in the muscles. This linear problem

is more numerically efficient than many of the previously described optimality

criterions as well.

The mathematical approach embedded within AnyBody assumes that muscles

are recruited according to an optimality criterion, and that minimizing maximal

muscle activity is physiologically reasonable as it corresponds to a minimum fatigue

criterion [64]. The problem of indeterminacy is achieved through an iterative solving

technique, and a Numerical Recipes (NR) Simplex approach [65]. This criterion

distributes forces over redundant muscles to minimize the maximum muscle activation

[63]. The optimality criterion defined within AnyBody is as follows:

$$G\left(f^{(M)}\right) = \max\left(\frac{f_i}{N_j}\right) + \varepsilon_1 \sum\left(\frac{f_i}{N_j}\right) + \varepsilon_2 \sum\left(\frac{f_i}{N_j}\right)^2 \qquad (1\text{-}15)$$

In other words, by minimizing the objective function, all relative muscle forces

must be simultaneously reduced, in turn putting additional constraints on the objective

function, which then produces physiologically realistic muscle forces for the defined

movement. This has been previously used by An, et al. [66] with good results to

predict muscle forces in the human forearm and elbow joint.

The min/max criterion has the algorithmic advantage that it eliminates the need

for additional constraints to avoid muscle forces exceeding the physiological

maximum. The min/max solution is characterized by the fact that the activation of one

muscle in the system cannot be further reduced by increasing the activation of another

muscle (except if this other muscle becomes more stimulated than the first muscle)

[62]. Therefore, if the min/max objective function predicts any muscle force in excess of the physiological strength, it is simply due to lack of strength to balance the external forces.

Like all models however, there are some restrictions to the AnyBody Modeling System as well. The objective function, in which the maximal muscle activity is minimized, may lead to too much muscle synergism [59], as it makes use of muscles with small moment arms which may not occur physiologically. The inventors of the software admit to the fact that this min/max criterion naturally contains indeterminacy for certain groups of sub-maximally activated muscles [59], however this problem is handled in the software with a keen iterative solution, as suggested by Damsgaard, et al., and Forster [64, 67].

In lieu of the few restrictions that the AnyBody Modeling System has, to our knowledge, no other software offers the coupling of a computationally efficient muscle recruitment analysis with such versatile model building capabilities. Similar software packages are SIMM, by Musculographics, Inc. [68], BRG.LifeModeler by Biomechanics Research Group, Inc. [69], and Armo by G-sport, Inc. [70]. While the two former systems do have some inverse dynamics capabilities, in their current versions they vary significantly in their muscle recruitment analysis and are fundamentally based on forward dynamics engines. The latter system is similar to AnyBody in its muscle recruitment analysis, however lacking in a model building interface.

Current Study

It is thought that prolonged wheelchair use and transfers may cause the high frequency of upper limb cumulative trauma and strain injuries in spinal cord injury [21]. However, prolonged wheelchair use and transfers cannot be avoided by those seeking an independent way of life. What can be changed though, is the magnitude of the forces experienced in the shoulder joint complex with an altered seating position. It is hypothesized that the magnitude of shoulder joint forces experienced throughout one propulsive stroke, multiplied by hundreds to thousands of pushes per day, may contribute to the cumulative trauma and strain injuries that so many MWUs experience. Minimizing shoulder joint forces may be critical to delaying or reducing shoulder pain and pathology in a MWU. By maximizing axle placement to minimize shoulder joint forces throughout propulsion, the cyclic load during an individual push will be smaller, as will the overall load that the shoulder experiences throughout daily propulsive activities.

The major aim of this research project is two-fold: 1.) simultaneously quantify and compare the push rim forces, upper limb kinematics, and shoulder EMG during wheelchair propulsion between able-bodied participants and individuals with paraplegia. The hypothesis is that an integrated, simultaneous data collection and interpretation will establish differences between kinematics, kinetics, and EMG profiles of these two groups. Ultimately, this serves as the *first step* in the determination of whether differences between groups exist, and thus, potentially lead to an associated intervention prescription that may aid in altering kinematics, kinetics,

and EMG to potentially prevent the shoulder pain that so many MWUs will experience. These data will serve in the next step of calculating joint forces via patient-specific modeling, which brings about the second part of the study. 2.) Create and validate a computational biomechanical model of the upper limbs to determine resulting shoulder joint forces throughout propulsion, and subsequently use the model to enhance wheelchair propulsion rehabilitation for individuals with paraplegia by minimizing these forces. The second hypothesis is that the use of a patient-specific computational biomechanical model of wheelchair propulsion may help guide rehabilitation that may improve clinical instruction and patient performance as well as improved wheelchair prescription.

In combining this two-fold approach, the discovery into whether differences between cohorts exist, coupled with resulting joint forces determined from a patient-specific model, may potentially lead to an associated intervention and/or prescriptive tool that may aide in minimizing shoulder joint forces in MWUs. This may potentially prevent the shoulder pain and pathology that so many wheelchair users experience. In summary, the use of a patient-specific computational biomechanical model of wheelchair propulsion may help guide rehabilitation that may improve clinical instruction and patient performance as well as improved wheelchair prescription.

The following topics will be addressed in the remaining chapters in the investigation towards identifying responsible factors and existing links between manual wheelchair propulsion and shoulder pain:

- Chapter 2 - Experimental Study: Methods, Results, and Conclusions.

- Chapter 3 - Computational Study: Analytical and Computational Analyses.

- Chapter 4 - Computational Study: Patient-Specific Model, Creation and Validation.

- Chapter 5 - Computational Study: Joint Force Investigation, Results, and Discussion.

- Chapter 6 - Conclusion to Address Shoulder Pain and Future Work.

The majority of the content of this thesis has been published. Data from Chapter 2 – Experimental Study: Methods, Results, and Conclusions, is in press, and the reference is as follows:

Dubowsky SR, Langrana NA, and SA Sisto, "Comparison of Kinematics, Kinetics, and EMG Throughout Wheelchair Propulsion in Able-Bodied and Persons with Paraplegia: An Integrative Approach," <u>Journal of Biomechanical Engineering</u>, in press, February 2008.

In addition, data from Chapter 4 – Computational Study: Patient-Specific Model, Creation and Validation, is under review in the Journal of Biomechanics. The corresponding reference is:

Dubowsky SR, et al., "Validation of a musculo-skeletal model of wheelchair

   propulsion and its application to minimizing shoulder joint forces," <u>Journal of

   Biomechanics</u>, submitted 12-28-07.

Lastly, the remaining data from this thesis has been published and/or presented in the

following conferences and web seminars:

Dubowsky SR. "Adjusting the Axle Placement in Wheelchair Users to Minimize

   Shoulder Joint Forces," International World Wide Web Broadcast: AnyBody

   Modeling System. Nov. 8, 2007.

Sullivan SR, Langrana NA, and SA Sisto, "Shoulder Mechanics: Analytical Modeling

   and Validation," American Society of Biomechanics (ASB) 2007 Annual

   Conference, Stanford, CA. August 22-25, 2007. Poster Presentation.

Sullivan SR, Langrana NA, and SA Sisto, "Correlating Kinematics, Kinetics, and

   EMG in Wheelchair Propulsion in Normal and Paraplegia Subjects," Page 290, in

   the <u>Proceedings of BMES Conference</u>, Chicago, MD, October 2006.

Sullivan SR, Langrana NA, and SA Sisto, "Comparison of Experimental Subject

   Electromyography and Computational Muscle Force in the Upper Body," 3rd

   Annual 2006 Biomedical Engineering Showcase, Woodbridge, NJ. March 10,

   2006. Poster Presentation.

Sullivan SR, Langrana NA, and SA Sisto "Upper Extremity Computational Muscle

   Forces in Comparison with Subject Electromyography," in <u>the Proceedings of the</u>

2006 Bioengineering Conference, Paper No. BIO2006-157469, ASME, Amelia

Island, Florida, June 21-25, 2006.

Sullivan SR, Langrana NA, and SA Sisto, "A Patient-Specific Upper Body

Computational Biomechanical Model," 2nd Annual 2005 Biomedical Engineering

Showcase, New Jersey Institute of Technology, Newark, NJ. March 11, 2005.

Poster Presentation.

Sullivan SR, Langrana NA, and SA Sisto, "A Patient-Specific Upper Body

Computational Biomechanical Model," Page 99, in the Proceedings of BMES

Conference, Baltimore, MD, October 2005.

Sullivan SR, Langrana NA, and SA Sisto, "Multibody Computational Biomechanical

Model of the Upper Body," in the Proceedings of ASME IDETC/CIE 2005,

September 2005, Long Beach, California.

CHAPTER 2

EXPERIMENTAL STUDY: METHODS, RESULTS, AND CONCLUSIONS

Experimental Procedure: Materials and Methods

A systematic integrated data collection and analysis of kinematics, kinetics, and EMG data allow for the comparison of differences in wheelchair propulsion between able-bodied individuals and persons with paraplegia. Bilateral kinematics data from a motion analysis system, kinetics data from force-sensing push rims, and EMG data from six upper-limb muscles, were collected for ten consecutive push strokes at a self-selected speed.

Review of the literature tends to show that studies either examine individually [28, 30], or couple together two of the following for analysis; kinematics, kinetics, and EMG, [21, 27, 29, 31-38]. An investigation by Kulig, et al., which focused on shoulder joint kinetics and kinematics during the push phase of wheelchair propulsion, concluded that to determine the true demands on the shoulder during wheelchair propulsion, the effects of kinematics, kinetics, and EMG need to be considered together [32]. While there exists multiple studies that compare a combination of participant kinematics, kinetics, and EMG, to my knowledge there are few that compare all three parameters *together* [20].

The primary purpose of this part of the biomechanical study is to simultaneously quantify and compare upper limb kinematics, push rim forces, and shoulder EMG during wheelchair propulsion between able-bodied participants and individuals with paraplegia. The hypothesis is that an integrated, simultaneous data collection and interpretation will establish differences between kinematics, kinetics, and EMG profiles of these two groups. It is anticipated that any differences that exist between the populations may result in an associated intervention prescription that may potentially prolong the shoulder integrity of MWUs.

Data Acquisition

<u>Participants</u>

Eleven participants – six able-bodied individuals and five participants with paraplegia – gave informed consent to participate in data collection. Subject data is summarized in Table 2-1. The Kessler Medical Rehabilitation and Research Education Center Institutional Review Board approved all experiments and each participant signed an informed consent form before participating in the study.

Table 2-1: Participant anthropometrics and demographics

AC to OL represents the upper arm length as measured from the acromion (AC) to the olecranon (OL), and OL to US is indicative of the lower arm length as measured from the olecranon (OL) to the ulnar styloid (US). The top table reports able-bodied anthropometrics and demographics, and the bottom table, persons with paraplegia.

	AB-1	AB-2	AB-3	AB-4	AB-5	AB-6
Sex	M	M	M	F	M	F
Age (yrs)	26	23	25	29	27	25
Ht (m)	1.83	1.83	1.83	1.52	1.66	1.63
Wt (kg)	84.4	83.5	104.3	50.8	65.8	53.8
Injury Level	n/a	n/a	n/a	n/a	n/a	n/a
Duration	n/a	n/a	n/a	n/a	n/a	n/a
Right AC to OL	41.5	36.0	38.0	29.5	30.5	33.0
Right OL to US	28.5	28.5	27.0	21.0	23.5	25.0
Left AC to OL	40.0	37.5	38.0	27.5	29.5	33.0
Left OL to US	28.0	28.0	27.0	21.5	23.0	24.5

	PP-1	PP-2	PP-3	PP-4	PP-5
Sex	M	M	F	M	M
Age (yrs)	51	29	31	43	47
Ht (m)	1.70	1.75	1.75	1.80	1.87
Wt (kg)	78.9	61.2	70.3	98.2	102.3
Injury Level	T3	T6	T10	T6	L1/L2
Duration	15.0	4.5	3.5	5.5	4.5
Right AC to OL	36.0	35.0	30.2	39.0	39.0
Right OL to US	27.5	29.0	23.0	27.0	28.0
Left AC to OL	35.5	35.0	31.0	42.0	39.0
Left OL to US	26.5	29.0	22.5	27.0	28.0

Kinematics

Each participant was outfitted with 14-mm reflective markers so that a 7-camera motion capture system (Vicon Peak, Lake Forest, CA) could record in real time the 3-D trajectory data of the participant's upper body during each propulsive stroke. Markers were placed bilaterally on the following bony landmarks: tempero-mandibular joints; lateral-superior border of the acromion; lateral epicondyle; olecranon; radial styloid; prominent tuberosity of the ulna; 3rd metacarpal; greater trochanter; hub; axle; the spinous processes of C7 and T3; and the sternum (Figure 2-1). Data from the shoulder and hub markers specifically, were used to determine each participant's mechanical advantage at the points of push rim contact and release. Kinematics data for paraplegia participant 1 (PP-1) were collected at 60 Hz, while all other participants were collected at 120 Hz. The collection of kinematics and kinetics data was synchronized in time. Kinematics data were reviewed immediately after testing to ensure proper data collection with minimal marker dropout.

Figure 2-1: Marker placement for kinematic data collection

Not shown – temporal-mandibular joint and sternum.
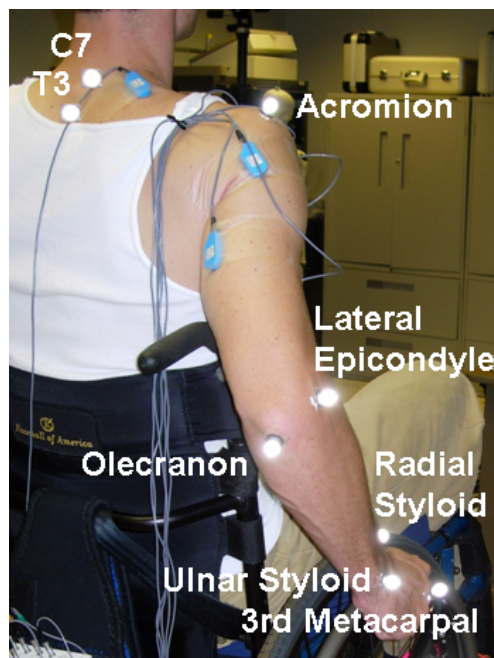
Kinetics

Previously tested and validated force- and moment- sensing push rims

(SmartWheel - Three Rivers Holdings, Inc., Mesa, AZ) were used to collect the kinetic

data of each participant as they propelled their wheelchair [71]. Each participant with

paraplegia, in their own wheelchair, swapped SmartWheel for their own wheels, while

able-bodied participants pushed a Kuschall Competitor (Kuschall, Longmont, CO),

also outfitted with SmartWheel (Figure 2-2). Each participant was given ample time

to become acclimated to pushing the chair on a dynamometer prior to data collection.

Bilateral push rim kinetic data were collected wirelessly at a sampling frequency of

240 Hz. Push rim force data were reviewed immediately after testing to ensure good signal quality.

Figure 2-2: SmartWheel coordinate system
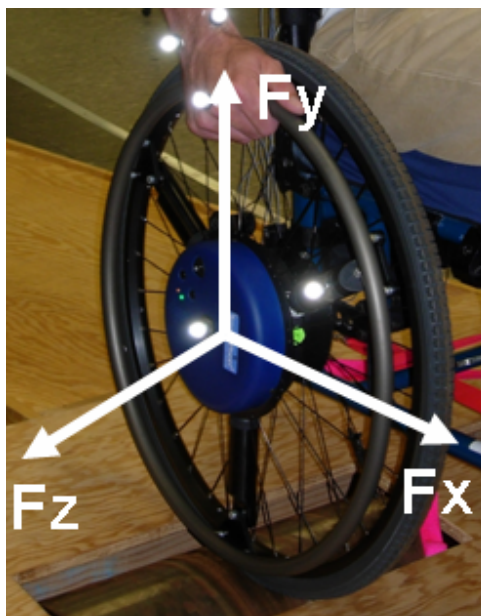
Electromyography

Shoulder muscle activities were documented with twelve bipolar pre-amplified surface electrodes (MA-300 EMG System, Motion Lab Systems, Inc., Baton Rouge, LA) with a single ground electrode, and were placed bilaterally on the anterior and posterior portions of the deltoid, upper trapezius, the sternal head of the pectoralis, biceps brachii, and the long head of the triceps.

The skin surface was prepared by first scrubbing the area with a scouring pad to remove dead skin cells, and then cleaning the area with an alcohol prep pad. Once the electrodes were properly placed, as described in the Anatomical Guide for the

Electromyographer [72], they were taped down tightly with Blenderm™ hypoallergenic surgical tape (3M, St. Paul, MN). After the electrodes were secured, the preamplifiers were plugged into the system backpack, which is connected to the computer via a coaxial cable. The data were collected at an anti-aliasing band width of 750 Hz, with gain settings ranging from 350 to 4000 times the input signal. The data were sampled and digitized on a computer at a rate of 1560 Hz for all subjects.

Prior to propulsion collection, electromyographic activity was obtained during maximal voluntary contraction (MVC). Testing was modified to allow all muscles to be assessed with the participant seated in his wheelchair in six standardized positions. The aforementioned muscles were tested as described by Mulroy, et al., in the following manner [38]:

Anterior Deltoid: 45° shoulder flexion, downward force applied to the elbow;

Posterior Deltoid: 90° shoulder abduction with forward force applied to elbow;

Upper Trapezius: Elevate shoulder girdle and provide strong downward force to the top of the shoulder halfway between the neck and tip of the acromion;

Sternal Pectoralis Major: 90° of shoulder abduction with instruction to pull toward contra-lateral knee with resistance applied in the upward and outward direction;

Biceps: 90° elbow flexion, full supination, downward force applied to the wrist;

Triceps: 90° shoulder abduction, full internal rotation, 45° elbow flexion, downward force applied to wrist.

During testing the participant's trunk and wheelchair were stabilized by the investigator. EMG data were reviewed immediately after testing to ensure proper gain settings and signal quality. The timing of muscle onset and cessation, burst duration, and the percent of muscle effort related to each subject's MVC were investigated. Results are reported as both a percentage of contact phase and degrees on the push rim.

Data Processing

This study focused on data derived only from the contact phase of the push stroke and did not include analysis of the recovery phase when the hand released from the push rim. Participants were asked to propel their wheelchair at a self-selected pace for 20 seconds. Kinematics, kinetics, and EMG from 10 successive push strokes were collected; once data collection began, the initial two push strokes were neglected, and the next 10 consecutive push strokes were saved for analysis. The remaining push strokes were neglected, so as to not have fatigue play a role in propulsion characteristics.

Kinematics

Kinematics data were pipelined from the Vicon Workstation to Microsoft Excel for processing in Matlab. Contact and release angles were calculated by coupling the trajectory between the wheelchair hub and the third metacarpal marker (from Vicon), with the contact and release points from force-sensing push rims. All contact angles are referenced from horizontal. Resulting shoulder and elbow flexion

and extension angles, as determined based on participant anthropometric data and assumed sagittal plane motion at the contact and release angles, are reported in Figures 2-3 and 2-4. From these data, a novel method was used to rank each participant's mechanical advantage based on clinical guidelines from the Paralyzed Veterans of America (PVA) [73]. Shoulder positioning, relative to the hub, was obtained from Vicon 3-D motion analysis data for contact and release positions. PVA guidelines recommend an inferior seat height to facilitate greater upper limb motion and hand contact angles, lower stroke frequency, and higher mechanical efficiency [73]. PVA guidelines also recommend an anterior axle position (without compromising the stability of the user) to assist in the following: increased hand contact time, decreased muscle effort, lower stroke frequency, lower peak forces, less rapid loading of the push rim, and fewer strokes to go the same speed [73]. Each participant's anterior-posterior posture was ranked according to these guidelines; the participant whose axle was the most anterior relative to their shoulder was ranked to have the greatest mechanical advantage.

Kinetics

Raw kinetics data from the SmartWheel was filtered by a 4th order, 20 Hz low pass Butterworth filter, and the resulting forces and moments were converted from volts to Newtons (or Newton-meters) by trigonometry from SmartWheel angle data. The propulsive phase of ten push strokes, as defined by palm strike to palm off, was then calculated   The onset of propulsion was visually defined as the point of

divergence of the F_x and F_y components, and the end of propulsion was visually

defined as the point of convergence of the F_x and F_y components [21]. This method of

defining propulsion has been found to be comparable to the method utilizing the

moment divergence from zero [74]. Resultant (F), tangential (F_t), and radial (F_r)

forces were analyzed from SmartWheel x-, y-, and z- output forces (Figure 2-2). The

conversion equations, as calculated by Robertson, et al. [29], are shown below:

$$F = \sqrt{F_x^2 + F_y^2 + F_z^2} \qquad (2\text{-}1)$$

$$F_t = \frac{M_z}{R} \qquad (2\text{-}2)$$

$$F_r = \sqrt{(F_x^2 + F_y^2) - F_t} \qquad (2\text{-}3)$$

Where F_x, F_y, and F_z are the raw SmartWheel force outputs, M_z is the moment

about the z-axis (from raw SmartWheel output), R is the radius of the push rim

(0.2667 m), F is the calculated resultant force, F_t is the calculated tangential force, and

F_r is the calculated radial force. Both the percentage of the propulsion phase and the

corresponding degrees on the push rim at which point the peaks occurred are reported.

Electromyography

EMG data were analyzed as previously described [75], where the onset of an

EMG burst was defined as the time when the signal amplitude remained above a

threshold defined by the mean of the baseline plus three standard deviations for 30 ms.

The end of the EMG burst was defined as the time when the signal amplitude

remained below the threshold level for 50 ms. Burst duration was then calculated as

the difference in time between the onset and the end of the EMG burst. Significant

EMG was defined as continuous activity for a duration of at least 5% of the propulsion

cycle [28]. Further analysis by visual inspection was necessary, as the Matlab

program that automated the EMG processing occasionally calculated bursts that were

shorter than the defined significant length. At that point, burst durations, including

start and stop times, were re-calculated manually.

Experimental Results

Kinematics

Shoulder and elbow flexion-extension angles, at contact and release, are shown

in Figures 2-3 and 2-4. Based on these postures, as previously discussed, a novel

method was used to rank each participant's mechanical advantage at contact time.

Results for the right side are as follows (ranked from greatest mechanical advantage to

least mechanical advantage and shown in Figure 2-3): AB-3, P-2, AB-2, AB-5, AB-6,

P-5, AB-4, AB-1, P-3, P-1, and P-4. Results from the left side are as follows (Figure

2-4): AB-3, AB-5, P-2, AB-6, P-5, AB-4, AB-1, P-3, P-1, P-4; results from the left-

hand side of AB-2 are unavailable due to a malfunction of the left SmartWheel.

In addition, trunk angle throughout propulsion was calculated

trigonometrically, and was found to be 2.5±0.4 and 4.1±1.0 degrees for participants

with paraplegia and able-bodied individuals, respectively. Resulting contact time, as

measured by degrees, varied between groups; the right side contact and release angles

for individuals with paraplegia and able-bodied participants were 63.2±11.0º and

69.7±8.3°, and 142.9±8.5° and 140.5±12.8°, respectively, and the left side were

65.5±10.2° and 71.1±6.9°, and 140.2±9.9° and 135.8±14.3°, respectively (Appendix B-

2-1). The self-selected propulsion speed varied between the groups as well; the group

with paraplegia propelled faster than the able-bodied group, at 1.4±0.1 versus 1.1±0.1

m/s, respectively (Appendix B-2-2).

Figure 2-3: Mechanical advantage results - right side

Participant contact and release angles – contact (top diagram) and release (bottom diagram) for able-bodied and persons with paraplegia, right side. Anterior axle positioning (relative to the shoulder) was obtained from Vicon. Upper and lower arm lengths were collected as part of the testing protocol. Most mechanically efficient (left) to least mechanically efficient (right) shown below. Figures drawn to scale. Two-dimensional motion assumed.

AB-3	P-2	AB-2	AB-5	AB-6	P-5	AB-4	AB-1	P-3	P-1	P-4
25° 98°	34° 131°	47° 81°	26° 127°	34° 86°	41° 98°	38° 94°	52° 89°	18° 165°	55° 99°	51° 113°
12° 156°	17° 148°	24° 174°	11° 139°	11° 131°	25° 180°	21° 159°	10° 144°	18° 180°	27° 92°	3° 148°
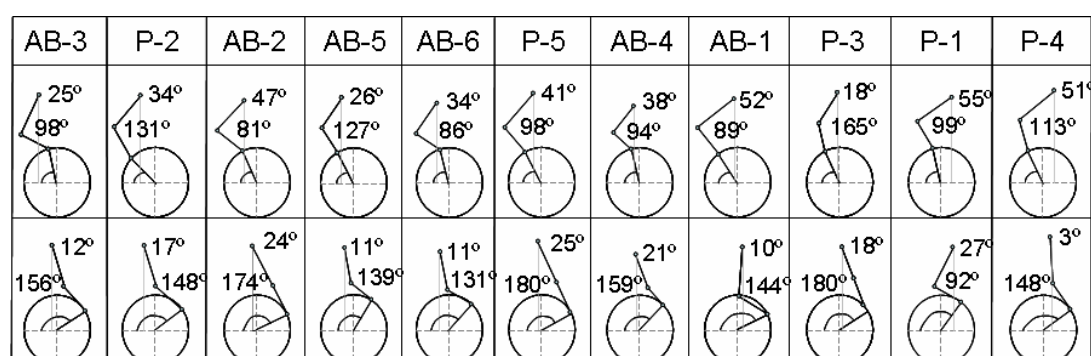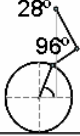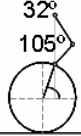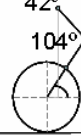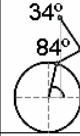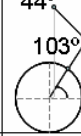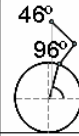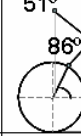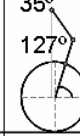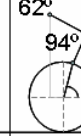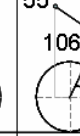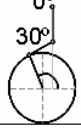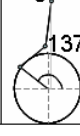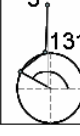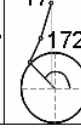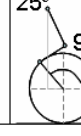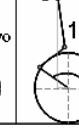
Figure 2-4: Mechanical advantage results - left side

Participant contact and release angles – contact (top diagram) and release (bottom diagram) for able-bodied and persons with paraplegia, left side. Ranking described above. AB-2 not included due to mechanical failure of the left SmartWheel.

AB-3	AB-5	P-2	AB-6	P-5	AB-4	AB-1	P-3	P-1	P-4
28° 96°	32° 105°	42° 104°	34° 84°	44° 103°	46° 96°	51° 86°	35° 127°	62° 94°	55° 106°
18° 162°	0° 30°	26° 176°	7° 122°	8° 137°	23° 160°	3° 131°	17° 172°	25° 97°	8° 129°

Kinetics

The majority of both groups demonstrated peak resultant, tangential, and radial forces subsequent to top dead center (90º) on the push rim during propulsion (Tables 2-2 and 2-3). There was also a noticeable trend that in general, the majority of participants with paraplegia reached peak resultant, tangential, and radial forces earlier on the push rim (in degrees) than their able-bodied counterparts (Tables 2-2 and 2-3).

Table 2-2: Kinetics results, right side

Percentage of propulsion and corresponding degrees where peak forces occur. Averaged over ten push strokes. Resultant, tangential, and radial forces as calculated by previously defined methods [29].

	Peak Force Occurrences					
	Resultant F		Tangential F_t		Radial F_r	
	%	°	*%*	°	*%*	°
AB-1	60.6±8.2	116.2±7.2	62.8±7.3	118.3±6.9	55.3±8.4	111.0±7.8
AB-2	61.7±5.6	121.1±5.5	62.8±5.1	122.1±5.3	60.9±5.3	120.3±5.4
AB-3	50.7±3.0	113.1±2.9	52.0±1.8	114.0±2.3	47.2±3.7	110.6±3.7
AB-4	54.0±5.6	107.1±3.1	54.8±4.9	107.5±3.0	33.0±10.2	95.4±6.1
AB-5	51.3±5.2	93.3±3.4	55.3±4.0	95.6±2.5	42.3±4.7	88.0±3.4
AB-6	52.5±6.1	105.6±5.0	53.8±4.6	106.3±4.5	37.2±13.2	97.0±8.1
PP-1	40.2±8.1	99.2±6.1	52.8±3.9	105.1±4.5	35.1±7.8	96.2±4.7
PP-2	64.3±4.4	107.8±4.9	64.4±4.5	108.0±5.0	50.1±20.7	94.2±19.3
PP-3	66.3±4.5	119.3±3.7	65.5±4.5	118.7±3.7	38.8±21.9	96.9±17.9
PP-4	42.9±14.2	98.6±11.4	49.5±4.8	104.0±4.9	33.8±15.3	91.3±13.0
PP-5	31.9±9.6	91.4±8.3	57.8±2.3	114.3±2.7	27.2±3.7	87.2±3.3

% Percentage of propulsion where peak forces occur
° Degrees where peak forces occur

Table 2-3: Kinetics results, left side

Percentage of propulsion and corresponding degrees where peak forces occur. Averaged over ten push strokes. Resultant, tangential, and radial forces as calculated by previously defined methods [29]. There is no data for AB-2 because there was a left SmartWheel malfunction during testing.

| | Peak Force Occurrences | | | | | |
| | Resultant F | | Tangential F_t | | Radial F_r | |
	%	°	%	°	%	°
AB-1	59.4±7.0	115.6±6.2	61.0±6.2	116.6±5.8	59.5±7.2	115.7±6.4
AB-2	n/a	n/a	n/a	n/a	n/a	n/a
AB-3[*]	50.8±5.0	108.6±4.5	52.8±4.2	110.25±4.2	51.7±4.5	109.4±4.4
AB-4	53.2±8.0	107.6±5.6	54.9±6.1	108.6±4.8	52.5±6.9	107.2±5.0
AB-5[t]	52.9±8.9	93.6±3.3	56.4±5.3	94.1±3.9	52.2±10.8	93.6±3.3
AB-6	51.5±4.3	104.1±3.5	54.3±4.6	105.6±3.6	50.6±4.1	103.7±3.8
P-1	34.0±13.0	94.7±8.0	56.4±4.5	107.0±4.7	31.4±11.1	92.9±6.6
P-2	65.2±2.6	117.0±6.3	65.3±3.6	116.7±7.9	65.0±2.5	116.8±6.3
P-3	50.9±13.3	105.4±10.5	55.7±7.3	107.6±8.4	55.6±15.3	108.5±11.1
P-4	48.9±7.3	103.6±7.9	51.5±5.1	105.7±5.8	50.8±6.9	105.1±7.3
P-5	32.7±8.6	85.3±5.7	51.3±1.9	101.2±2.4	32.6±8.7	85.2±5.9

[*]   Data from trial III
[t]   Data from 9 out of 10 push strokes
%   Percentage of propulsion where peak forces occur
°   Degrees where peak forces occur

Electromyography

It is well known that the shoulder muscle complex offers a wide range of movements and, as a result, has a large compensatory ability [76]. This may partially explain why upper limb repetitive movements have been found to be so variable in able-bodied and persons with paraplegia [77]. The functioning of muscle groups may be directly responsible for the observable differences between and within the studied groups. Right and left side burst duration, maximum percentage MVC, and the percentage of propulsion where this maximum occurs are summarized for all muscles and all subjects in Appendix Tables B-2-3 and B-2-4. "Muscle energy," as defined by

the area under the curve of the percentage of EMG plotted throughout propulsion, in addition to the peak EMG amplitudes for all subjects and all muscles, are reported below. Tables 2-4 and 2-5 are the right and left sides, respectively, of the muscle energy differences between participants with paraplegia and able-bodied participants, and Tables 2-6 and 2-7 are the right and left sides, respectively, of the peak percentage of MVC for all participants.

Right Side

Anterior deltoid: The burst duration and peak EMG amplitude during propulsion was similar between the able-bodied individuals and persons with paraplegia (Appendix B-2-3). Peak firing for nearly all subjects in both groups coincided with the impact spike (as defined by Robertson, et al. [29]) on the resultant, tangential, and radial force profiles; however persons with paraplegia achieved peak anterior deltoid firing nearly 5% earlier in the contact phase.

Posterior deltoid: Peak EMG amplitude between groups varied dramatically; participants with paraplegia used 45.0±12.0% of MVC at peak, while able-bodied participants used 29.7±6.6%. The percent phase of propulsion at which persons with paraplegia and able-bodied individuals achieved these peaks varied as well; participants with paraplegia had peak posterior deltoid firing over 10% later in the push stroke than the able-bodied group. In addition, participants with paraplegia used

36% greater "muscle energy" throughout propulsion than the able-bodied group (Table 2-4).

Trapezius: The trapezius demonstrated a marked number of differences between the two groups. Contrary to all other muscles, the able-bodied participants had dramatically higher peak EMG amplitude than those with paraplegia, 43.8±8.9% versus 31.8±7.6%, respectively. Where during the contact phase of the push stroke this peak occurred varied considerably as well, with the able-bodied group reaching peak EMG amplitude at 62.7±7.5% of the push stroke, while the participants with paraplegia reached peak amplitude at 45.8±14.0%. In addition, the total trapezius burst duration varied, with the able-bodied individuals having trapezius activity for 76.1±8.2% of the push stroke, and the participants with paraplegia having a burst duration of 61.6±9.7%.

Pectoralis Major: Peak EMG amplitude between groups was similar (Table 2-6), however where throughout the contact phase this peak occurred varied dramatically. Peak pectoralis firing for able bodied participants was over 10% later on in the push stroke than for participants with paraplegia (41.5±3.3 versus 29.6±8.3). The total burst duration between groups varied dramatically as well, with the able-bodied and participants with paraplegia burst durations being 62.0±7.1% and 77±8.4%, respectively.

Biceps brachii: Peak EMG amplitude between groups varied dramatically; participants with paraplegia used 36.8±10.3% of MVC at peak, while able-bodied participants used 20.8±8.7%. The "muscle energy" differences between groups, as described above, are dramatic; participants with paraplegia use 132% greater biceps "muscle energy" (Table 2-4). The angle at which both groups achieved these peaks was similar, and again coincided with the impact spike (as defined by Robertson, et al. [29]) on all force profiles for nearly every subject in both groups.

Triceps: Obvious differences in triceps muscle activity between able-bodied and persons with paraplegia can be seen in Figure 2-5. It is clear that all five participants with paraplegia had triceps activity early on in the push stroke while none of the able-bodied participants had any initial activity. As a result, the participants with paraplegia had a longer triceps burst duration in comparison with the able-bodied participants (85.2±8.3% versus 58.4±6.5%). Peak EMG amplitude between groups varied dramatically as well; participants with paraplegia used 43.0±6.4% of MVC at peak, while able-bodied participants used 24.9±4.3% (Table 2-6). In addition, participants with paraplegia used 67.1% greater triceps "muscle energy" (Table 2-4). The angle at which both groups achieved these peaks however, was similar, and coincided with peak resultant, tangential, and radial forces for the majority of participants.

Left Side

Anterior deltoid: The burst duration during propulsion was similar between the able-bodied individuals and participants with paraplegia (Appendix B-2-4). However, there were differences in peak EMG amplitude and where on the push rim this peak occurs. Participants with paraplegia have a noticeably larger peak EMG value than their able-bodied counterparts (45.1±9.0 vs. 28.7±6.6), and achieve this peak firing nearly 8% earlier in the contact phase (35.1±10.8% vs. 42.5±8.2%).

Posterior deltoid: The only noticeable difference between the groups for the left posterior deltoid is the fact that participants with paraplegia use 83.6% greater "muscle energy" throughout propulsion than the able-bodied group (Table 2-5).

Trapezius: Once again, contrary to all other muscles, the able-bodied participants had a dramatically higher peak EMG amplitude than the persons with paraplegia, 42.9±10.0 versus 20.5±8.7, respectively. Where during the contact phase of the push stroke this peak occurred varied considerably as well, with the able-bodied group reaching peak EMG amplitude at 77.4±6.1% of the push stroke, while the participants with paraplegia reached peak amplitude at 58.9±11.5%.

Pectoralis Major: Contrary to the right side, the peak EMG amplitude varied noticeably between groups; participants with paraplegia used 34.0±7.1 percent of their MVC, while able-bodied participants used 46.9±12.8%. The overall "muscle energy"

for able-bodied participants was 52.5% greater than for participants with paraplegia. Similar to findings on the right, peak pectoralis firing for able-bodied participants was 7% later throughout the push stroke than for participants with paraplegia (39.9±3.5% versus 32.9±9.5%). Overall burst durations were comparable.

Biceps brachii: Peak EMG amplitude between groups varied dramatically; participants with paraplegia used 26.9±5.3% of MVC at peak, while able-bodied participants used 17.5±4.4% (Table 2-7). The percentage of where this peak occurred is comparable between groups. Overall burst duration varied as well; participants with paraplegia had a burst duration of 77.1±7.5 while their able-bodied counterparts had a burst duration of 45.1±8.6. In addition, participants with paraplegia use 97.5% greater "muscle energy" throughout propulsion than the able-bodied group.

Triceps: It is clear that all five participants with paraplegia had triceps activity early on in the push stroke while only one of the able-bodied participants had any initial activity. As a result, the participants with paraplegia had a longer triceps burst duration in comparison with the able-bodied participants (76.4±8.7% versus 62.9±6.5%). Peak EMG amplitude between groups varied slightly as well; contrary to the findings from the right side, participants with paraplegia used 23.6±5.8% of MVC at peak, while able-bodied participants used 29.4±7.1% (Table 2-7). In addition, the angle at which both groups achieved these peaks varied, with participants with

paraplegia achieving peak amplitude at 67.4±5.2 percent of the push stroke versus the

able-bodied 58.7±5.8% (Figure 2-6).

Table 2-4: "Muscle energy" comparison, right side

"Muscle energy," as calculated from the area under the curve of the graph of the magnitude of muscle activity throughout propulsion. A positive result in the percent difference in effort means that the persons with paraplegia needed a greater muscle effort throughout propulsion than the able-bodied group.

Muscle	Population	"Energy"	% Difference in Energy
Anterior Deltoid	Able-Bodied	1862.2	- 5.1 %
	Paraplegia	1772.1	
Posterior Deltoid	Able-Bodied	1009.5	+ 36.0 %
	Paraplegia	1372.7	
Upper Trapezius	Able-Bodied	2033.0	- 82.4 %
	Paraplegia	1114.4	
Pectoralis Major	Able-Bodied	1301.0	- 6.1 %
	Paraplegia	1221.9	
Biceps Brachii	Able-Bodied	764.5	+ 132.0 %
	Paraplegia	1778.5	
Long Head of the Triceps	Able-Bodied	1087.7	+ 67.1 %
	Paraplegia	1817.1	

Table 2-5: "Muscle energy" comparison, left side

Left side results. See definition of "muscle energy" above. A positive result in the percent difference in effort means that the persons with paraplegia needed a greater muscle effort throughout propulsion than the able-bodied group.

Muscle	Population	"Energy"	% Difference in Energy
Anterior Deltoid	Able-Bodied	1823.0	- 19.8 %
	Paraplegia	1521.3	
Posterior Deltoid	Able-Bodied	908.4	+ 83.6 %
	Paraplegia	1668.0	
Upper Trapezius	Able-Bodied	1773.9	+ 26.0 %
	Paraplegia	2234.8	
Pectoralis Major	Able-Bodied	2328.9	- 52.5 %
	Paraplegia	1527.5	
Biceps Brachii	Able-Bodied	593.9	+ 97.5 %
	Paraplegia	1173.0	
Long Head of the Triceps	Able-Bodied	1269.5	+ 12.0 %
	Paraplegia	1421.7	

Table 2-6: Peak percentage of MVC, right side

	Participants with Paraplegia	Able-Bodied Participants
Anterior Deltoid	39.1±9.0	38.5±7.8
Posterior Deltoid	45.0±12.0[*]	29.7±6.6
Trapezius	31.8±7.6	43.8±8.9[+]
Pectoralis Major	28.2±5.5	32.9±7.7
Biceps Brachii	36.8±10.3[t]	20.8±8.7
Long Head of the Triceps	43.0±6.4	24.9±4.3

[*]   For four participants – one had physiologically unrealizable results
[t]   For three participants – two had physiologically unrealizable results
[+]   For five participants – one had physiologically unrealizable results

Table 2-7: Peak percentage of MVC, left side

	Participants with Paraplegia	Able-Bodied Participants
Anterior Deltoid	45.1±9.0	28.7±6.6[t]
Posterior Deltoid	27.4±10.1[•]	25.8±5.0
Trapezius	20.5±8.7[•]	42.9±10.0[t]
Pectoralis Major	34.0±7.1	46.9±12.8[*]
Biceps Brachii	26.9±5.3[+]	17.5±4.4
Long Head of the Triceps	23.6±5.8[+]	29.4±7.1

[*]   For five participants – one had physiologically unrealizable results
[t]   For four participants – two had physiologically unrealizable results
[+]   For four participants – one had physiologically unrealizable results
[•]   For three participants – two had physiologically unrealizable results

Figure 2-5: Comparing triceps activity, right side

Right side muscle activity normalized to propulsion with peak muscle activity denoted by the triangles on the graph. Contrary to able-bodied participants, persons with paraplegia have a longer burst duration, with activity early on in the propulsion cycle. Raw EMG (Appendix Table B-2-3) was processed in Matlab, and then resulting burst durations were further visually processed (as described previously). Additional processing for peak %MVC and percentage of propulsion where the peak occurs was done by neglecting any values that were two standard deviations above and/or below the calculated mean to neglect any outliers (from the raw processed EMG data).
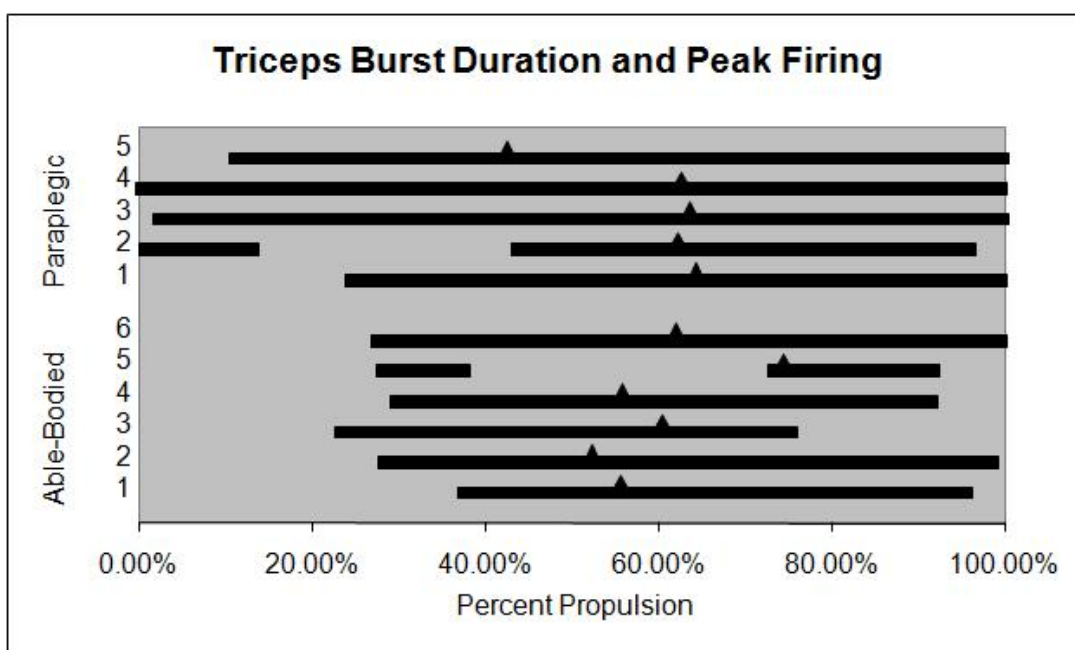
Figure 2-6: Comparing triceps activity, left side

Left side muscle activity normalized to propulsion with peak muscle activity denoted by the triangles on the graph. Processing techniques described above. PP-5 had no clear burst onset or offset.
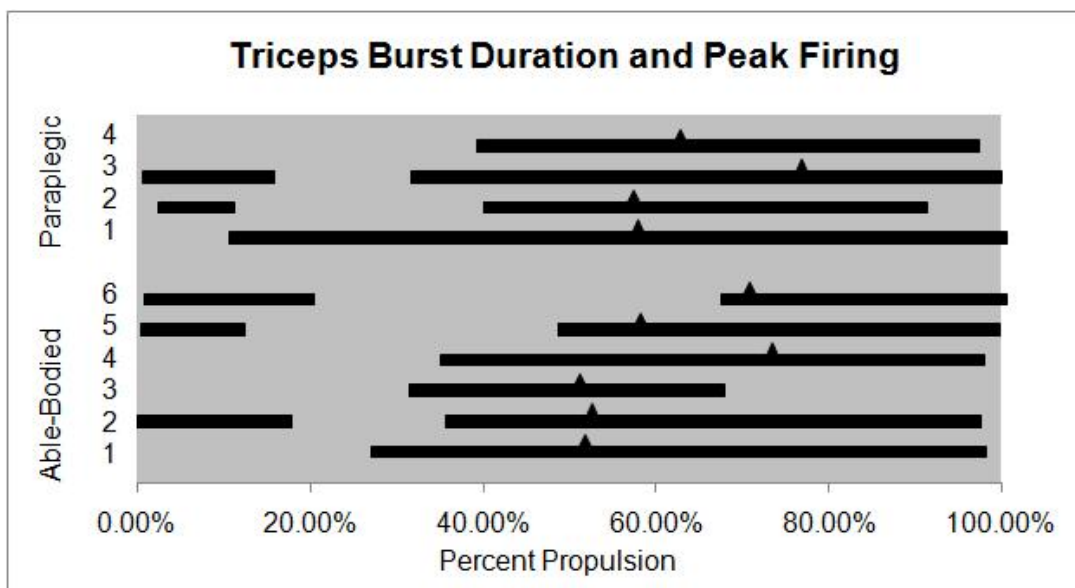
Summary

A systematic integrated data collection and analysis of kinematics, kinetics, and EMG data allow for the comparison of differences in wheelchair propulsion between able-bodied individuals and persons with paraplegia. Kinematics data from a motion analysis system, kinetics data from force-sensing push rims, and EMG data from six upper-limb muscles, were collected for ten consecutive push strokes at a self-selected speed. Putting the entire picture together results in a more comprehensive view, which may allow an understanding of differences that may exist between participants with paraplegia and able-bodied individuals to become clear (Figure 2-7). Results are as follows: In general, individuals with paraplegia tend to use a greater

percentage of the majority of muscles in relation to MVC; participants with paraplegia reach peak EMG amplitude prior to their able-bodied counterparts, when measured as a function of the percentage of propulsion; the majority of able-bodied individuals had no triceps activity in the initial stages of propulsion; burst durations for about half of the investigated muscles were considerably longer for the participants with paraplegia than their cohorts; and able-bodied participants had, on average, peak resultant, tangential, and radial forces occurring later on the push rim (in degrees).

Figure 2-7: Kinetics, EMG, and contact and release angles for two participants
Muscle labels are as follows: 1) Anterior Deltoid; 2) Posterior Deltoid; 3) Trapezius; 4) Pectoralis Major; 5) Biceps Brachii; 6) Triceps. Left side, sagittal view; right side, sagittal - but looking in the lateral direction. Tangential force traces as a function of contact time on the push rim. Peak muscle activities denoted by triangles.

Left Side: Push Force, Contact Angle, and EMG Bursts for AB-1

Right Side: Push Force, Contact Angle, and EMG Bursts for AB-1
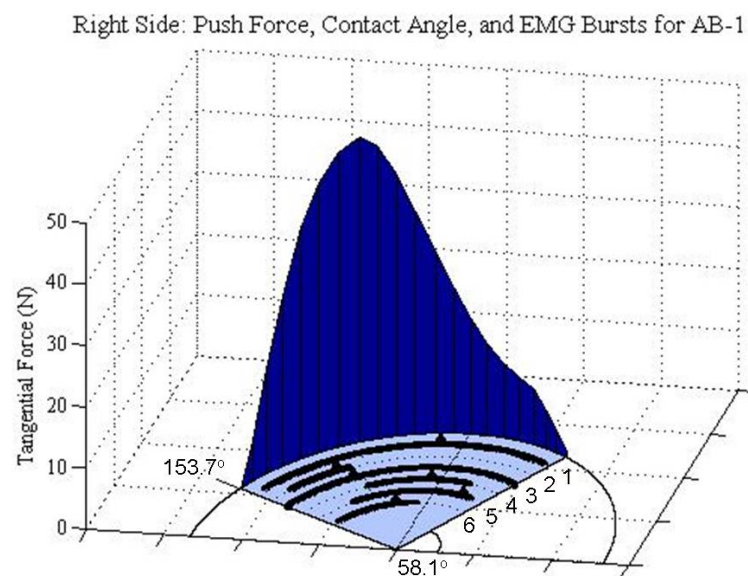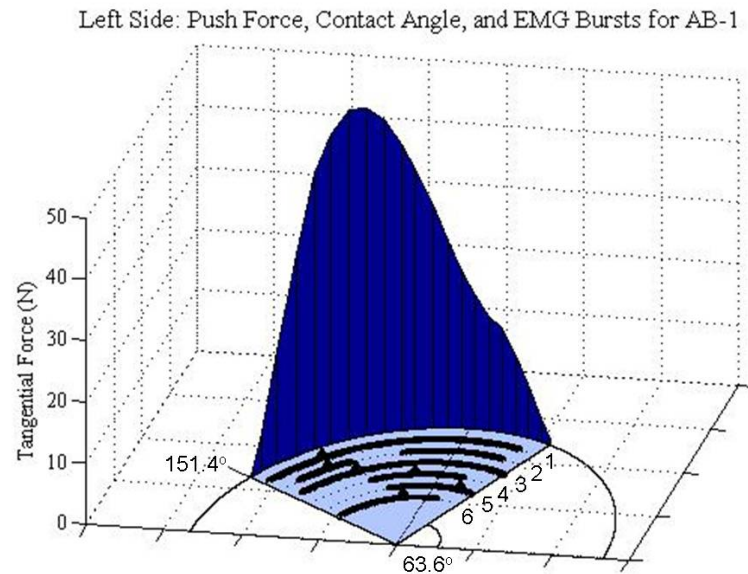
Left Side: Push Force, Contact Angle, and EMG Bursts for PP-2
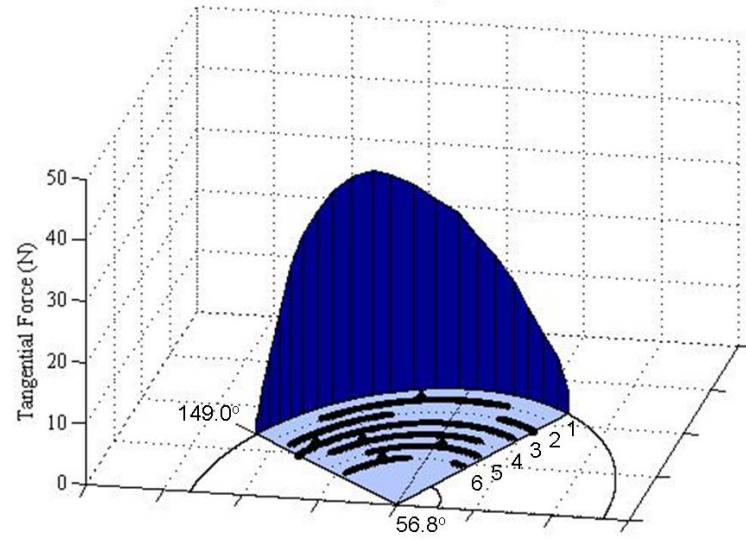
Right Side: Push Force, Contact Angle, and EMG Bursts for PP-2
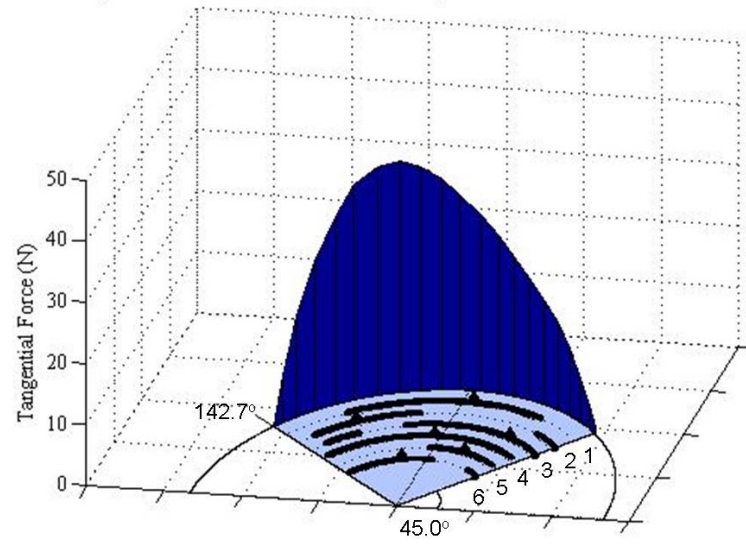
Conclusion

There are two main conclusions that can be drawn from this integrative investigation: 1.) A greater "muscle energy," as measured by the area under the curve of the percentage of EMG throughout propulsion, results in a greater resultant joint force in the shoulder and elbow, thus potentially resulting in shoulder pathology. 2.) Similarly, a greater "muscle energy" may result in fatigue and play a factor in the development of shoulder pain and pathology over time; fatigue may compromise an effective propulsive stroke placing undue stresses on the joint capsule.

Muscle activity differences may be responsible for the observed kinematic and kinetic differences between the two groups. The high incidence of shoulder pain in MWUs as compared to the general population may be the result of such differences, although the results from this biomedical investigation should be examined with caution. Future research into joint forces may shed light on this. Further investigation needs to focus on whether the pattern of kinematics, kinetics, and muscle activity during wheelchair propulsion is compensatory or evolutionary by tracking individuals longitudinally.

CHAPTER 3

COMPUTATIONAL STUDY: ANALYTICAL AND COMPUTATIONAL ANALYSIS

The motivating factor behind the creation of a patient-specific biomechanical model of the upper limb is to investigate the potential link between wheelchair use and shoulder pain. Gellman, et al., reports that 16 years post injury, 100% of MWUs have experienced some degree of shoulder pain during transfers [12]. Another study, by Boninger, et al., concluded that prolonged wheelchair use and transfers may cause this high frequency of upper limb cumulative trauma and strain injuries in MWUs [21]. The high incidence of shoulder pain in MWUs as compared to the general population may be the result of muscle activity differences, however further investigation into the connection between this link cannot be achieved without the aid of a computational model to potentially provide insight into the cyclic-propulsion and cumulative-trauma link. A fully-validated patient-specific upper limb model allows for the quantification of the magnitude of shoulder joint forces throughout propulsion. Investigating the effects of wheelchair set-up on the magnitude of these forces may shed light on detrimental axle placements that should be avoided due to the high shoulder joint forces that result.

As previously described, the AnyBody Modeling System is a software system for simulation of human movement [59]. It can model any part of the musculoskeletal system and compute muscle forces, joint reactions, metabolism, mechanical work, and

efficiency for given movements. Every property of a model created in AnyBody is parametric, and the software can be used for optimization of movement patterns, working positions, anthropometric data, and boundary conditions, using non-linear or linear optimization criteria. Non-linear optimization solution techniques are available for use within AnyBody, however they are considered to be time-consuming numerical methods. Criteria leading to linear optimization problems however, are attractive in terms of efficiency and ease of implementation; linear optimization problems, or min/max criteria, can be considered to be minimum fatigue criteria, formulated as minimization of the maximum relative muscle load as previously discussed. AnyBody can be used to investigate a number of fundamental questions as well as to solve practical problems of ergonomics.

However, prior to using AnyBody for practical ergonomic problems which are commonly complicated indeterminate calculations, a better understanding of how the software solves simpler problems is necessary. To do this, several analytical analyses were run, after which an equivalent model was created in AnyBody, and results from both were compared. The overall goal in creating and comparing outputs from these models was to better understand the mathematical processes within the software.

2-Segment Model

A rigid-body model was created analytically, representative of a 2-segment arm model (upper arm and forearm), in which a 100 Newton force was applied at the end of the forearm. The free body diagram of the analytical model used for analyses is

shown in Figure 3-1. There were five muscles available for analyses, and their origins
and insertions are shown below (Figure 3-1). Two separate analytical analyses were
run calculating the muscle and joint reaction forces for a static scenario in which the
elbow was in 90° flexion. One scenario investigated the muscle and joint reaction
force outputs calculated when the deltoid and biceps short were active, and another in
which the brachialis and biceps long were active. The primary difference between the
two scenarios is the level of difficulty in solving for the muscle and joint forces. In
the first scenario, the system is perfectly constrained – there are an equal number of
equations and unknowns. However in the second scenario there are more unknowns
than equations (as both the brachialis and biceps long insert onto the forearm), so the
solution is solved by setting one muscle as a function of the other while solving the
problem. Analytical analyses and associated free body diagrams for each scenario
follow.

Figure 3-1: 2-segment arm model

(1) Deltoid; (2) Biceps Long; (3) Biceps
Short; (4) Brachialis; (5) Brachioradialis
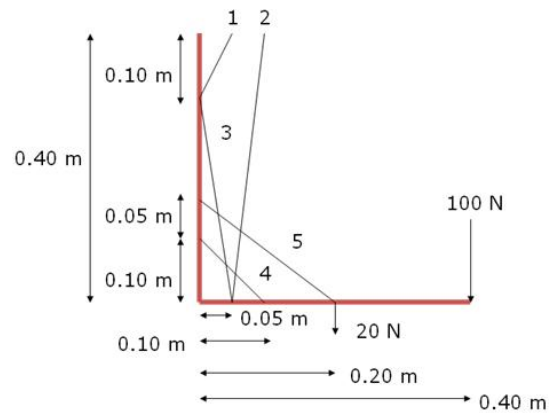
Analytical Analysis I: Deltoid and Biceps Short

Figure 3-2: Free body diagram, analytical analysis I
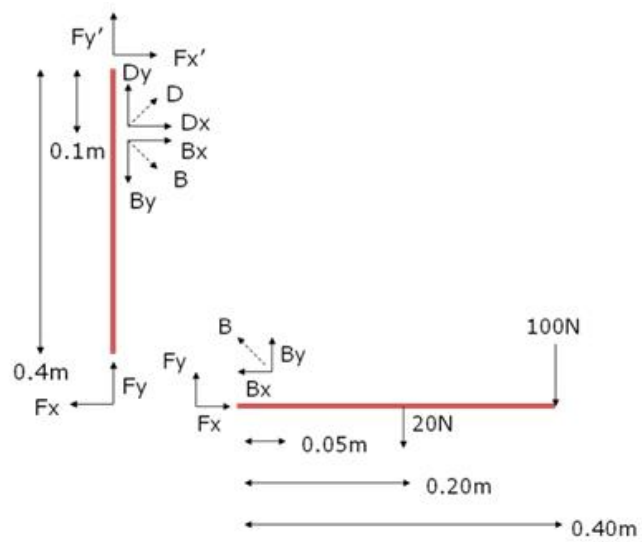
Analytical analysis and results (Figure 3-2):

$$\sum M = 0; (-100N)(0.4m) - (20N)(0.2m) + B_Y(0.05m) = 0$$

$$\sum F_X = 0; F_X - B_X = 0$$

$$\sum F_Y = 0; F_Y + B_Y - 100N - 20N = 0$$

Solving the above equations yield the following results, summarized in Table 3-1.

Table 3-1: Analytical results, analytical analysis I

B_y = 880 N
B_x = 147 N
B = 892 N
F_x = 147 N
F_y = -760 N
D_x = 440 N
D_y = 880 N
D = 984 N
F_x' = -440 N
F_y' = -760 N

Analytical Analysis II: Brachialis (BR) and Biceps Long (BL)

Figure 3-3: Free body diagram #1, analytical analysis II
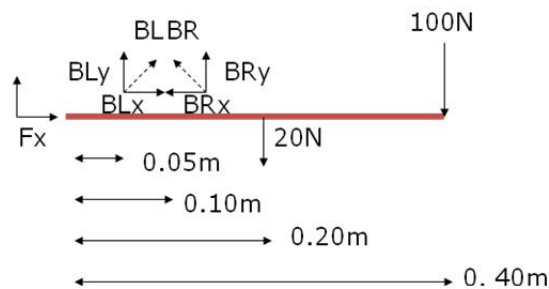
Trigonometric results for x- and y- force components for each muscle:

$$BR_Y = \frac{BR}{\sqrt{2}}; BL_Y = \frac{BL}{\sqrt{2}}$$

Analytical analyses (Figure 3-3):

$$\sum M = 0; (-100N)(0.4m) - (20N)(0.2m) + BR_Y(0.1m) + BL_Y(0.05m) = 0$$

$$BR_Y(0.1m) + BL_Y(0.05m) = 44$$

$$2BR_Y + BL_Y = 880$$

Substitute in BR$_y$ and BL$_y$ values:

$$\frac{2BR}{\sqrt{2}} + \frac{8BL}{\sqrt{65}} = 880$$

Setting BR = 0; BL = 887 N

Setting BL = 0; BR = 622 N

Graphing the above result:

Figure 3-4: First step analytical analysis II

The result of setting BR to zero and solving for BL, followed by separately setting BL to zero and solving for BR. Axes are labeled accordingly.
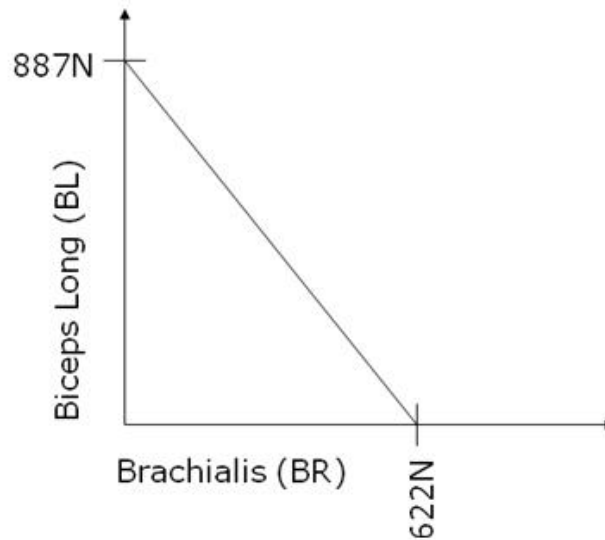
$$\sum F_Y = 0; F_Y + BR_Y + BL_Y - 100N - 20N = 0$$

$$F_Y + \frac{BR}{\sqrt{2}} + \frac{8BL}{\sqrt{65}} = 120N$$

$$F_Y = 120 - \frac{BR}{\sqrt{2}} + \frac{8BL}{\sqrt{65}}$$

$$\sum F_X = 0; F_X - \frac{BR}{\sqrt{2}} + \frac{BL}{\sqrt{65}}$$

$$F_X = \frac{BR}{\sqrt{2}} - \frac{BL}{\sqrt{65}}$$

Figure 3-5: Free body diagram #2, analytical analysis II
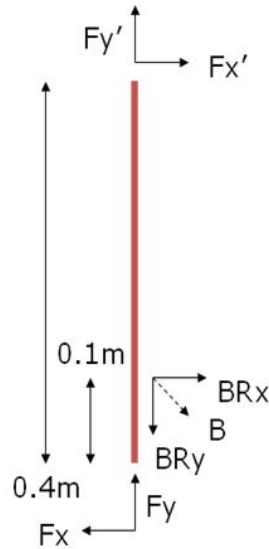
$$\sum M = 0; BR_X(0.3m) - F_X(0.4m) = 0$$

$$\frac{BR(0.3m)}{\sqrt{2}} - \left[\frac{BR}{\sqrt{2}} - \frac{BL}{\sqrt{65}}\right](0.4m) = 0$$

$$BL = \left(\frac{(\sqrt{65})BR}{\sqrt{2}} - \frac{0.3(\sqrt{65})BR}{0.4(\sqrt{2})}\right)$$

$$BL = 1.425BR$$

Set the moment equations equal to each other:

$$\frac{BR(0.3m)}{\sqrt{2}} - \left[\frac{BR}{\sqrt{2}} - \frac{BL}{\sqrt{65}}\right](0.4m) = \frac{2BR}{\sqrt{2}} + \frac{8BL}{\sqrt{65}} - 880$$

$$\frac{2.1BR}{\sqrt{2}} + \frac{7.6BL}{\sqrt{65}} = 880$$

Setting BR = 0; BL = 934 N

Setting BL = 0; BR = 593 N

Graphing this result on the same axes as the first graph results in an intersection point

of (313, 442). The result of this analysis is: Brachialis = 313 N, and Biceps Long =

442 N (Figure 3-6).

Figure 3-6: Resulting graph, multi-step analytical analysis II
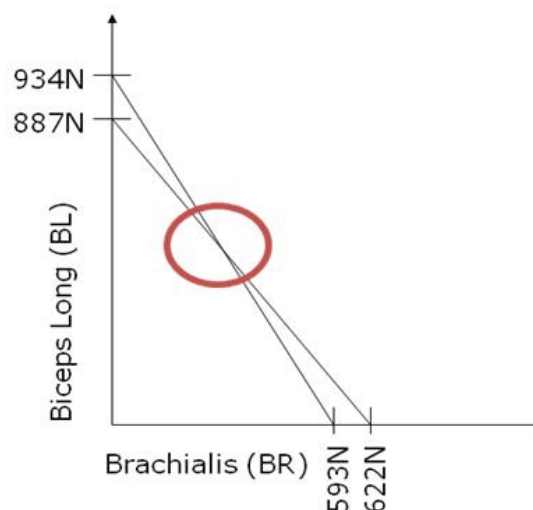
Computational and Analytical Comparison

An equivalent rigid-body model was created in AnyBody for use in comparing

analytical and computational results (AnyBody code in Appendix A). For each

scenario, the deltoid and biceps short, and the brachialis and biceps long,

computational results matched the analytical calculations. Further validations for

more complicated models were run, with the addition of more segments, muscles, and degrees of freedom.

Anthropometrically Correct 2- and 3-Segment Arm Models

To further validate AnyBody outputs, a similar 2-segment arm model was again constructed to once again compare the analytical and computational muscle and joint force outputs [78], this time based on anthropometric dimensions (Figure 3-7). Each segment's length, center of mass, and inertial properties, as well as the muscle origin and insertion points of the biceps, triceps, and brachialis, were based on the data and modeling assumptions of the Dutch Shoulder Model [45]. As in the previous validation experiments, the elbow joint of the arm-complex was held in 90° flexion with the lower arm parallel to the ground, however for this calculation, the distal end of the lower arm held a 5-pound dumbbell. An inverse-dynamics analysis was run, and the resulting muscle and joint forces were compared to the long-hand calculations of the same problem. Investigated muscles include the biceps long and short, and the long head, medial head, and lateral head of the triceps, each divided into two muscle sections (resulting in 8 total muscle fibers). Muscle and joint forces were calculated first when one muscle contributed to holding the arm in the flexed position, up to when eight muscles contributed. As muscles were added to the system, the model became indeterminate. In the case of indeterminacy, muscles flexors and extensors were individually grouped and set in terms of each other based on their physiological cross sectional areas (PCSA). The resulting muscle force values, as calculated

analytically and computationally, were equivalent. Results are summarized in (Table 3-2).

Adding a third dimension to the bicep-curl model added another level of complication. The forearm was split into the radius and the ulna, as were the appropriate muscle origins and insertions. This model has the advantage of a high level of detail making it a fairly accurate replication of the human musculoskeletal system. However this added dimension created an indeterminate system. Validation at this point, became more difficult to achieve long-hand. To verify the mathematics within the software, the three-dimensional model was restricted to movement in two-dimensional space. Results, as optimized by an objective function built into the AnyBody Modeling System, were comparable to those calculated via long-hand in two-dimensions.

Figure 3-7: Computational and analytical models

Upper left: Initial rigid-body 2-segment model based on measurements from the Dutch Shoulder model [45]. Lower left: 3-D skeleton. Right: Free-body diagram associated with left-hand figures for analytical analysis.
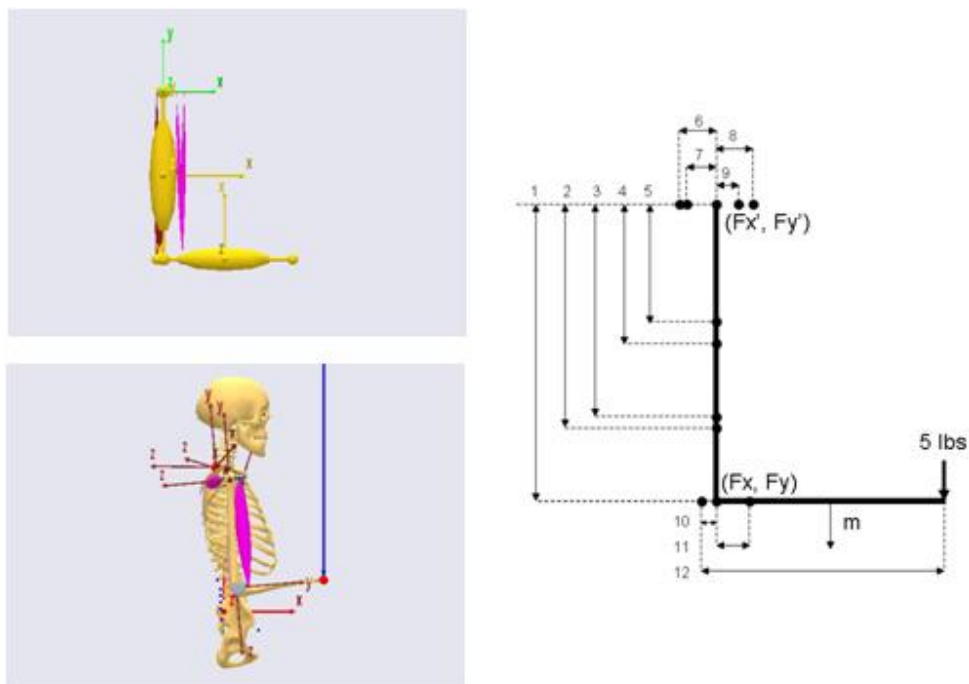
Table 3-2: Results for the anthropometrically correct model

Muscle/Joint Force	Results (N)
Biceps Breve	103.9
Biceps Long	107.6
Lateral Head of the Triceps I	12.4
Lateral Head of the Triceps II	12.4
Medial Head of the Triceps I	23.5
Medial Head of the Triceps II	23.5
Long Head of the Triceps I	0
Long Head of the Triceps II	0
Elbow Joint F_x	-5.3
Elbow Joint F_y	248.5
Shoulder Joint F_x	2.8
Shoulder Joint F_y	-156.7

The fact that there was parity in muscle forces between AnyBody outputs and long-hand calculations validated the mathematics within the software. By completely validating simple, and then more complicated physiologically-representative models through analytical analyses, confidence in the mathematics within the AnyBody Modeling System was obtained. This further lends assurance to the validity of future outputs calculated from patient-specific models.

CHAPTER 4

COMPUTATIONAL STUDY: PATIENT-SPECIFIC MODEL, CREATION AND VALIDATION

To follow up the previous chapter comparing analytical and computational results, the focus now shifts to an approach for the calculation of patient-specific shoulder joint reaction forces using a rigid body musculoskeletal model of the upper limb based on inverse dynamics. This approach is validated multiple ways. Historically, comparing the calculated muscle activities of biomechanical models with experimental EMG has long been an accepted means of model validation [79]. Qualitatively, the experimental and computational muscle burst output graphs are visually inspected and compared. Quantitatively, the muscle activity envelopes between the experimentally collected and computationally calculated are compared with a mean absolute error (MAE) analysis. The model is also validated by a means of comparing calculated joint reaction forces at the hand with SmartWheel outputs (further explained in the chapter), as well as with comparisons between shoulder joint forces as reported in literature. The primary focus of this chapter is to present and validate a rigid-body musculoskeletal model of the upper limb for later investigation into the effect that altered seat axles have on shoulder joint forces.

Creation of the Model

A patient-specific three-dimensional musculoskeletal model of the upper body was built using the previously discussed AnyBody Modeling System. The upper half of a previously created skeleton was downloaded from the public domain AnyBody Model Repository (www.anybody.aau.dk), and was used as the base for this model. The skeleton was then scaled anthropometrically to reflect the individual upper limb parameters of each participant (Table 2-1). In addition, each participant's wheelchair measurements were collected and used in construction of the model and are summarized in Table 4-1.

The model consisted of 21 rigid bodies; the skull, upper spine, lower spine (divided into 5-lumbar vertebrae), pelvis, thorax, and bilateral scapula, clavicle, humerus, radius, ulna, and hand. The model was equipped with 32 bilateral upper-body muscles (represented as over 225 muscle elements), as well as the rectus and transversus abdominal muscles, for controlling the upper body movement. Properties of muscles used in this model (such as PCSA, strength, origin and insertion) were derived from cadaver studies by the Dutch Shoulder Group [45] and are fully adjustable. For our study, the only muscle property that was adjusted was the strength in the core to reflect different levels of injury. For example, the able-bodied subjects and the individual with low-level paraplegia (PP-5 with an L1/L2 injury) were considered to have full core strength, whereas mid-level thoracic injuries were given half core strength, etc. All arm muscles are left at full strength as we only investigated individuals with paraplegia (who have fully innervated arm muscles).

The model was driven with 3-D trajectory inputs corresponding to each subject's propulsion kinematics. The model has 22 individual degrees of freedom; 2-degrees of freedom in the wrist, 1 in the elbow, 1 in the forearm (pronation/supination), 3 in the shoulder, 2 in the sterno-clavicular joint (elevation/depression and protraction/retraction), 1 in the neck, and 3 between the trunk and pelvis (flexion/extension, lateral bending, and rotation). The model was also driven with 3-dimensional forces, as recorded by force-sensing push rims, and were applied to the third metacarpal joint. Resulting joint and muscle forces were then calculated via inverse dynamics. Set-up and data collection and analysis were discussed previously.

Table 4-1: Wheelchair data

The participants with paraplegia used their own wheelchairs and the able-bodied participants used a lab wheelchair.

	Participants					
	PP-1	PP-2	PP-3	PP-4	PP-5	AB[*]
Backrest Height (cm)	54.0	35.0	43.0	49.0	40.0	n/a[t]
Seat Height (cm)	48.0	48.0	45.0	46.6	45.5	n/a[t]
Seat Angle (deg)	3.9	8.6	13.6	7.2	8.4	5.2
Horizontal Axle Position (cm)	3.0	2.0	4.0	12.5	10.0	7.0
Vertical Axle Position (cm)	14.0	11.0	4.8	16.1	4.0	16.0
Distance Between Rear Wheels (cm)	57.0	49.0	53.0	69.2	58.5	65.0
Self-Selected Speed (mph)	2.9±0.2	3.4±0.4	2.8±0.3	3.3±0.3	2.7±0.3	--

[*] One wheelchair was used for all able-bodied participants.
[t] This information was never collected
-- Self selected speed varied for all able-bodied participants, a full summary can be found in the Appendix, Table B-2-2.

Driving the Model

Coordinate Manipulation for Model Inputs

In order for the model to be run driven by patient-specific kinematics and kinetics, coordinate transformations were necessary to align the various coordinate systems in the model. The SmartWheel and the AnyBody modeling environment coordinate systems are set up in correspondence to the ISB Global Coordinate system where x is positive anterior, y is positive superior, and z is positive lateral (on the right side), Figure 4-1a. Since the SmartWheel and AnyBody model environments are already in the same coordinate system, to kinetically drive the model no coordinate transformation was necessary. However, there was a minor manipulation of the raw SmartWheel data for input into the model; the "equal and opposite" equivalent of the measured SmartWheel forces were calculated and then applied to the third metacarpal area up into the palm.

To kinematically drive the model, the raw Vicon 3-D coordinate outputs had to be manipulated for use with the AnyBody model. Vicon has the global coordinate system set up so that the z-direction is inferior/superior, the x-direction is anterior/posterior, and the y-direction is medial/lateral, Figure 4-1 b. To transform these Vicon global coordinates into the ISB Global Coordinate System, the following coordinate transformation matrices were applied to the 3-dimensional outputs for each reflective marker:

$$R_x = \begin{bmatrix} 1 & 0 & 0 \\ 0 & \cos(90) & -\sin(90) \\ 0 & \sin(90) & \cos(90) \end{bmatrix} = \begin{bmatrix} 1 & 0 & 0 \\ 0 & 0 & -1 \\ 0 & 1 & 0 \end{bmatrix}$$

$$R_y = \begin{bmatrix} \cos(180) & 0 & \sin(180) \\ 0 & 1 & 0 \\ -\sin(180) & 0 & \cos(180) \end{bmatrix} = \begin{bmatrix} -1 & 0 & 0 \\ 0 & 1 & 0 \\ 0 & 0 & -1 \end{bmatrix}$$

$$R_x R_y = \begin{bmatrix} -1 & 0 & 0 \\ 0 & 1 & 1 \\ 0 & 1 & 0 \end{bmatrix}$$

After transformation, each individual reflective marker, defined in the reference frame of the global coordinate system in the AnyBody model, can be used as input to drive the model kinematically. Upon completion of these transformations, the model is fully able to be driven by patient-specific inputs.

Figure 4-1: Coordinate systems in the model

a.)   AnyBody / SmartWheel

Environment   X – positive forward

Y   Y – positive vertical

Z – positive lateral (right side)

X   Z – positive medial (left side)

Z

b.)   Vicon Environment   X – positive forward

Z   Y – positive medial (right side)

Y – positive lateral (left side)

Y   Z – positive vertical

X
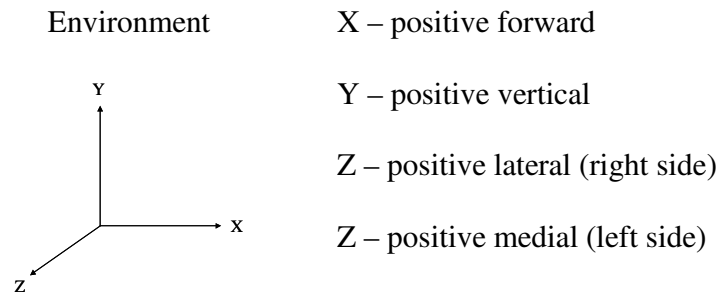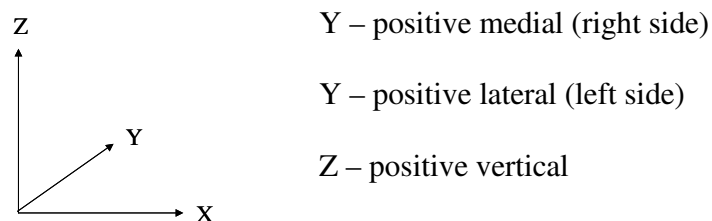
Validation of the Model

Validation of a musculoskeletal model is necessary, however there is no direct way to accurately measure muscle force in vivo to compare to that calculated in our computational model. However, EMG activity profiles can be compared between those collected experimentally and those calculated computationally. Similarly, the best way to compare shoulder joint forces as calculated computationally would be to compare them to in-vivo measurements obtained throughout the same movements, however to our knowledge, no such data exists for wheelchair propulsion. Each model was validated by comparing: 1.) experimental and computational EMG activity profiles (as mentioned above), 2.) experimental kinetics SmartWheel outputs to computationally calculated contact forces at the hand, 3.) the calculated shoulder joint forces with literature previously citing joint forces determined from other computational models, and 4.) in-vivo shoulder joint forces obtained from an instrumented shoulder joint implant throughout a variety of movements (however no wheelchair propulsion).

Comparison of Numerical and Experimental Data

EMG Validation

Computationally, for physiologically more realizable results, muscles with large origin and insertion areas need to be divided into multiple fibers. Van der helm developed a model calculating the number of muscle force vectors capable of representing the mechanical effect of muscles with large attachment sites, and found

that most muscles in the shoulder require at least 6 force vectors to be modeled accurately [80]. It can be concluded then, that different fibers of the same muscle can have different activity profiles, depending on what area of a large muscle is being investigated. So to compare the computational outputs to the experimental results, it was necessary to make sure that the fibers that were being analyzed computationally for comparison to experimentally derived participant EMG corresponded to the correct area on the participant where the surface EMG electrodes were placed. For example, the trapezius is a large muscle that spans a broad area of the back of the neck and the upper shoulders. From Figure 4-2e, one can see that there are multiple pink fibers that span the neck to the spine of the scapula (six), and one has been highlighted purple to represent the section of the trapezius that is being analyzed computationally for experimental EMG comparison. Based on both experimental placement and computational comparison, it is from that muscle fiber that the computational results are being compared to the experimental results.

All muscles investigated, anterior and posterior deltoids, trapezius, pectoralis major, biceps, and triceps, are represented computationally by multiple muscle fibers. The highlighted (purple) muscles in Figure 4-2 are those that are being compared computationally to experimentally collected data. Often times, the activity from multiple adjacent fibers is investigated, and is representative of a surface electrode that spans multiple parts of a muscle resulting in the production of activity that corresponds to more than one muscle fiber.

Once it has been determined which muscle fiber(s) should be analyzed for model validation for each subject, data is collected for two forms of validation – qualitative and quantitative analyses. Qualitatively, each of the ten analyzed push strokes was normalized and the muscle activity – as calculated computationally by AnyBody – was averaged and plotted in 10% increments on a graph showing muscle activity (as a percent of MVC) versus the percentage of propulsion. The start and end times, for each experimentally collected muscle burst, were averaged as a percentage of the propulsive stroke over the ten analyzed push strokes, and were graphed on the same axes as the computational results. The trace of muscle activities for computational and experimental outputs are nearly identical for PP-5, as shown in Figure 4-3.

Quantitatively, the mean absolute error (MAE), previously used to validate a computational musculoskeletal mandible model [81], was calculated for each muscle's activity envelope (both experimental and computational) with the following equation:

$$MAE = \frac{1}{n}\sum_{i=1}^{n}\left|MA_i - EA_i\right| \tag{4-1}$$

Where n is the number of push strokes, MA_i is the measured activity at push stroke i and EA_i is the estimated activity at push stroke i. The amount of time, measured as a percentage of the propulsive cycle, that each muscle was considered "on," in both the experimental and computational results for every push stroke, went into the above equation for determining the mean absolute error for each muscle. Results are summarized in Table 4-2 below, and are comparable in magnitude to MAE results used as a previous means of validation [81].

Figure 4-2: Experimentally collected EMG represented computationally

4-2 a: Anterior deltoid
4-2 b: Biceps brachii
4-2 c: Pectoralis major
4-2 d: Posterior deltoid
4-2 e: Trapezius
4-2 f: Triceps

a.)

b.)

c.)

d.)

e.)

f.)
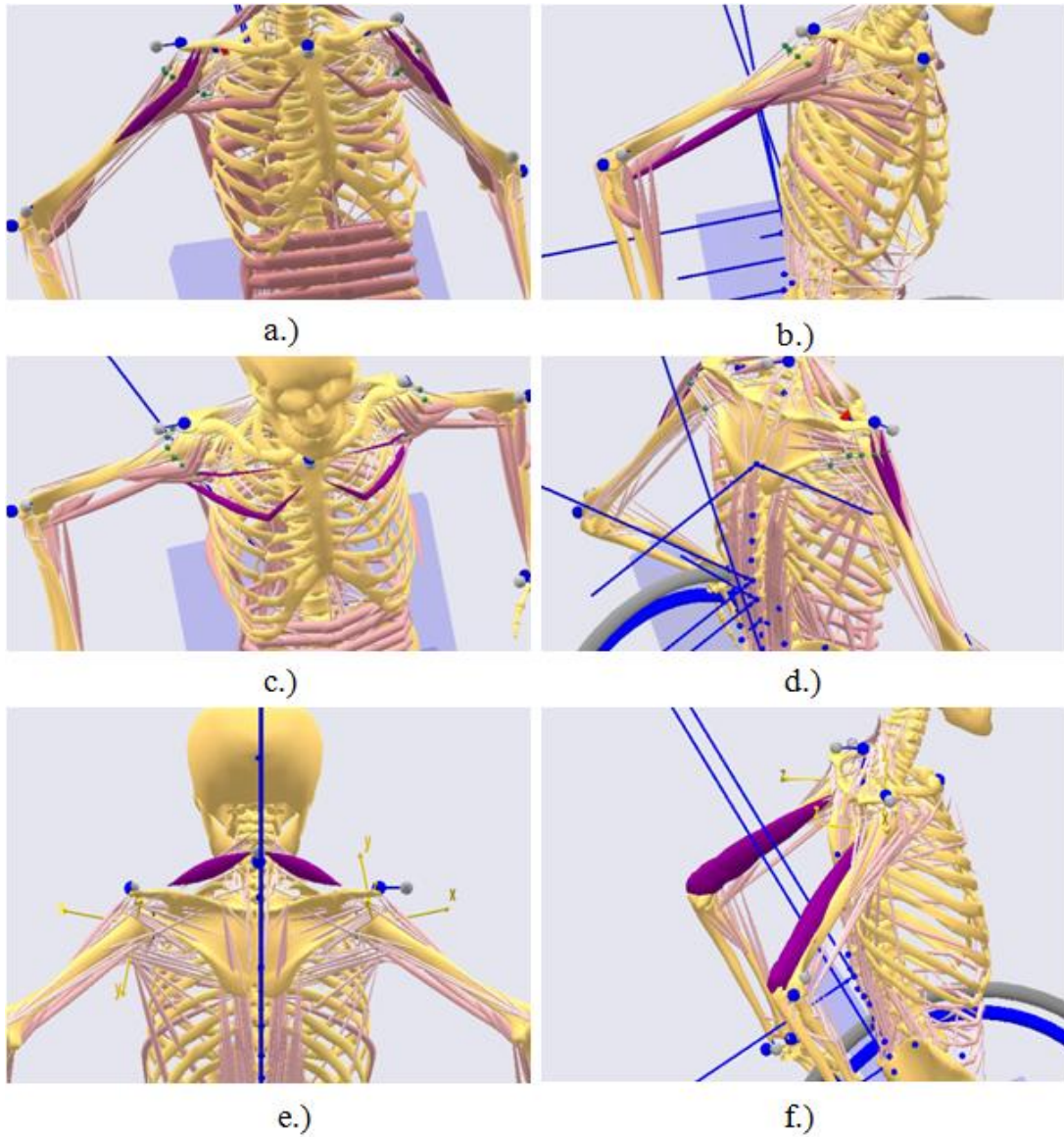
Table 4-2: MAE results for three participants

Muscles	Subject			Mean
	PP-2	PP-5	AB-1	
Biceps Left	0.210	0.138	0.068	0.139
Biceps Right	0.075	0.224	0.080	0.126
Anterior Deltoid Left	0.071	0.052	0.076	0.066
Anterior Deltoid Right	0.101	0.070	0.093	0.088
Posterior Deltoid Left	0.222	0.198	0.117	0.179
Posterior Deltoid Right	0.123	0.096	0.140	0.120
Pectoralis Major Left	0.173	0.068	0.068	0.103
Pectoralis Major Right	0.255	0.094	0.050	0.133
Trapezius Left	0.221	0.189	0.088	0.142
Trapezius Right	0.158	0.078	0.141	0.126
Triceps Left	0.177	0.558	0.433	0.389
Triceps Right	0.265	0.547	0.295	0.369
Mean	0.165	0.193	0.137	0.165

Figure 4-3: Qualitative model validation

Experimentally measured (solid lines) versus computationally calculated (dashed lines) muscle activities for 10 consecutive push strokes for PP-5. Each push stroke was normalized, and the activities were graphed at 10% increments of the contact phase (x-axis).
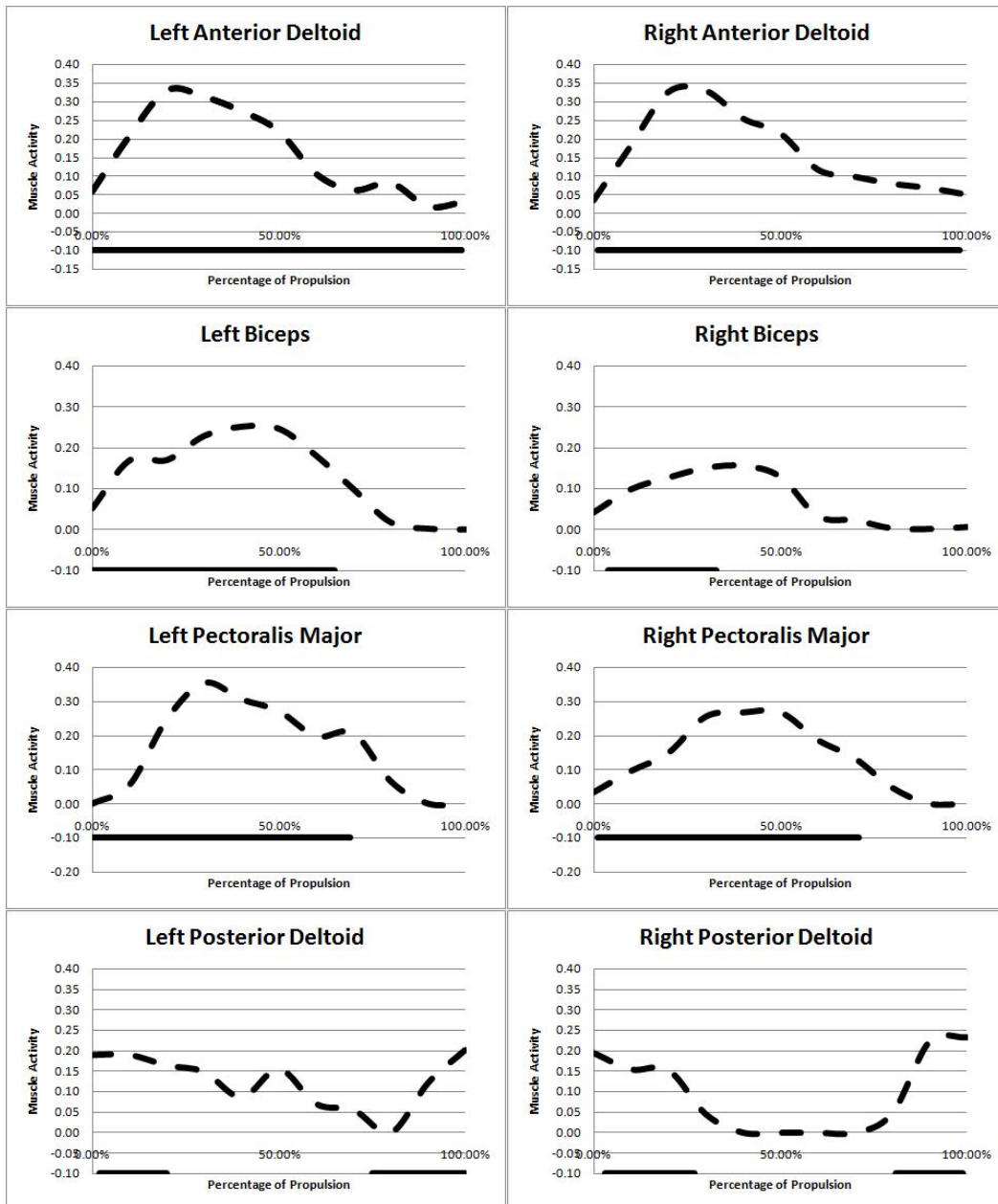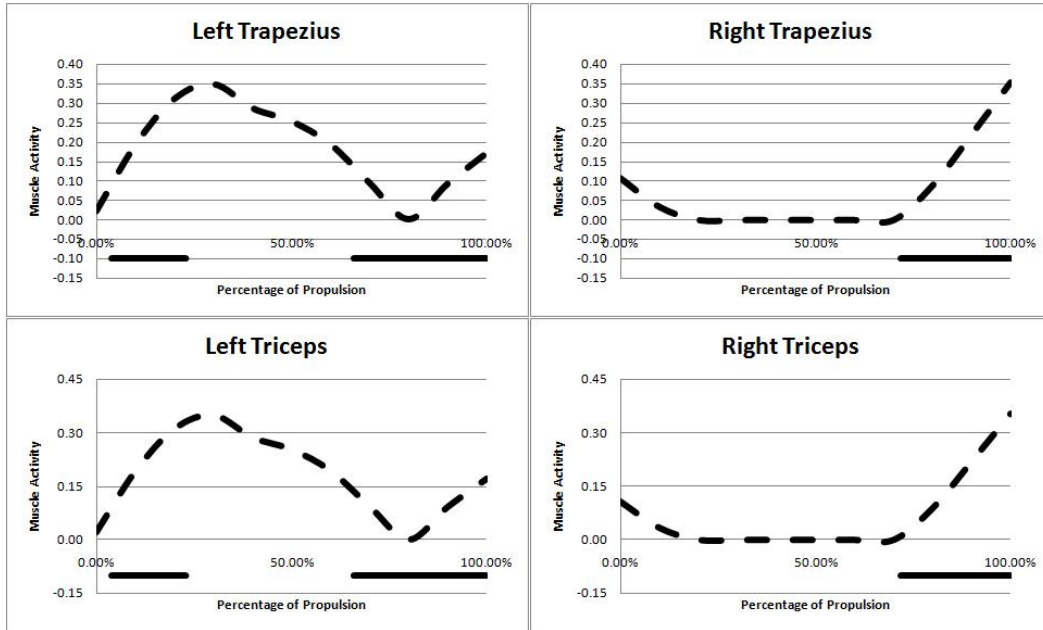
Kinetics Validation

In addition to muscle activity comparisons, another means of indirect validation is possible for further confidence in the model. The assumption has to be made, however, that the muscle forces and activities that have been calculated via inverse dynamics, as calculated and validated in the first section on model validation, are correct. This is a reasonable assumption if the qualitative experimental and computational muscle activity traces appear to align graphically, and if the MAE from the first validation is relatively low.

For this second means of validation, instead of driving the model by applying the SmartWheel x-, y-, and z- output forces to the hand, it is possible to derive the torque at the hub of the wheel with the following equation:

$$\tau = F \times R \tag{4-2}$$

Where the radius of the push rim, *R*, is a constant 0.2667 meters, and the force applied to the wheel *F*, varies depending on each subject. The model was then driven using the above calculated value coupled with the patient-specific kinematics. Each subject maintained their own constant self-selected speed throughout the propulsion process (Table 4-1 and Appendix Table B-2-2), although the torque, as described above, was constantly changing based on SmartWheel outputs throughout propulsion. After running the inverse dynamics analysis, the computationally calculated contact forces in the x-, and y-directions between the hand and the push rim are compared to the original SmartWheel output forces in the x- and y- directions. The z-direction force is neglected due to its negligible magnitude as compared to the x- and y- forces. The overall traces in the x- and y- directions between both experimentally collected and computationally calculated data align well qualitatively (Figures 4-4 and 4-5), however the resulting computationally calculated output forces are not as smooth as the SmartWheel forces (below), most likely due, in part, to the fact that the SmartWheel collects and smoothes data at 240 Hz, while the kinematics used to drive the model are collected at 120 Hz. In addition, due to the inherent nature of inverse dynamics, each point in space is discretized to solve for resulting joint and muscle forces based on the kinetics and kinematics inputs; in forward dynamics current solutions are used as predictive indicators in calculating the next step in an analysis which may produce a smoother output curve. However, the overall qualitative result that the two scenarios – computationally calculated and experimentally derived – comparably follow the same trend line, serves as another means of validation.

Figure 4-4: Kinetics validation results, right side, PP-5

Solid lines are the original SmartWheel x- (left), and y- (right) outputs. The dotted lines are the computationally calculated x- (left), and y- (right) outputs, as determined based on a kinematics and torque-driven model.
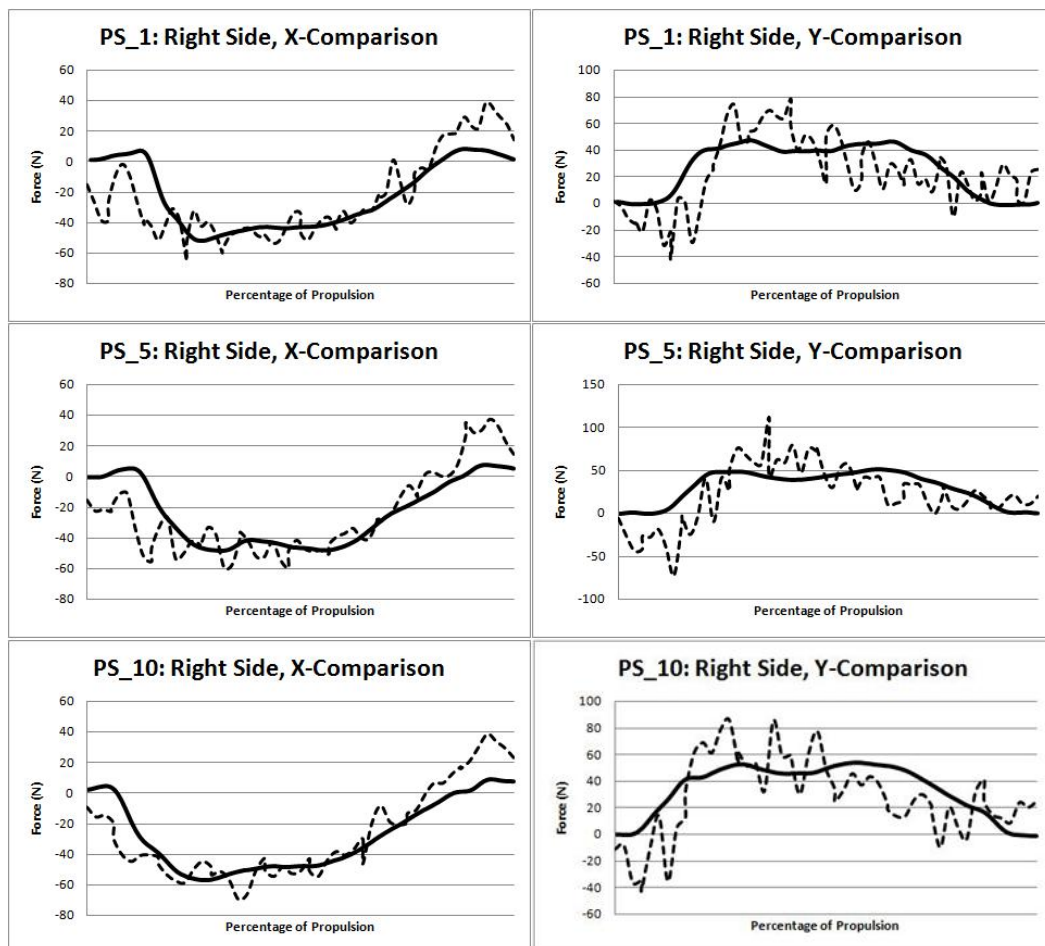
Figure 4-5: Kinetics validation results, left side, PP-5

Solid lines are the original SmartWheel x- (left), and y- (right) outputs. The dotted lines are the computationally calculated x- (left), and y- (right) outputs, as determined based on a kinematics and torque-driven model.
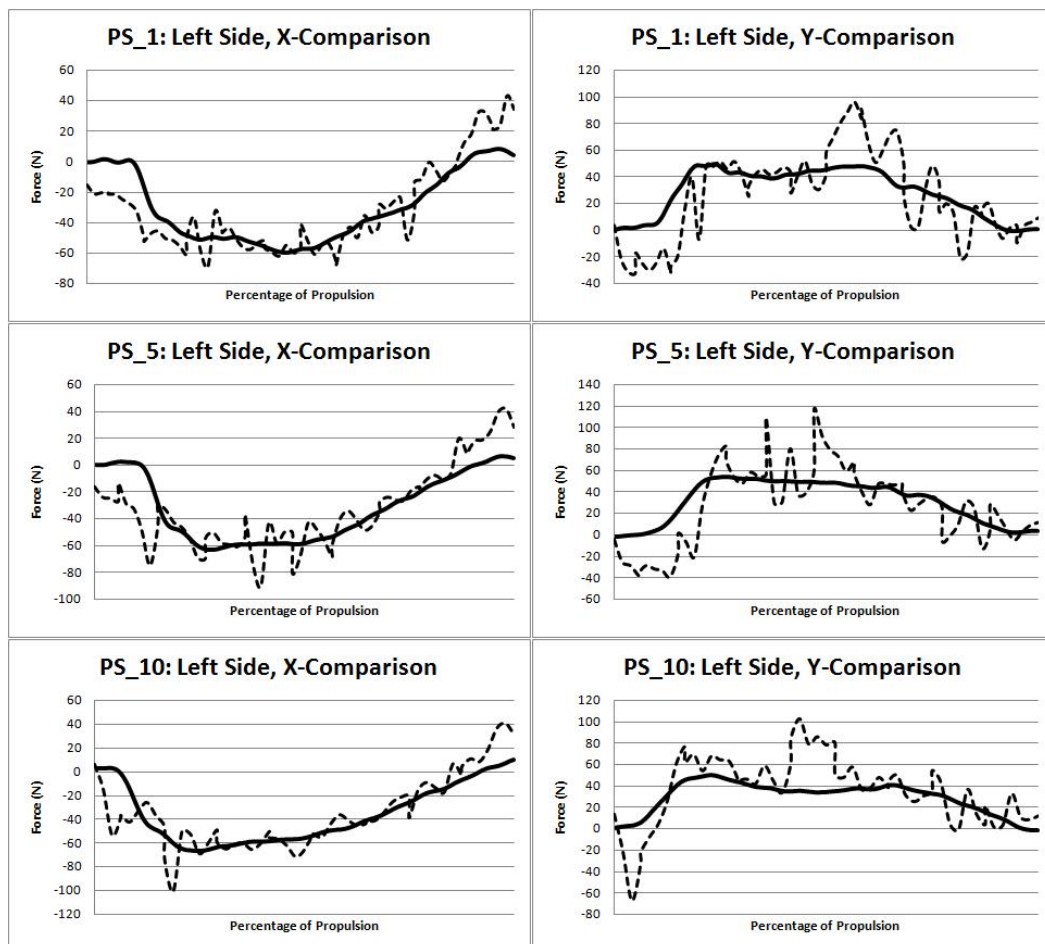
Comparison to Previous Studies

Comparison to In-vivo Measurements

As mentioned previously, the best way to compare shoulder joint forces as calculated computationally would be to compare them to in-vivo measurements obtained throughout the same movements, however to our knowledge, no such data exists. However, a previous study by Bergmann, et al., investigates in-vivo shoulder joint forces during a variety of activities of daily living, albeit no wheelchair propulsion [82]. A 6-degree-of-freedom instrumented shoulder was implanted into the right side of a male patient who had been suffering from primary humeral head arthrosis. Seven months postoperatively, data was collected on the subject and results from the first ever in-vivo shoulder joint force analyses were reported for various activities of daily living. The wide range of investigated activities includes abduction, flexion, and extension of the arm (with and without weights), lifting a 1.4 kilogram coffeepot, hammering a nail, steering, combing hair, and crutch-assisted walking. No wheelchair propulsion data was collected, however the activity of walking with two crutches most closely mimics the cyclic motion of wheelchair propulsion. Partial weight-bearing walking resulted in a shoulder load of approximately 65% of this individual's body weight (BW), and full weight-bearing (no foot-floor contact) resulted in a range of approximately 102% to 118% BW; in a 100 kilogram man, this results in joint force magnitudes of 638 – 1158 N. As this is an in-vivo study, this becomes the gold standard for validating biomechanical models, however these results are limited to the right side of only one person, and it should also be noted that this

subject had minor functional supraspinatus deficits resulting from surgery upon testing.

Comparison with Literature Results

Another means of model validation is to compare the current results to results found in literature. There are a number of previous studies investigating shoulder joint forces throughout a variety of activities. Table 4-3 summarizes the activities and associated contact force for the shoulder joint for each study.

Table 4-3: Glenohumeral contact forces in literature

Study	Motion	Resultant Contact Force
Van der Helm [83]	w/out weight abduction and anteflexion	~ 400 N
Van der Helm and Veeger [50]	Quasi-static WC propulsion	~ 300 – 1900 N
Van Drongelen, et al. [84]	Low-level WC propulsion	~ 300 – 400 N
	Weight relief	~ 1100 – 1600 N
	Reaching	~ 600 – 750 N
Veeger, et al. [85]	WC propulsion, 10 Watts	~ 800 – 1000 N
	WC propulsion, 20 Watts	~ 1100 – 1400 N
Anglin, et al. [86]	Standing	~ 300 – 2800 N
	Sitting	~ 300 – 2500 N
	Cane walking	~ 400 – 2300 N
Van Drongelen, et al. [87]	Weight relief	~ 1000 – 1700 N

The Dutch Shoulder Model was used for the majority of the reported studies above. When investigating wheelchair propulsion, van Drongelen, Veeger, and van der Helm and Veeger, each drove the Dutch Shoulder Model with subject kinematics and kinetics [50, 84, 85]. Van Drongelen investigated the glenohumeral contact forces of able-bodied individuals, and persons with para- and tetraplegia during three

different tasks assumed to be activities of daily living [84]. Veeger collected data from three male subjects with paraplegia at two different speeds and at two different resistances; the peak glenohumeral contact forces varied depending on the resistance of the set-up (10 Watts versus 20 Watts), however it was independent of the velocity of the pushing speed [85]. Van der Helm and Veeger used the Dutch Shoulder Model to determine shoulder joint and muscle forces at static points throughout propulsion for four healthy male subjects [50]. Another study, investigating the muscle and shoulder joint forces for four able-bodied and four subjects with tetraplegia determined the effect of the loss of a triceps muscle in a weight relief (not wheelchair propulsion) scenario [87]. No mention is made for the above investigations regarding model patient-specificity (to reflect subject anthropometrics), or model validation.

Using the Dutch Shoulder Model in arenas other than wheelchair propulsion and associated activities of daily living, van der Helm analyzed the positioning of 10 healthy subjects during loaded and unloaded abduction and anteflexion of the humerus [83]. Unlike many previous models, the thorax is included as a rigid-body in this study. EMG signals are recorded in 12 subjects, however not all of the subjects participated in the motion recording part of the experiment. The model then calculated the forces and moments exerted by individual muscles to maintain and counterbalance the external load. This was the most complete model regarding validation, however it was acknowledged within the paper that validation via muscle on/off patterns is difficult because in the motions analyzed there were limited on/off times.

Lastly, Anglin, et al., was the only group in the table above to use the Swedish shoulder model for the analysis of glenohumeral contact force for a variety of activities (unrelated to wheelchair propulsion). The model was driven with subject kinematics and kinetics, however it was acknowledged that although the magnitude of shoulder joint forces are comparable to findings from other studies, this particular model cannot be validated directly.

Current results mimic findings in literature. Resultant shoulder joint force results will be discussed in greater detail in the following chapter, but the magnitude of participant results fell within the above ranges (200 – 800 Newtons). The magnitude of joint force results vary between the right and the left sides. For PP-5, for example, the average range of the resultant shoulder joint force throughout propulsion on the right hand side was between 200 and 500 Newtons, however the left hand side had a range of 200 to 800 Newtons. Differences between the right and the left sides could be the result of dominance – this individual was left-handed and may, as a result, show greater favoritism to the left-hand side, resulting in greater resultant joint forces. Regardless though, the low end of our results align well with van Drongelen's low-level wheelchair propulsion findings and the high end of our results align well with Veeger's 10 Watt wheelchair propulsion results. On another positive note, the current findings are comparable to those reported from in-vivo measurements.

CHAPTER 5

COMPUTATIONAL STUDY: JOINT FORCE INVESTIGATION, RESULTS AND DISCUSSION

With a complete and fully validated musculoskeletal model of the upper limb, the focus shifts to the functional outcomes and overall goals of the research at hand. While previous chapters have focused on the kinematics, kinetics, and EMG differences between able-bodied and participants with paraplegia, the underlying question still remains regarding what exactly is the magnitude of shoulder joint forces throughout propulsion, and how do the differences between the two cohorts, as well as how does proper wheelchair set-up, affect the magnitude of these forces? The magnitude of shoulder joint forces throughout propulsion, as calculated with the upper limb musculoskeletal model, and the effect that a parametrically calculated axle placement has on these forces, then becomes the focus of the current chapter.

Joint Force Analyses Results

Joint force results are reported in the ISB scapular coordinate frame (Figure 5-1) [88]. On the right side, positive x- is forward, positive y- is pointing upward, and positive z- is pointing laterally. On the left side the only difference is that positive y- points downwards. This coordinate system is set up based on the following anatomical landmarks: the most dorsal point on the acromioclavicular (AC) joint, the

midpoint of the triangular surface on the medial border of the scapula in line with the scapular spine (TS), the most caudal point of the scapula (AI), and the most laterodorsal point of the scapula (AA), as shown in Figure 5-1 [88].

The resulting shoulder joint forces for participant PP-5 – for both the right and the left shoulders – normalized and averaged in 10% increments throughout propulsion, are shown in Figures 5-2 and 5-3. The overall traces of the curves (F_x, F_y, F_z, and resultant graphs), are similar for both the right and the left sides (Figures 5-2 and 5-3). The magnitudes of peak F_x and F_y forces, in addition to the resultant force (as calculated with Equation 1-1 in Chapter 2), are greater on the left side of this participant than on the right. Also differing between the sides, is the percentage of propulsion where the peak shoulder joint force occurs. For the left side, the peak F_x occurs at 50% of propulsion, the peak F_y occurs at 40% of propulsion, the peak F_z occurs at 20% of propulsion, and the peak resultant force occurs at 50% of propulsion. For the right side, peaks tend to occur earlier in propulsion, with peak F_x at 40%, peak F_y at 30%, peak F_z at 70% (an exception to the right side), and peak resultant at 40% of propulsion. When comparing where the peak resultant, tangential, and radial forces occur on the push rim, participant PP-5 achieves these peaks *earlier* on the left side (than the right side) as a function of degrees on the push rim.

For PP-2, the results are summarized as follows: similar to the findings from PP-5, the magnitudes of peak F_x and F_y forces, in addition to the resultant force, are greater on the left side of this participant than on the right (Figures in Appendix B-5-1 and B-5-2). In addition, the percentage of propulsion where these peaks occurs is at

60% for the left side for all forces, and at 50% for the right side (with the exception of the F_z peak occuring at 70%). For this individual, the difference in where on the push rim peak resultant, tangential, and radial forces occur, as a function of the percentage of propulsion, is negligible. Contrary to PP-5, PP-2 achieves peak resultant, tangential, and radial forces later on the left side (than the right side) as a function of degrees on the push rim.

AB-1 results are summarized as follows: the magnitudes of peak F_x and F_y forces, in addition to the resultant force, are greater on the right side of this participant than on the left (Figures in Appendix B-5-3 and B-5-4). Unlike either PP-2 or PP-5, the percentage of propulsion where these peaks occurs is the same on both sides – at 50% of propulsion (for *all* force values) – however on the left side, the peak at 50% is not dramatically different than the value at 60%, leading to the conclusion that this individual maintains that peak value for longer on the left than on the right. For this individual, the difference in where on the push rim peak resultant and tangential forces occur, as a function of both the percentage of the propulsive stroke and the associated degrees on the push rim, is negligible. The radial forces, however, vary between sides, with the right side achieving peak earlier than the left side (as a function of both the percentage of the propulsive stroke and the associated degrees on the push rim).

Figure 5-1: Scapula coordinate system

The origin of the scapula is coincident with AA, the Z-axis (Z_s) is the line connecting TS and AA, pointing to AA, the X-axis (X_s) is formed from the line perpendicular to the plane formed by AI, AA, and TS, pointing forward, and the Y-axis (Y_s) is the common line perpendicular to the X_s- and Z_s-axis, pointing upward [88].
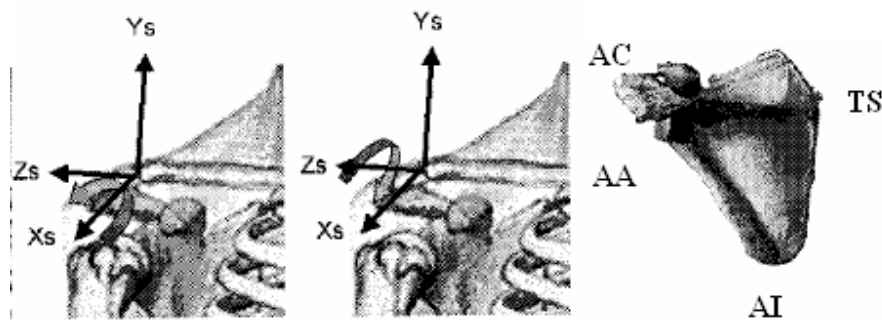
Figure 5-2: Right shoulder joint force results, PP-5

Top graph: F_x, F_y, and F_z forces. Bottom graph: Resultant force. The graphs are calculated by normalizing the joint forces throughout propulsion and then graphing the resulting joint forces in 10% increments.
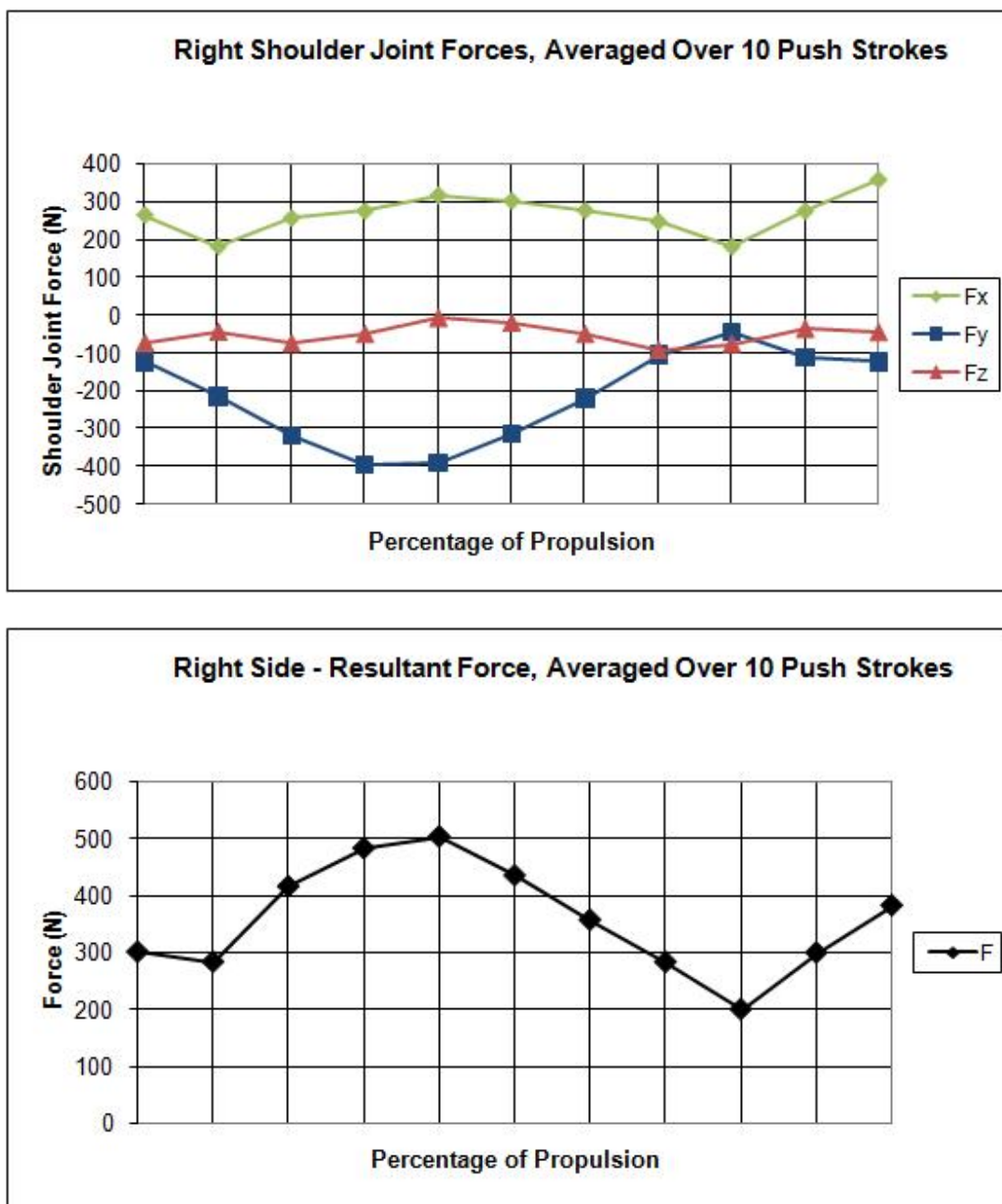
Figure 5-3: Left shoulder joint force results, PP-5

Top graph: F_x, F_y, and F_z forces. Bottom graph: Resultant force. The graphs are calculated by normalizing the joint forces throughout propulsion and then graphing the resulting joint forces in 10% increments.
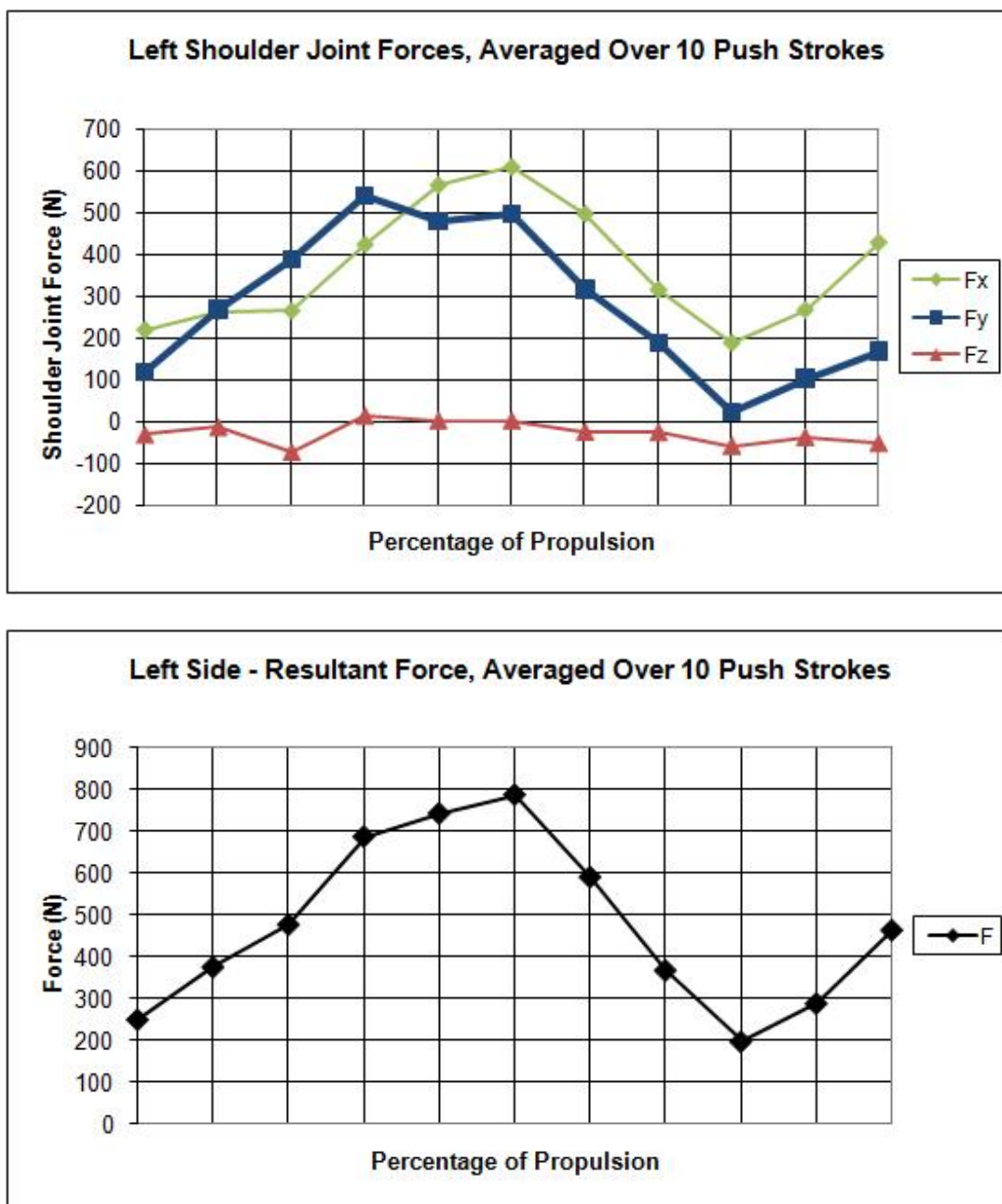
Discussion

The most obvious explanation for the differences between the right and left sides of participant PP-5 is the fact that this individual is left handed. That may most easily explain why the forces in the left shoulder joint are so much higher than in the right side. In general, overall strength is related to dominance, and, based on the conclusions from the first part of the investigation to determine if kinematic, kinetic, and EMG differences exist between able-bodied and participants with paraplegia, greater "muscle energy," most likely results in a greater resultant joint force in the shoulder and elbow. Therefore, one can make the conclusion that the reason joint forces on the left side are so much greater than on the right side is due to the fact that this individual is left handed. This argument is supported with the results from the magnitude of the shoulder joint forces for AB-1 throughout propulsion; both the individual force components, as well as the resultant forces, on the right side – this participants dominant side – are much higher in magnitude than the forces on the left side (Figures in Appendix B-5-3 and B-5-4).

This is, however, a potentially controversial argument. Much more goes into the actual act of wheelchair propulsion than sheer strength. There is a learning curve with many cyclic tasks such as wheelchair propulsion. The very opposite of the above argument could hold true; an individual's dominant side could actually be more efficient in a task, as defined by a minimum in the duration and magnitude of muscle activity. This, for example, may be the reasoning behind the confounding results from PP-2, in which the magnitude of shoulder joint forces from the dominant side is

actually less than those from the non-dominant side (Figures in Appendix B-5-1 and B-5-2). This argument speaks to a level of coordination between dominant and non-dominant sides; an uncoordinated non-dominant limb may actually compensate for dexterity with muscle inefficiencies. This argument is supported by the fact that of the six analyzed muscles, the duration of activity on the left side is noticeably longer in three muscles (biceps brachii, posterior deltoid, and trapezius), and only noticeably shorter in the pectoralis major (the durations of the anterior deltoid and long head of the triceps were comparable). It is possible that longer muscle activity duration may lead to fatigue which may in turn compromise an effective propulsive stroke placing undue stresses on the joint capsule. Findings from the first part of this bi-fold study support this explanation as well. A greater "muscle energy" may result in fatigue and play a factor in the development of shoulder pain and pathology over time; fatigue may compromise an effective propulsive stroke placing undue stresses on the joint capsule.

In conclusion, there is a valid explanation for both scenarios which further demonstrate the need for truly patient-specific models for analysis. While dominance may be the underlying factor in explaining the current findings, the interpretation of how dominance plays a role varies between both situations. Each case should be evaluated individually and no generalizations should be made, as evidence supports the fact that one explanation does not cover all scenarios.

Parametric Study Set-Up

At this point, clinically speaking it is not a matter of 'if' a MWU will experience or develop shoulder pain as they go about their daily lives, but it is a matter of 'when;' the reported prevalence of shoulder pain in MWUs is an astounding 31% - 73% [7-16]. It is anticipated that by adjusting the axle placement of a MWU to a position that minimizes shoulder joint forces, as determined from parametric study results, the integrity of a MWU's upper limbs may be prolonged, and pain and pathology may be postponed or altogether prevented.

There is no debate regarding the structural differences that exist between the human hip joint, which was made for the cyclic pounding of walking and running (in excess of our body weight) versus the human shoulder joint, which was made for range-of-motion and mobility. The shoulder joint is not made for the role reversal of cyclic pounding to loco-mote the body after a spinal cord injury. In fact, as mentioned previously, it is thought that prolonged wheelchair use, transfers, and pressure relief techniques may cause the high frequency of upper limb cumulative trauma and strain injuries in spinal cord injury [21]. It should stand to reason then, that by taking action to minimize the magnitude of shoulder joint forces throughout everyday activities with the simple adjustment of the axle placement in a wheelchair set-up, the integrity of the upper limb joints can be saved.

A parametric study was set-up to investigate the influence that axle placement had on the magnitude of shoulder joint forces. The parameter study is a cyclic step-wise investigation that calculates the resulting joint forces at each defined parameter.

Patient-specific data drives the model for each of the parameter steps. The initial model's environmental set-up represents the current axle positioning of the subject, as measured at the time of data acquisition. The positioning of the axle was allowed to move five centimeters in each of the four directions: anterior, posterior, inferior, and superior. The model is driven so that a total of five anterior/posterior seat positions and five inferior/superior seat heights are investigated. When combined, this results in a parameter study with 25 outputs (2-parameters, 5-values in each parameter equals 5^2 or 25).

Parametric Study Results

The minimum values of shoulder joint forces throughout propulsion for PP-5 are summarized in Table 5-1 (right) and Table 5-2 (left), and are the result of averaging the results from push strokes 1, 3, and 5. On the right side, the magnitude of the shoulder joint forces ranges from 275 to 363 Newtons over the defined boundaries (Table 5-1). The minimum of these values coincides with the current seat height set-up, however the seat position should be moved forward 2.5 centimeters for a true shoulder joint minimum (although the difference in shoulder joint forces between the current set up and the ideal set-up that minimizes shoulder joint forces is small). Resulting shoulder joint forces for the right side are listed in Table 5-1 (the minimum is bolded and outlined), and visually represented with a 3-D mesh grid and corresponding contour graph in Figure 5-4.

The left side results are slightly different; the range in the magnitude of the resulting shoulder joint forces is slightly smaller, with forces ranging from 278 to 324 Newtons (Table 5-2). The minimum of these values again coincides with the current set-up with regards to seat height, however contrary to the results from the right side, the seat positioning on the left side should actually be moved backward five centimeters from its current position. Resulting shoulder joint forces for the left side are listed in Table 5-2 (the minimum is bolded and outlined), and visually represented with a 3-D mesh grid and corresponding contour graph in Figure 5-5.

Table 5-1: Parameter study results, right side

Right side average joint forces (N), for push strokes 1, 3, and 5.

PP_5 – Right Side						
		Seat Position (m)				
		0.0500	**0.0750**	**0.1000**[*]	**0.1250**	**0.1500**
Seat Height (m)	**0.1002**	363.46	300.82	300.94	304.56	322.41
	0.1252	285.04	281.17	280.90	283.17	294.40
	0.1502[t]	281.18	**275.50**	275.90	282.06	296.30
	0.1752	294.48	291.53	292.43	291.19	293.39
	0.2002	292.44	290.18	290.13	289.78	286.63

[*]   Current anterior/posterior axle position
[t]   Current inferior/superior axle position

Table 5-2: Parameter study results, left side

Left side average joint forces (N) for push strokes 1, 3, and 5.

PP_5 – Left Side						
		Seat Position (m)				
		0.0500	**0.0750**	**0.1000**[*]	**0.1250**	**0.1500**
Seat Height (m)	**0.1002**	324.35	307.48	304.01	306.97	311.50
	0.1252	305.15	295.99	287.79	282.73	282.10
	0.1502[t]	306.34	299.25	291.86	283.35	**277.54**
	0.1752	279.09	290.63	299.36	294.08	290.81
	0.2002	291.22	292.44	292.38	291.94	291.22

[*]   Current anterior/posterior axle position
[t]   Current inferior/superior axle position

Figure 5-4: Parameter study results, right side

Right side parameter study results averaged over push strokes 1, 3, and 5. Top graph, resulting 3D mesh grid, middle graph, 2D graph, and bottom graph, filled contour plot coinciding with the top and middle plots.

Parameter Study Results: Right Side
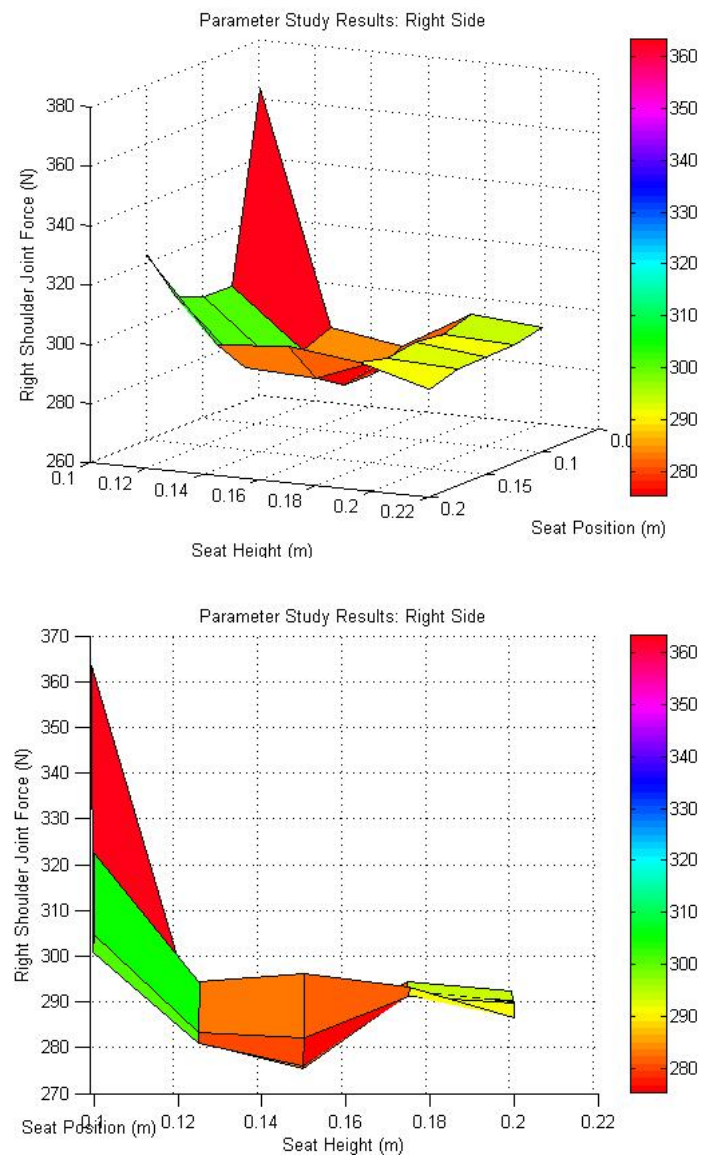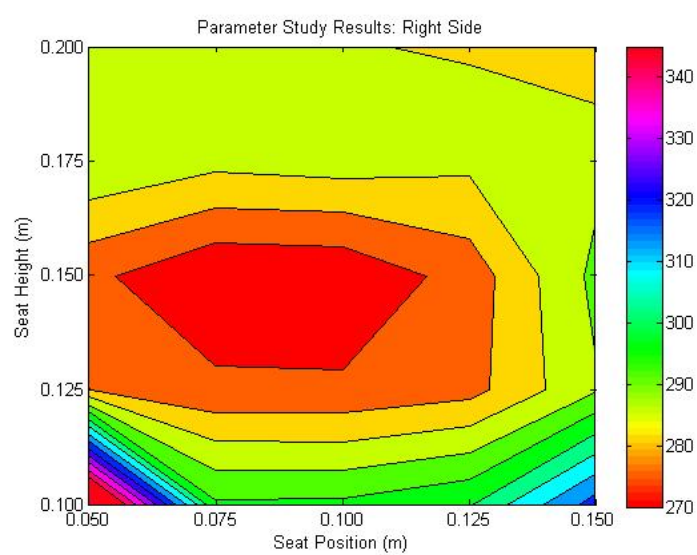
Figure 5-5: Parameter study results, left side

Left side parameter study results averaged over push strokes 1, 3, and 5. Top graph, resulting 3D mesh grid, middle graph, 2D graph, and bottom graph, filled contour plot coinciding with the top and middle plots.

Parameter Study Results: Left Side
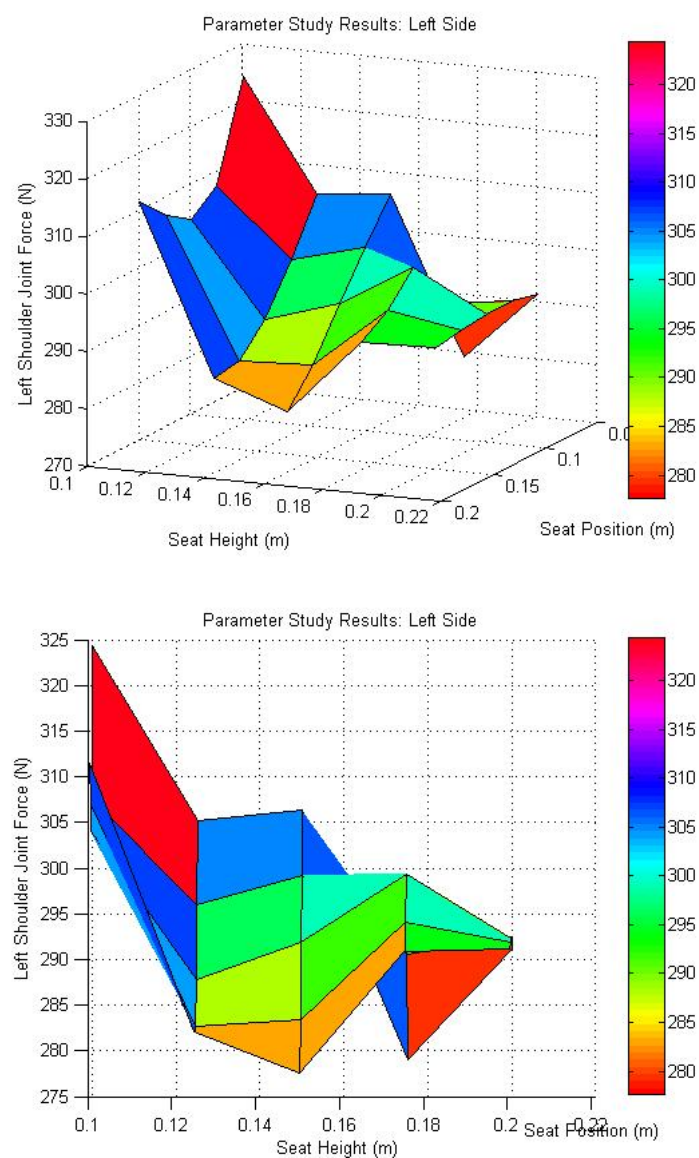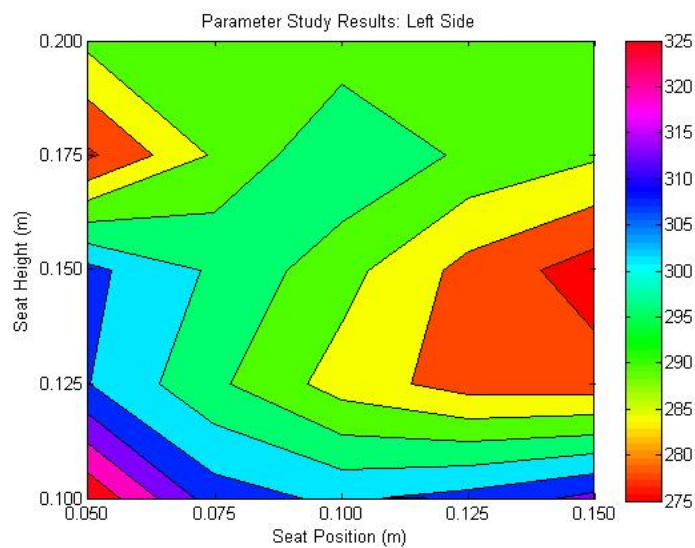
Discussion

It is not surprising that the parametric studies for PP-5 do not produce identical results on the left and right sides regarding recommendations for axle placement positioning to minimize shoulder joint forces. It is encouraging to note though, that for the subjects with paraplegia, the actual seat height that the subjects were fitted for resulted in a shoulder joint force minimum as calculated parametrically, for both the left and right sides. This would suggest that the Paralyzed Veterans of America recommendation guidelines for determining proper seat height is highly effective as a placement in which shoulder joint forces are at a minimum [73]. The guidelines recommend a seat height determined by aligning the tip of a subject's middle finger with height of the axle, when they are comfortably seated in their chair with their arms hanging loosely at their sides.

Results from the parametric study suggest that while the current seat height is ideal for minimizing shoulder joint forces, the ideal seat placement for the right side is 7.5 centimeters further forward than the left side's recommendations. One would anticipate that postural differences, handedness, and asymmetry between the right and left hemispheres may play a role in the different recommendations for joint force minimums. It is obvious that it is an unrealistic idea to set up the seat to reflect the parametric results regarding the anterior/posterior seating positions, as this would result in the subject's right side twisted slightly more forward than the left side. One can imagine the implications for potentially pushing in circles with this sort of set up.

Since the right and left sides do not match up, decisions have to be made as to how to compromise the axle placement. If the shoulder joint force on the right and left sides are simply averaged, a minimum exists 2.5 centimeters further backward (more posterior) than the current axle placement (Table 5-3). This can clearly be seen on the contour plot in Figure 5-6. There is a large red circle corresponding to an area where axle placement is ideal to minimize shoulder joint forces. While slight shifts forward and backward from this position result in slightly greater shoulder joint forces, seat positions above and below this result in dramatic changes in these forces and should be avoided.

Table 5-3: Parameter study results, right and left

Parameter study results, right and left sides averaged together for push strokes 1, 3, and 5.

PP_5 – Left & Right Sides Averaged						
		Seat Position (m)				
		0.0500	**0.0750**	**0.1000***	**0.1250**	**0.1500**
Seat Height (m)	**0.1002**	343.90	304.15	302.48	305.77	316.96
	0.1252	295.10	288.58	284.34	282.95	288.25
	0.1502t	293.76	287.37	283.88	**282.70**	286.92
	0.1752	286.78	291.08	295.89	292.64	292.10
	0.2002	291.83	291.31	291.26	290.86	288.93

Figure 5-6: Parameter study results, right and left sides averaged

Right and left side parameter study results averaged over push strokes 1, 3, and 5. Top graph, resulting 3D mesh grid, middle graph, 2D graph, and bottom graph, filled contour plot coinciding with the top and middle plots.
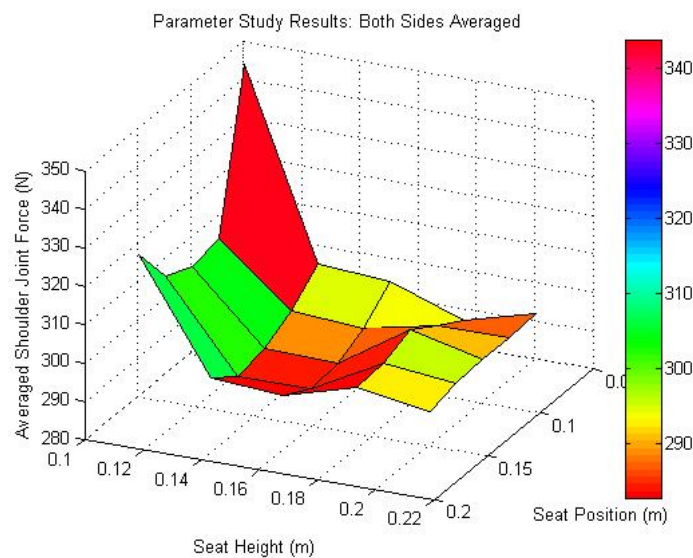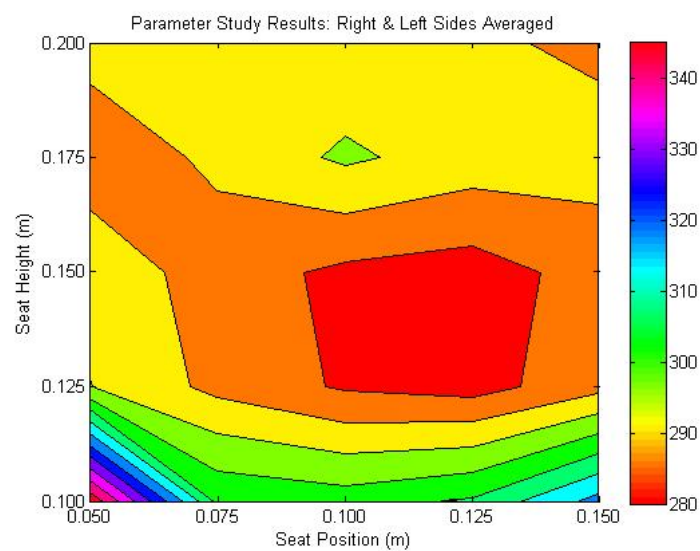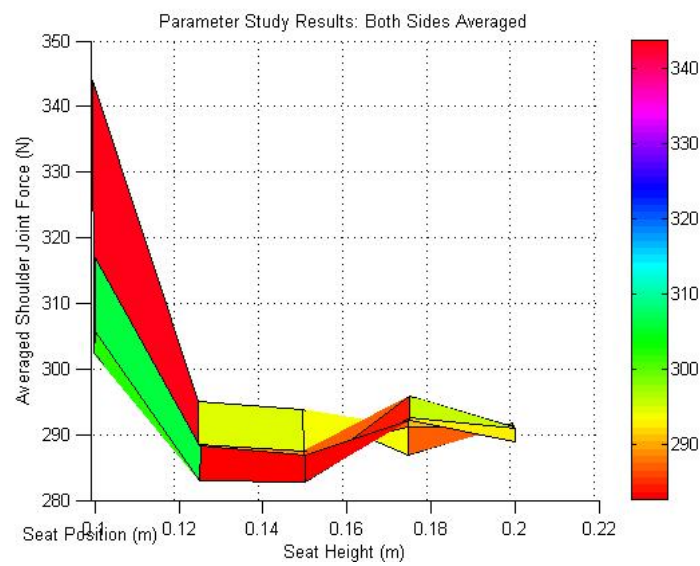
Proper wheelchair set-up is imperative. These contour maps serve as a good prescriptive tool for individualized axle set-up. It is clear that altering the axle placement even slightly can have dramatic and significant results on the magnitude of the shoulder joint forces throughout propulsion, especially in the inferior and superior

directions. However, shoulder joint force results and trends are so individualized that any broad generalizations for prescriptive guidelines cannot be made. This fact alone demonstrates the true need for patient specificity, as accurate results are dependent on the model truly reflecting every aspect of the patient. In addition, it is also important to note that this analysis assumes that aside from axle placement, everything else remains the same – subject kinematics, kinetics, and EMG – however this may not be true. This fact demonstrates the need for quantifiable results from a pre- and post-axle placement intervention strategy, which is a section in the next chapter, Future Work.

CHAPTER 6

CONCLUSION TO ADDRESS SHOULDER PAIN AND

FUTURE WORK

Conclusions

In identifying and addressing potential causes of shoulder pain and pathology in MWUs, the quality of life for a majority of this population will be dramatically improved. There were two major parts to the current study: 1.) the integration of data collection and analysis of participant kinematics, kinetics, and EMG, for investigating if there are differences between able-bodied and participants with paraplegia during wheelchair propulsion, and 2.) the use of these data in the creation and validation of a patient-specific computational model of the upper limb for investigating the magnitude of shoulder joint forces throughout propulsion. More specifically, the latter part of this bi-fold study was used to investigate the effect axle placement had on the magnitude of shoulder joint forces.

The advantage of the first part of the study over previous studies investigating the biomechanics of wheelchair propulsion is the fact that the integrated approach of a simultaneous collection and analysis of kinematics, kinetics, and EMG is novel; while many previous studies look at either one or two of the aforementioned parameters, there are few studies that simultaneously integrate all three [20]. By looking at all three parameters simultaneously, noticeable differences between able-bodied and

participants with paraplegia emerged. The high incidence of shoulder pain in MWUs as compared to the general population may be the result of such differences, suggesting that a need existed for further investigation into the magnitude of shoulder joint forces throughout propulsion.

This naturally segues into the creation and validation of a patient-specific musculoskeletal biomechanical model of the upper limb for such purposes. The advantage of the patient-specific model that was created in the second part of the study as compared to previously created and used shoulder models is multi-fold: 1.) the level of patient-specificity was unprecedented; not only was the model driven by participant kinematics and kinetics, with results compared to participant EMG, but the actual model was scaled anthropometrically to exactly reflect participant dimensions, including height, weight, upper arm and forearm length, and wheelchair measurements, and 2.) the level of validation was more extensive than previously constructed upper limb models with computationally calculated joint forces compared to those found in literature (both in vivo and computational results), in addition to muscle activity comparisons between those obtained experimentally and those calculated computationally, and kinetics comparisons between those obtained experimentally via the SmartWheels, and contact forces calculated computationally at the hand.

From the patient-specific model, resulting joint forces throughout propulsion were investigated. In addition, this study was unique in its goal to computationally identify axle placements (with a parametric investigation), that minimize the

magnitude of shoulder joint forces throughout the contact phase of propulsion. The overall major strength of the investigation is its potential for immediate clinical and societal impact for thousands of clinicians and MWUs themselves. It is the hope that a patient-specific intervention or prescription tool may potentially prolong or prevent the shoulder pain that so many in this population will experience by advising on correct axle placement to minimize shoulder joint forces, thus potentially prolonging a pain-free way of life for MWUs.

Key Points

Many important ideas emerged from the two studies. Several differences were identified between able-bodied and participants with paraplegia in the first part of the current study, and there are two main conclusions that can be drawn from the integrative investigation:

- A greater "muscle energy," as measured by the area under the curve of the percentage of EMG throughout propulsion, may result in a greater resultant joint force in the shoulder and elbow, thus potentially resulting in shoulder pathology.
- Similarly, a greater "muscle energy" may result in fatigue and play a factor in the development of shoulder pain and pathology over time; fatigue may compromise an effective propulsive stroke placing undue stresses on the joint capsule.

Following the investigation into experimental differences between cohorts, the creation and validation of a computational biomechanical model of the upper limb has yielded the following additional information:

- Computational shoulder joint force results and trends are so individualized that any broad generalizations for any group of people seem not to apply. This fact alone demonstrates the true need for patient specificity, as accurate results are dependent on the model truly reflecting every aspect of the patient, from anthropometrics and wheelchair measurements to build the model, patient kinematics and kinetics to drive the model, and EMG to validate the model.

- Altering the axle placement even slightly can have dramatic and significant results on the magnitude of the shoulder joint forces throughout propulsion. As a result, proper wheelchair set-up is imperative.

In summary, there are clear differences between able-bodied individuals and persons with paraplegia when it comes to propulsion parameters and characteristics. Since the investigation focused on individuals with paraplegia – who have full upper limb muscle innervation – the differences observed between the cohorts, assuming that muscle activity differences may be responsible for the observed kinematics and kinetic differences between the two groups, cannot be faulted on the original spinal cord injury. It is possible that such differences instead are the result of adaptation to life in

a wheelchair. It would be recommended then, that parametric studies investigating the ideal axle placement for a participant's specific kinematics, kinetics, and wheelchair set-up be run yearly, as over time adaptations may result in unfavorable shoulder joint forces. A routine monitoring program may be able to identify adverse wheelchair set-ups and should therefore be employed to focus on maintaining an environment in which participant shoulder joint forces are at a minimum. It is the hope that in doing so, the onset of shoulder pain that so many MWUs experience is either delayed, or altogether prevented, so that MWUs can continue to lead active, independent, confident lives.

Outstanding Questions

Although many points emerged from the combination of experimental and computational results, a few assumptions and questions arose as well. In the first part of the investigation in which the differences between able-bodied participants and those with paraplegia were examined, an assumption was made that just because the two cohorts are engaged in the same activity (wheelchair propulsion), that due to the fact that only fully innervated muscles were analyzed there were no glaring physiological differences between the two cohorts. It is possible that an able-bodied individual using a wheelchair does not accurately mimic an individual with paraplegia using a wheelchair due to the possible leverage that full use of the lower limbs may provide the able-bodied participants during propulsion. The fact that each participant pushed at their own self-selected speed, coupled with the fact that there was little

upper body trunk motion, help to assuage the concerns surrounding this variable, however a future study looking into the differences between able-bodied individuals pushing a wheelchair with and without leverage aid (via some means of tying down the legs) should be investigated.

Regarding the second part of the investigation, an assumption was made in the computational model that the frictional coefficient between the seat (and backrest) of the wheelchair and each participant's pants (and shirt) was equal to 0.75. The material of each participant's wheelchair seat and backrest, in addition to the fabrics of the clothes that were worn on the day of testing, were not recorded, so to keep the system balanced in order that the individual in the wheelchair would not "slide" out of the chair, the assumption was made for all participants that the frictional coefficient between the two surfaces was 0.75. This seemed reasonable as results from the muscle validation study computationally aligned with the experimental data.

In addition, as thorough as the validation on the current model has been, a joint force comparison between the computational results and the gold standard of an in-vivo shoulder joint measurement has yet to be completed. It is not so much that such a level of validation has been neglected; it is more the result of a lack of subjects that fit the criteria. Were the opportunity to present itself, the computational outputs could be compared to the in-vivo measurements, resulting in a more thorough validation and subsequent gold standard for shoulder modeling.

Future Work

Following the successful completion of a patient-specific computational model, its use as a laboratory tool should be expanded on and parlayed for use in a clinical setting. There are two immediate uses that may have significant impact on the lives of those with spinal cord injury that use a manual wheelchair:

i.) Individuals who are being fitted for a newly prescribed wheelchair, and

ii.) Current MWUs, who may, or may not, have existing shoulder pain, looking to prolong the general health of their shoulders.

It is anticipated that a patient-specific biomechanical model determining appropriate axle-placement to minimize shoulder joint loads, will provide additional tools and methods to assist therapists in both of the above-mentioned arenas. When pain is resolved, MWUs tend to participate more in community activities and have a better quality of life.

Clinical Validation Studies

A pre- and post- intervention study should be run to demonstrate the effectiveness and applicability of a patient-specific model in a clinical setting. Multiple subjects who use a manual wheelchair as their primary means of locomotion should be recruited for this analysis and should have wheelchairs with adjustable axles. The first part of the study will be much like the data investigation that has currently been discussed at length, with the collection of each subject's patient-specific anthropometrics, wheelchair measurements (including current axle

placement), kinematics, kinetics, and EMG throughout a predetermined time at their self-selected propulsion speed. The data will be processed and a patient-specific model will be created. A subsequent inverse dynamics analysis will be run, calculating each participant's shoulder joint forces and muscle activities throughout propulsion, with the latter being used as a means of validation against the experimentally collected participant EMG. With assurance of a valid computational model, a parameter study investigating the effect of axle placement on the magnitude of shoulder joint forces will be run. The resulting 3-D graph, on which the dependency of shoulder joint forces associated with various anterior/posterior and inferior/superior axle placements is clear, can be used to determine which axle position results in a shoulder joint force minimum. Following the determination of a more favorable axle position, the participant will be asked to come back for a follow-up, during which time their axle position will be re-adjusted to reflect that which resulted in a shoulder joint minimum, and another round of data will be collected for use to re-run the model. With the new axle-placement, it is anticipated that the results from the inverse dynamics analysis (after full-validation) will demonstrate a lower shoulder joint force than those calculated with the previous axle-placement. Ideally, the magnitude of new shoulder joint forces should mimic the minima determined from the computational parametric study. If necessary, more parameter studies can be run to follow up and see if the axle-placement can be refined to further minimize shoulder joint forces.

Depending on findings from this pre- and post- intervention study, generalizations may be able to be formulated that may be applicable to all physical therapists fitting an individual with a spinal cord injury with a newly prescribed wheelchair. In the future, clinics and research laboratories may be able to use the model to determine optimal axle placement based on such previously observed trends from the model, as well as measurable wheel characteristics like push frequency, perhaps even without a force sensitive push-rim.

Long Term

In terms of a long-term outcome to assist spinal cord injury subjects, this biomechanical computational methodology will be very valuable. This cost-effective methodology will benefit all involved, both researchers and individuals with spinal cord injury. This user-friendly model will allow therapists to insert an individual's patient-specific anthropometrics, kinematics, kinetics, and compute. Observing the computational information can enhance a therapist's decision-making and instruction for each individual subject. In the future, clinics and research laboratories will be able to use the model to determine optimal axle placement to minimize shoulder joint loads which may ultimately reduce or eliminate pain and pathology among MWUs, prolonging an independent and pain-free way of life.

REFERENCES

1.   Dvir, Z. and N. Berme, "The shoulder complex in elevation of the arm: a mechanism approach," Journal of Biomechanics, 1978. 1: p. 219-25.

2.   Dubowsky, S.R., N.A. Langrana, and S.A. Sisto, "Comparison of Kinematics, Kinetics, and EMG Throughout Wheelchair Propulsion in Able-Bodied and Persons with Paraplegia: An Integrative Approach," Journal of Biomechanical Engineering, in press, February 2008.

3.   Anglin, C. and U.P. Wyss, "Review of arm motion analyses," Proceedings of the Institution of Mechanical Engineers [H], 2000. 214(5): p. 541-55.

4.   Martini, F.H., M.J. Timmons, and M.P. McKinley, Human Anatomy. 3rd ed. 2000, Upper Saddle River: Prentice Hall.

5.   Lal, S., "Premature degenerative shoulder changes in spinal cord injured patients," Spinal Cord, 1998. 36: p. 186-9.

6.   Mercer, J.L., et al., "Shoulder joint kinetics and pathology in manual wheelchair users," Clinical Biomechanics, 2006. 21: p. 791-9.

7.   Ballinger, D., D. Rintala, and K. Hart, "The relation of shoulder pain and range-of-motion problems to functional limitations, disability, and perceived health of men with spinal cord injury: a multifaceted longitudinal study," Archives of Physical Medicine and Rehabilitation, 2000. 81: p. 1575-81.

8.   Bayley, J.C., T.P. Cochran, and C.B. Sledge, "The weight-bearing shoulder: The impingement syndrome in paraplegics," The Journal of Bone & Joint Surgery - American Volume, 1987. 69(5): p. 676-8.

9.   Boninger, M.L., et al., "Shoulder imaging abnormalities in individuals with paraplegia," Journal of Rehabilitation Research & Development, 2001. 38(4): p. 301-8.

10.   Curtis, K.A., et al., "Shoulder pain in wheelchair users with tetraplegia and paraplegia," Archives of Physical Medicine and Rehabilitation, 1999. 80(4): p. 453-7.

11.   Finley, M.A. and M.M. Rodgers, "Prevalence and identification of shoulder pathology in athletic and nonathletic wheelchair users with shoulder pain: A pilot study," Journal of Rehabilitation Research & Development, 2004. 41(3B): p. 395-402.

12. Gellman, H., I. Sie, and R.L. Waters, "Late complications of the weight-bearing upper extremity in the paraplegic patient," <u>Clinical Orthopaedics</u>, 1988. 233(132-5).

13. Nichols, P.J., P.A. Normal, and J.R. Ennis, "Wheelchair user's shoulder? Shoulder pain in patients wtih spinal cord lesions," <u>Scandinavian Journal of Rehabilitation</u>, 1979. 42: p. 41-6.

14. Pentland, W. and L.T. Twomey, "The weight-bearing upper extremity in women with long-term paraplegia," <u>Paraplegia</u>, 1991. 29: p. 521-30.

15. Samuelsson, K.A.M., H. Tropp, and B. Gerdloe, "Shoulder pain and its consequences in paraplegic spinal cord-injured, wheelchair users," <u>Spinal Cord</u>, 2004. 42: p. 41-6.

16. Subbarao, J., J. Klopfstein, and R. Turpin, "Prevalence and impact of wrist and shoulder pain in patient with spinal cord injury," <u>The Journal of Spinal Cord Medicine</u>, 1995. 18(1): p. 9-13.

17. Rose, M., et al., "Pain following spinal cord injury: results from a postal survey," <u>Pain</u>, 1988. 34: p. 101-102.

18. Rao, S.S., et al., "Three-dimensional kinematics of wheelchair propulsion," <u>IEEE transactions on rehabilitation engineering: a publication of the IEEE Engineering in Medicine and Biology Society</u>, 1996. 4(3): p. 152-60.

19. Rodgers, M.M., "Three-dimensional dynamic analysis of joint reaction forces and moments during wheelchair propulsion," <u>Clinical Kinesiology</u>, 1994. 47: p. 98.

20. Rodgers, M.M., et al., "Biomechanics of Wheelchair Propulsion During Fatigue," <u>Archives of Physical Medicine and Rehabilitation</u>, 1994. 75(1): p. 85-93.

21. Boninger, M.L., et al., "Propulsion Patterns and Pushrim Biomechanics in Manual Wheelchair Propulsion," <u>Archives of Physical Medicine and Rehabilitation</u>, 2002. 83: p. 718-23.

22. Brubaker, C.E., "Wheelchair prescription: an analysis of factors that affect mobility and performance," <u>Journal of Rehabilitation Research & Development</u>, 1986. 23(4): p. 19-26.

23. Costic, R.S., et al., "Joint compression alters the kinematics and loading patterns of the intact and capsule-transected AC joint," <u>Journal of Orthopaedic Research</u>, 2003. 21(3): p. 379-85.

24. Gokeler, A., et al., "Quantitative analysis of traction in the glenohumeral joint. In vivo radiographic measurements," <u>Manual Therapy</u>, 2003. 8(2): p. 97-102.

25. McLaurin, C.A. and C.E. Brubaker, "Biomechanics and the wheelchair," <u>Prosthetics and Orthotics International</u>, 1991. 15(1): p. 24-37.

26. Remia, L.F., et al., "Biomechanical evaluation of multidirectional glenohumeral instability and repair," <u>Clinical Orthopaedics and Related Research</u>, 2003. 416: p. 225-36.

27. Cooper, R.A., et al., "Projection of the point of force application onto a palmar plane of the hand during wheelchair propulsion," <u>IEEE transactions on rehabilitation engineering: a publication of the IEEE Engineering in Medicine and Biology Society</u>, 1996. 4(3): p. 133-42.

28. Mulroy, S.J., et al., "Electromyographic activity of shoulder muscles during wheelchair propulsion by paraplegic persons," <u>Archives of Physical Medicine and Rehabilitation</u>, 1996. 77(2): p. 187-93.

29. Robertson, R.N., et al., "Pushrim forces and joint kinetics during wheelchair propulsion," <u>Archives of Physical Medicine and Rehabilitation</u>, 1996. 77(9): p. 856-64.

30. Roux, L.S., S. Hanneton, and A. Roby-Brami, "Shoulder movements during the initial phase of learning manual wheelchair propulsion in able-bodied subjects," <u>Clinical Biomechanics</u> (Bristol, Avon), 2006. 21(S): p. S45-51.

31. Kulig, K., et al., "The effect of level of spinal cord injury on shoulder joint kinetics during manual wheelchair propulsion," <u>Clinical Biomechanics</u>, 2001. 16(9): p. 744-51.

32. Kulig, K., et al., "Shoulder joint kinetics during the push phase of wheelchair propulsion," <u>Clinical Orthopaedics and Related Research</u>, 1998. 354: p. 132-43.

33. Lin, H.T., et al., "Muscle force analysis in the shoulder mechanism during wheelchair propulsion," <u>Proceedings of the Institution of Mechanical Engineers, Part H, Journal of engineering in medicine</u>, 2004. 218(4): p. 213-21.

34. Sabick, M.B., B.R. Kotajarvi, and K.N. An, "A New Method to Quantify Demand on the Upper Extremity During Manual Wheelchair Propulsion," <u>Archives of Physical Medicine and Rehabilitation</u>, 2004. 85(7): p. 1151-9.

35. de Groot, S., et al., "Effect of wheelchair stroke pattern on mechanical efficiency," <u>American Journal of Physical Medicine and Rehabilitation / Association of Academic Physiatrists</u>, 2004. 83(8): p. 640-9.

36. Au, A.T. and R.F. Kirsch, "EMG-Based Prediction of Shoulder and Elbow Kinematics in Able-Bodied and Spinal Cord Injured Individuals," <u>IEEE transactions on rehabilitation engineering: a publication of the IEEE Engineering in Medicine and Biology Society</u>, 2000. 8(4): p. 471-80.

37. de Groot, S., et al., "Short-term adaptations in co-ordination during the initial phase of learning manual wheelchair propulsion," <u>Journal of Electromyography and Kinesiology</u>, 2003. 13(3): p. 217-28.

38. Mulroy, S.J., et al., "Effects of spinal cord injury level on the activity of shoulder muscles during wheelchair propulsion: an electromyographic study," <u>Archives of Physical Medicine and Rehabilitation</u>, 2004. 85(6): p. 925-34.

39. Karlsson, D. and B. Peterson, "Towards a model for force predictions in the human shoulder," <u>Journal of Biomechanics</u>, 1992. 25(2): p. 189-99.

40. van der Helm, F.C., "A finite element musculoskeletal model of the shoulder mechanism," <u>Journal of Biomechanics</u>, 1994. 27(5): p. 551-69.

41. Hogfors, C., G. Singholm, and P. Herberta, "Biomechanical model of the human shoulder - I. Elements," <u>Journal of Biomechanics</u>, 1987. 20(2): p. 157-66.

42. Karlsson, D. and U. Jarvholm, "Force-producing ability in all shoulder muscles, as determined by cross-sectional areas," Center for Biomechanics, 1988.

43. Pheasant, S., <u>Bodyspace: Anthropometry, Ergonomics, and Design</u>. 1986, London: Taylor & Francis.

44. Wood, J.E., S.G. Meek, and S.C. Jacobsen, "Quantitation of human shoulder anatomy for prosthetic arm control - I. Surface modelling," <u>Journal of Biomechanics</u>, 1989. 22(273-92).

45. van der Helm, F.C., "Geometry parameters for musculoskeletal modelling of the shoulder system," <u>Journal of Biomechanics</u>, 1992. 25(2): p. 129-44.

46. van der Helm, F.C. and R. Veenbaas, "Modelling the mechanical effect of muscles with large attachment sites: Application to the shoulder mechanism," <u>Journal of Biomechanics</u>, 1991. 24(12): p. 1151-63.

47. Veeger, H.E., "Inertia and muscle contraction parameters for musculoskeletal modelling of the shoulder mechanism," <u>Journal of Biomechanics</u>, 1991. 24(7): p. 615-29.

48. van der Helm, F.C. and G.M. Pronk, "Three-dimensional recording and description of motions of the shoulder mechanism," <u>Journal of Biomechanical Engineering</u>, 1995. 117(1): p. 27-40.

49. Happee, R. and F.C. van der Helm, "The control of shoulder muscles during goal directed movements, an inverse dynamic analysis," <u>Journal of Biomechanics</u>, 1995. 28(10): p. 1179-91.

50. van der Helm, F.C. and H.E. Veeger, "Quasi-static analysis of muscle forces in the shoulder mechanism during wheelchair propulsion," <u>Journal of Biomechanics</u>, 1996. 29(1): p. 39-52.

51. Johnson, G.R., "Modelling the muscles of the scapula, morphometric and coordinate data and functional implications," <u>Journal of Biomechanics</u>, 1996. 29: p. 1039-51.

52. de Leva, P., "Adjustments to Zatsiorsky-Seluyanov's segment inertia parameters," <u>Journal of Biomechanics</u>, 1996. 29: p. 1223-30.

53. Hogfors, C., D. Karlsson, and B. Peterson, "Structure and internal consistency of a shoulder model," <u>Journal of Biomechanics</u>, 1995. 28: p. 767-77.

54. Charlton, I.W. and G.R. Johnson, "Application of spherical and cylindrical wrapping algorithms in a musculoskeletal model of the upper limb," <u>Journal of Biomechanics</u>, 2001. 34(9): p. 1209-16.

55. Maurel, W., "3D Modeling of the Human Upper Limb including the Biomechanics of Joints, Muscles and Soft Tissues," in Laboratoire d'Infographie. 1998, Ecole Polytechnique Federale: Lausanne.

56. Garner, B.A. and M.G. Pandy, "A Kinematic Model of the Upper Limb Based on the Visible Human Project (VHP) Image Dataset," <u>Computer Methods in Biomechanics and Biomedical Engineering</u>, 1999. 2(2): p. 107-24.

57. Garner, B.A. and M.G. Pandy, "Musculoskeletal model of the upper limb based on the visible human male dataset," <u>Computer Methods in Biomechanics and Biomedical Engineering</u>, 2001. 4(2): p. 93-126.

58. Garner, B.A. and M.G. Pandy, "The Obstacle-set Method for representing muscle paths in musculoskeletal models," <u>Computer Methods in Biomechanics and Biomedical Engineering</u>, 2000. 3: p. 1-30.

59. AnyBody Software. [cited; Available from: www.anybodytech.com].

60. van Bolhius, B.M. and C.C. Gielen, "A comparison of models explaining muscle activation patterns for isometric contractions," Biological Cybernetics, 1999. 81: p. 249-61.

61. Challis, J.H. and D.G. Kerwin, "An analytical examination of muscle force estimations using optimization techniques," Proceedings of the Institution of Mechanical Engineers, Part H, Journal of engineering in medicine, 1993. H.

62. Rasmussen, J., M. Damsgaard, and M. Voigt, "Ergonomic Optimization of a Bicycle," Aalborg University: Aalborg.

63. Damsgaard, M., J. Rasmussen, and S.T. Christenson, "Inverse dynamics of musculoskeletal systems using an efficient min/max muscle recruitment model," in IDETC: 18th Biennial Conference on Mechanical Vibration and Noise, 2001: Pittsburgh, Pennsylvania.

64. Damsgaard, M., S.T. Christensen, and J. Rasmussen, "An efficient numerical algorithm for solving the muscle recruitment problem in inverse dynamics simulations," in International Society of Biomechanics, XVIIth Congress, 2001: Zurich, Switzerland.

65. Rasmussen, J., "The role of mechanics and optimization in ergonomics," Aalborg University: Aalborg.

66. An, K.N., et al., "Determination of Muscle and Joint Forces: A new Technique to Solve the Indeterminate Problem," Journal of Biomechanical Engineering, 1984. 106(4): p. 364-7.

67. Forster, E., "Predicting Muscle Forces in the Human Lower Limb during Locomotion," 2003. Ulm University: Dusseldorf, Germany.

68. MusculoGraphics, Inc.   [cited; Available from: www.musculographics.com].

69. Biomechanics Research Group, Inc.   [cited; Available from: www.lifemodeler.com].

70. G-sport, Inc.   [cited; Available from: www.gsport.co.jp].

71. Asato, K.T., et al., "SMARTWheels: development and testing of a system for measuring manual wheelchair propulsion dynamics," IEEE transactions on bio-medical engineering, 1993. 40(12): p. 1320-4.

72. Anatomical Guide for the Electromyographer: The Limbs and Trunk.

73. Paralyzed Veterans of America Consortium for Spinal Cord Medicine, "Preservation of upper limb function following spinal cord injury: a clinical

practice guideline for health-care professionals," <u>The Journal of Spinal Cord Medicine</u>, 2005. 28(5): p. 434-70.

74.   Boninger, M., et al., "Three-dimensional pushrim forces during two speeds of wheelchair propulsion," <u>American Journal of Physical Medicine and Rehabilitation / Association of Academic Physiatrists</u>, 1997. 76(5): p. 420-6.

75.   Beres-Jones, J.A. and S.J. Harkema, "The human spinal cord interprets velocity-dependent afferent input during stepping," <u>Brain</u>, 2004. 127: p. 2232-46.

76.   Schantz, P., et al., "Movement and muscle activity pattern in wheelchair ambulation by persons with para- and tetraplegia," <u>Scandinavian Journal of Rehabilitation Medicine</u>, 1999. 31(2): p. 67-76.

77.   Veeger, H.E., L.H. van der Woude, and L.A. Rozendaal, "The effect of rear wheel camber in manual wheelchair propulsion," <u>Journal of Rehabilitation Research & Development</u>, 1989. 26(2): p. 37-46.

78.   Dubowsky, S.R., N.A. Langrana, and S.A. Sisto, "Shoulder Mechanics: Analytical Modeling and Validation," American Society of Biomechanics, 2007 Annual Conference. August 22-25, 2007.

79.   Crowninshield, R.D., "Use of optimization techniques to predict muscle forces," <u>Journal of Biomechanical Engineering</u>, 1978. 100: p. 88-92.

80.   van der Helm, F.C. and R. Veenbaas, "Modelling the mechanical effect of muscles with large attachment sites: application to the shoulder mechanism," <u>Journal of Biomechanics</u>, 1991. 24: p. 1151-63.

81.   de Zee, M., et al., "Validation of a musculo-skeletal model of the mandible and its application to mandibular distraction osteogenesis," <u>Journal of Biomechanics</u>, 2007. 40: p. 1192-1201.

82.   Bergmann, G., et al., "In vivo glenohumeral contact forces - measurements in the first patient 7 months postoperatively," <u>Journal of Biomechanics</u>, 2007. 40(10): p. 2139-49.

83.   van der Helm, F.C., "Analysis of the kinematic and dynamic behavior of the shoulder mechanism," <u>Journal of Biomechanics</u>, 1994. 27(5): p. 527-50.

84.   Van Drongelen, S., et al., "Glenohumeral contact forces and muscle forces evaluated in wheelchair-related activities of daily living in able-bodied subjects versus subjects with paraplegia and tetraplegia," <u>Archives of Physical Medicine and Rehabilitation</u>, 2005. 86: p. 1434-40.

85.   Veeger, H.E., L.A. Rozendaal, and F.C. van der Helm, "Load on the shoulder in low intensity wheelchair propulsion," <u>Clinical Biomechanics</u>, 2002. 17(3): p. 211-8.

86.   Anglin, C., U.P. Wyss, and D.R. Pichora, "Glenohumeral contact forces during five activities of daily living," in the <u>Proceedings of the First Conference of the International Shoulder Group</u>, 1997. The Netherlands: Shaker Publishing BV.

87.   van Drongelen, S., et al., "Glenohumeral joint loading in tetraplegia during weight relief lifting: A simulation study," <u>Clinical Biomechanics</u>, 2006. 21: p. 128-37.

88.   Wu, G., et al., "ISB recommendation on definitions of joint coordinate systems of various joints for the reporting of human joint motion - Part II: shoulder, elbow, wrist and hand," <u>Journal of Biomechanics</u>, 2005. 38: p. 981-92.

APPENDIX A

AnyBody code for simple arm model

```
Main = {

  AnyFolder ArmModel = {

  // Global Reference Frame

  AnyFixedRefFrame GlobalRef = {

   AnyDrawRefFrame DrwGlobalRef = {};

   AnyRefNode Shoulder = {

    sRel = {0,0,0};

   };

   AnyRefNode DeltodeusA = {

    sRel = {0.05,0,0};

   };

   AnyRefNode DeltodeusB = {

    sRel = {-0.05,0,0};

   };

   AnyRefNode BicepsLong = {

    sRel = {0.1,0,0};

   };

   AnyRefNode TricepsLong = {

    sRel = {-0.1,0,0};

   };
```

```
};  // Global reference frame

// Segments

AnyFolder Segs = {

  AnySeg UpperArm = {

    r = {0,0,0};

    Axes = {{0,1,0},{-1,0,0},{0,0,1}};

    Mass = 2.0;

    Jii = {0.005,0.01,0.01};

    AnyDrawSeg DrwSeg = {};

    AnyRefNode ShoulderNode = {

      sRel = {-0.2,0,0};

    };

    AnyRefNode ElbowNode = {

      sRel = {0.2,0,0};

    };

    AnyRefNode DeltodeusA = {

      sRel = {-0.1,0,0.0};

    };

    AnyRefNode DeltodeusB = {

      sRel = {-0.1,0,0.0};

    };

    AnyRefNode Brachialis = {
```

```
  sRel = {0.1,0,0.0};

};

AnyRefNode BicepsShort = {

 sRel = {-0.1,0,0.0};

};

AnyRefNode Brachioradialis = {

 sRel = {0.05,0,0.0};

};

AnyRefNode TricepsShort = {

 sRel = {-0.1,0,0.0};

};

}; // Upper Arm

AnySeg LowerArm = {

 r = {0,0,0};

 Mass = 2.0;

 Jii = {0.005,0.01,0.01};

 AnyRefNode ElbowNode = {

  sRel = {-0.2,0,0};

 };

 AnyRefNode HandNode = {

  sRel = {0.2,0,0};

 };
```

```
    AnyRefNode Brachialis = {

      sRel = {-0.1,0,0.0};

    };

    AnyRefNode Brachioradialis = {

      sRel = {0.0,0,0.0};

    };

    AnyRefNode Biceps = {

      sRel = {-0.15,0,0.0};

    };

    AnyRefNode Triceps = {

      sRel = {-0.25,0,0.0};

    };

    AnyDrawSeg DrwSeg = {};

  }; // Lower Arm

}; // Segments folder

AnyFolder Muscles = {

  AnyMuscleModel MusMdl = {

    F0 = 300;

  };


  //-------------------------------

  AnyViaPointMuscle Brachialis = {
```

```
  AnyMuscleModel &MusMdl = ..Muscles.MusMdl;

  AnyRefNode &Org = ..Segs.UpperArm.Brachialis;

  AnyRefNode &Ins = ..Segs.LowerArm.Brachialis;

  AnyDrawMuscle DrwMus = {};

};

//-------------------------------

AnyViaPointMuscle DeltodeusA = {

  AnyMuscleModel &MusMdl = ..Muscles.MusMdl;

  AnyRefNode &Org = ..GlobalRef.DeltodeusA;

  AnyRefNode &Ins = ..Segs.UpperArm.DeltodeusA;

  AnyDrawMuscle DrwMus = {};

};

//-------------------------------

AnyViaPointMuscle DeltodeusB = {

  AnyMuscleModel &MusMdl = ..Muscles.MusMdl;

  AnyRefNode &Org = ..GlobalRef.DeltodeusB;

  AnyRefNode &Ins = ..Segs.UpperArm.DeltodeusB;

  AnyDrawMuscle DrwMus = {};

};

//-------------------------------

AnyViaPointMuscle Brachioradialis = {

  AnyMuscleModel &MusMdl = ..Muscles.MusMdl;
```

```
AnyRefNode &Org = ..Segs.UpperArm.Brachioradialis;

  AnyRefNode &Ins = ..Segs.LowerArm.Brachioradialis;

  AnyDrawMuscle DrwMus = {};

};

//-------------------------------

AnyViaPointMuscle BicepsShort = {

  AnyMuscleModel &MusMdl = ..Muscles.MusMdl;

  AnyRefNode &Org = ..Segs.UpperArm.BicepsShort;

  AnyRefNode &Ins = ..Segs.LowerArm.Biceps;

  AnyDrawMuscle DrwMus = {};

};

//-------------------------------

AnyViaPointMuscle TricepsShort = {

  AnyMuscleModel &MusMdl = ..Muscles.MusMdl;

  AnyRefNode &Org = ..Segs.UpperArm.TricepsShort;

  AnyRefNode &Ins = ..Segs.LowerArm.Triceps;

  AnyDrawMuscle DrwMus = {};

};

//-------------------------------

AnyViaPointMuscle BicepsLong = {

  AnyMuscleModel &MusMdl = ..Muscles.MusMdl;

  AnyRefNode &Org = ..GlobalRef.BicepsLong;
```

```
    AnyRefNode &Ins = ..Segs.LowerArm.Biceps;

    AnyDrawMuscle DrwMus = {};

  };

  //-------------------------------

  AnyViaPointMuscle TricepsLong = {

    AnyMuscleModel &MusMdl = ..Muscles.MusMdl;

    AnyRefNode &Org = ..GlobalRef.TricepsLong;

    AnyRefNode &Ins = ..Segs.LowerArm.Triceps;

    AnyDrawMuscle DrwMus = {};

  };

}; // Muscles Folder

AnyFolder Loads = {

  AnyForce3D Dumbbell = {

    AnyRefNode &PalmNode = ..Segs.LowerArm.HandNode;

    F = {0,-100,0};  // N

  };

}; // Loads Folder

AnyFolder Jnts = {

  AnyRevoluteJoint Shoulder = {

    Axis = z;

    AnyRefNode &GroundNode = ..GlobalRef.Shoulder;

    AnyRefNode &UpperArmNode = ..Segs.UpperArm.ShoulderNode;
```

```
    };  // Shoulder Joint

    AnyRevoluteJoint Elbow = {

      Axis = z;

      AnyRefNode &UpperArmNode = ..Segs.UpperArm.ElbowNode;

      AnyRefNode &LowerArmNode = ..Segs.LowerArm.ElbowNode;

    };  // Elbow Joint

  };  // Joints Folder

  AnyFolder Drivers = {

    AnyKinEqSimpleDriver ShoulderMotion = {

      AnyRevoluteJoint &Jnt = ..Jnts.Shoulder;

      DriverPos = {-((90)*(pi/180))};

      DriverVel = {0};

      Reaction.Type = {0};

    };  // Shoulder Driver

    AnyKinEqSimpleDriver ElbowMotion = {

      AnyRevoluteJoint &Jnt = ..Jnts.Elbow;

      DriverPos = {((90)*(pi/180))};

      DriverVel = {0};

      Reaction.Type = {0};

    };  // Elbow Driver

  };  // Driver Folder

  AnyForceMomentMeasure ElbowReaction = {
```

```
    AnySeg &Ref = .Segs.LowerArm.ElbowNode;

    AnyFolder &Reac = .Jnts.Elbow.Constraints.Reaction;

  };

  AnyForceMomentMeasure ShoulderReaction = {

    AnySeg &Ref = .Segs.UpperArm.ShoulderNode;

    AnyFolder &Reac = .Jnts.Shoulder.Constraints.Reaction;

  };

}; // ArmModel

// The study: Operations to be performed on the model

AnyBodyStudy MyStudy = {

  AnyFolder &Model = .ArmModel;

  RecruitmentSolver = MinMaxNRSimplex;

  Gravity = {0.0, -9.81, 0.0};

  //RecruitmentQpPenalty = 1.0;

};

}; // Main
```

Matlab code for surface plots

x = [5-seat height positions]

y = [5-seat ant/post positions]

[X, Y] = meshgrid(x, y)

Z = [25 joint forces]

surf(X,Y,Z)

colormap hsv

colorbar

Matlab code for contour plots

x = [5-seat height positions]

y = [5 seat ant/post positions]

[X, Y] = meshgrid (x,y)

Z = [25 joint forces]

[XI, YI] = meshgrid(x,y)

ZI = interp2(X, Y, Z, XI, YI)

[C, h] = contourf (XI, YI, ZI)

Clabel(C, h)

APPENDIX B

Chapter 2

Table B-2-1: Participant contact and release angles, right and left sides

Averaged over ten consecutive push strokes

		Right Side		Left Side	
		Contact Angle	Release Angle	Contact Angle	Release Angle
Able-Bodied	AB-1	58.1±5.3	153.7±5.0	63.6±3.3	151.4±3.84
	AB-2	65.7±4.0	155.4±3.2	--*	--*
	AB-3	77.9±2.4	147.2±2.8	68.4±2.6	147.6±1.8
	AB-4	77.2±1.9	132.4±1.2	75.3±2.5	136.2±1.4
	AB-5	63.4±1.5	121.6±1.7	70.8±8.9^t	112.0±4.8^t
	AB-6	75.7±2.6	132.5±2.1	77.3±5.5	129.4±2.5
Paraplegia	P-1	78.5±1.8	129.0±7.5	75.8±3.9	131.0±7.0
	P-2	45.0±3.1	142.7±1.4	56.8±11.8	149.0±6.4
	P-3	64.8±1.1	147.1±1.0	72.9±8.3	133.7±13.0
	P-4	64.7±3.0	144.0±2.1	64.1±2.7	145.0±2.1
	P-5	63.1±2.2	151.6±2.3	58.0±2.8	142.3±4.2

*   Mechanical failure of the equipment for this subject on the left side.
^{t} Contact and release angles determined from 9 push strokes, not 10.

Table B-2-2: Participant self-selected propulsion speeds

Averaged over ten consecutive push strokes

		Speed (mph)
Able-Bodied	AB-1	3.6±0.4
	AB-2	2.5±0.4
	AB-3	1.9±0.2
	AB-4	2.3±0.2
	AB-5	1.9±0.2
	AB-6	2.2±0.2
Paraplegia	P-1	2.9±0.2
	P-2	3.4±0.4
	P-3	2.8±0.3
	P-4	3.3±0.3
	P-5	2.7±0.3

Table B-2-3: EMG results, right side

		Muscle Activity % of Push Stroke		% Prop. Of Max MVC	Max % MVC
		Burst 1	Burst 2		
Anterior Deltoid	AB-1	2.5±2.5 – 95.9±4.3		44.5±15.2	34.6±5.1
	AB-2	5.5±4.7 – 86.8±7.4		39.2±10.4	23.0±8.6
	AB-3	2.6±2.2 – 77.5±2.7		45.6±9.7	41.5±8.6
	AB-4	0.7±0.7 – 76.6±8.1		31.6±13.4	67.4±10.4
	AB-5	0.6±0.7 – 99.9±0.2		59.7±3.7	10.6±2.7
	AB-6	0.2±0.3 – 98.3±2.5		24.8±4.0	54.4±9.4
	P-1	1.1±1.7 – 100.0±0.0		82.8±16.0	72.4±12.3
	P-2	19.6±5.4 – 77.6±10.2		43.2±7.3	27.8±6.6
	P-3	1.3±2.2 – 98.6±2.6		47.6±8.2	38.2±7.8
	P-4	0.7±0.6 – 94.8±5.6		22.2±9.4	28.1±6.4
	P-5	1.3±2.0 – 97.6±3.8		17.4±17.1	26.2±3.9
Biceps Brachii	AB-1	9.9±7.2 – 76.8±8.5		16.5±15.2	34.6±5.2
	AB-2	15.3±5.1 – 64.3±9.2		21.2±8.8	5.0±4.6
	AB-3	2.2±1.9 – 50.2±6.2	64.5±6.2 – 82.4±8.9	15.6±6.8	38.8±10.9
	AB-4	1.1±1.0 – 56.6±7.5		13.8±4.8	16.4±4.1
	AB-5	0.7±0.6 – 78.1±4.5		14.8±2.7	13.4±3.2
	AB-6	7.9±8.7 – 26.2±8.1	74.8±2.5 – 87.8±6.4	15.0±11.9	9.2±3.4
	P-1	0.3±0.3 – 26.4±12.0	64.0±9.2 – 98.4±2.0	0.1±0.0	77.5±15.9
	P-2	4.7±5.2 – 49.2±3.9		30.8±6.4	26.7±8.6
	P-3	0.8±1.2 – 97.7±1.9		18.6±6.0	60.2±8.2
	P-4	2.7±2.2 – 40.8±6.0	77.9±5.1 – 99.7±0.8	21.6±7.4	n/a[*]
	P-5	4.3±3.2 – 33.1±14.1		9.7±4.3	22.7±5.82
Pectoralis Major	AB-1	20.4±6.9 – 67.5±6.8		41.3±9.4	68.5±10.2
	AB-2	0.8±1.4 – 94.0±5.1		37.7±6.1	52.4±8.9
	AB-3	5.7±7.1 – 68.7±5.4		38.7±9.7	27.3±9.3
	AB-4	6.1±4.2 – 77.7±10.9		33.5±10.3	22.6±3.5
	AB-5	8.3±4.6 – 63.7±7.3		41.3±10.2	9.6±1.8
	AB-6	20.3±8.9 – 64.8±3.0		42.1±6.2	41.0±7.7
	P-1	0.9±0.7 – 38.5±12.0	72.5±9.9 – 97.9±2.6	12.8±11.7	9.1±3.5
	P-2	4.6±5.5 – 94.6±8.4		52.0±7.7	41.8±9.4
	P-3	0.5±0.5 – 99.8±0.4		43.5±10.8	27.3±3.9
	P-4	6.1±4.6 – 74.6±16.1		34.6±8.1	27.8±7.6
	P-5	0.8±0.9 – 70.7±5.0		12.3±14.9	31.2±6.3
Posterior Deltoid	AB-1	71.0±8.8 – 90.7±8.5		73.6±8.5	30.8±8.6
	AB-2	0.5±0.9 – 19.4±10.5	48.4±6.6 – 99.8±0.4	81.1±12.3	34.3±7.7
	AB-3	36.1±3.1 – 49.0±4.1	64.0±2.9 – 92.8±8.3	42.1±10.6	24.7±5.1
	AB-4	6.0±7.1 – 98.2±2.9		84.8±15.2	16.5±3.8
	AB-5	0.5±0.8 – 99.7±0.5		7.7±9.4	12.4±1.2
	AB-6	71.0±2.3 –		81.8±10.2	53.0±12.8

Muscle	ID				
		100.0±0.0			
	P-1	47.1±7.6 – 99.9±0.3		71.7±10.6	n/a[*]
	P-2	0.3±0.3 – 13.8±5.8	59.1±10.5 – 91.4±3.2	77.1±4.5	70.0±8.9
	P-3	3.9±5.5 – 95.1±4.8		76.0±7.5	26.9±6.7
	P-4	0.6±1.3 – 100.0±0.0		70.1±6.5	67.4±11.5
	P-5	2.9±3.1 – 26.6±8.9	81.1±2.5 – 98.8±2.1	96.8±7.9	22.2±10.0
Trapezius	AB-1	0.3±0.3 – 99.7±0.7		75.1±13.6	35.0±9.4
	AB-2	1.0±1.0 – 34.9±5.4	65.7±5.3 – 99.9±0.3	74.8±9.6	51.0±7.4
	AB-3	1.3±2.0 – 100±0.00		79.5±15.2	100.0±0.0
	AB-4	9.6±6.7 – 70.8±13.4		34.2±11.7	8.5±1.6
	AB-5	7.4±6.8 – 96.5±8.0		61.8±8.2	55.3±10.6
	AB-6	1.5±1.6 – 28.1±12.3	68.3±2.5 – 100.0±0.0	79.7±14.3	63.9±8.8
	P-1	41.4±9.6 – 100.0±0.1		70.6±11.6	32.4±7.5
	P-2	0.5±0.7 – 62.8±5.9	77.6±2.6 – 90.0±6.0	54.0±15.6	7.6±4.9
	P-3	9.1±4.8 – 67.0±8.5		13.0±4.4	28.2±9.6
	P-4	1.3±1.4 – 43.9±9.6	58.4±9.8 – 99.9±0.2	80.9±17.1	52.5±16.23
	P-5	72.3±3.0 – 99.6±0.8		74.2±3.4	48.6±7.4
Triceps	AB-1	41.2±9.2 – 95.4±6.7		55.9±10.2	24.0±5.8
	AB-2	32.1±6.8 – 98.3±2.5		52.8±6.0	41.7±14.5
	AB-3	23.8±5.1 – 75.7±3.1		60.5±9.2	31.7±6.3
	AB-4	30.8±8.7 – 92.5±5.7		55.2±5.2	23.7±3.1
	AB-5	70.2±3.4 – 92.7±7.5		77.4±11.7	9.3±1.5
	AB-6	27.7±4.7 – 99.4±0.7		62.6±11.7	29.3±9.1
	P-1	24.5±26.5 – 99.7±0.6		64.4±13.8	32.3±8.9
	P-2	0.7±1.7 – 13.1±6.0	46.7±2.6 – 96.1±3.3	61.7±5.1	65.9±13.6
	P-3	2.3±2.2 – 99.8±0.3		60.6±12.4	52.7±9.6
	P-4	0.4±03 – 99.6±0.6		61.2±8.5	47.7±8.3
	P-5	11.0±8.4 – 99.8±0.3		42.3±9.1	24.9±3.3

[*] Physiologically unrealizable

Table B-2-4: EMG results, left side

		Muscle Activity % of Push Stroke		% Prop. Of Max MVC	Max % MVC
		Burst 1	Burst 2		
Anterior Deltoid	AB-1	8.3±7.9 – 96.9±5.6		81.8±10.1	n/a[*]
	AB-2	21.8±10.3 – 78.8±10.0	--	44.7±14.4	20.0±4.7
	AB-3	3.1±3.4 – 80.8±6.1		41.0±10.9	44.2±8.5
	AB-4	1.0±0.8 – 92.0±6.4		32.6±13.9	n/a[*]
	AB-5	1.8±2.7 – 82.1±10.3		42.7±12.2	13.5±2.9
	AB-6	3.1±4.5 – 52.7±7.2	67.4±5.3 – 91.4±4.1	20.5±6.5	31.2±7.6
	P-1	0.2±0.2 – 26.9±8.0	48.0±6.4 – 97.5±5.1	3.4±5.3	66.2±22.6
	P-2	17.5±6.1 – 72.3±7.5		43.3±7.5	40.7±8.6
	P-3	17.0±5.5 – 87.4±5.3		39.2±15.5	29.5±4.7
	P-4	0.9±0.6 – 87.4±5.8		71.1±5.2	63.7±18.8
	P-5	0.1±0.0 – 99.2±1.1		18.6±15.6	28.0±5.3
Biceps Brachii	AB-1	3.4±4.5 – 63.9±14.3		17.7±9.0	36.6±15.1
	AB-2	16.9±7.9 – 37.7±4.4		26.1±13.6	5.5±1.4
	AB-3	1.7±2.5 – 41.2±9.0	68.5±6.3 – 99.2±1.3	11.4±5.4	29.8±10.9
	AB-4	2.9±2.3 – 61.3±19.7		16.8±6.3	17.8±4.8
	AB-5	7.4±3.7 – 40.6±6.7		23.6±9.7	12.2±4.8
	AB-6	16.2±8.5 – 40.5±7.0		23.5±7.4	7.9±2.2
	P-1	0.1±0.0 – 25.6±12.1	49.7±5.9 – 99.0±1.0	0.1±0.0	15.2±5.7
	P-2	4.3±3.7 – 62.7±17.0		28.1±6.8	25.7±7.2
	P-3	4.0±3.8 – 96.5±4.4		25.1±8.7	36.8±9.7
	P-4	0.5±0.7 – 91.7±9.3		17.8±3.9	n/a[*]
	P-5	0.1±0.1 – 64.6±9.4	82.8±9.5 – 95.9±3.4	13.6±8.9	38.4±6.9
Pectoralis Major	AB-1	17.6±8.0 – 68.1±7.7		45.4±8.4	100.0±12.4
	AB-2	1.6±2.3 – 77.4±8.0		46.8±4.3	33.3±9.6
	AB-3	6.6±4.9 – 68.2±5.7		31.2±16.1	95.9±4.9
	AB-4	6.9±6.6 – 79.5±14.4		37.5±7.7	45.0±10.9
	AB-5	13.8±5.2 – 64.0±8.8		32.6±12.7	10.8±2.2
	AB-6	13.7±5.6 – 97.4±2.1		40.6±5.8	52.5±7.7
	P-1	0.9±1.2 – 30.0±13.1		4.5±5.6	26.0±9.0
	P-2	13.9±9.0 – 80.9±4.5		61.5±6.4	29.4±10.7
	P-3	11.4±6.0 – 89.6±6.8		40.9±9.4	34.6±7.9
	P-4	4.0±3.1 – 84.4±8.3		33.4±7.4	64.4±11.0
	P-5	0.3±0.3 – 69.2±7.0		16.7±13.5	21.0±2.8
Posterior Deltoid	AB-1	9.3±6.8 – 53.8±8.0	73.4±6.4 – 91.4±7.4	79.9±5.9	21.2±7.4
	AB-2	0.1±0.1 – 20.3±8.0	54.9±9.3 – 99.1±2.4	13.7±21.7	38.3±6.0
	AB-3	0.5±1.1 – 99.8±0.4		82.3±14.9	10.7±2.5
	AB-4	1.3±1.4 – 30.2±13.5	50.0±11.6 – 98.9±1.7	73.8±7.9	30.1±11.1
	AB-5	0.1±0.1 – 59.0 – 6.8	70.3±4.6 – 99.8±0.3	85.5±12.5	12.7±1.4
	AB-6	74.0±2.5 – 100.0±0.1		88.1±10.4	40.5±7.0

|					
	P-1	47.4±6.5 – 100.0±0.1		85.1±15.6	n/a[*]
	P-2	0.1±0.0 – 15.9±4.1	52.3±5.2 – 93.5±3.8	77.2±4.8	52.9±9.7
	P-3	1.4±1.8 – 92.8±0.3		78.9±6.3	13.5±5.1
	P-4	0.5±0.5 – 99.8±0.3		73.7±15.0	24.8±4.7
	P-5	3.3±2.5 – 37.8±14.1	77.5±4.0 – 100.0±0.0	98.8±3.9	n/a[*]
Trapezius	AB-1	0.2±0.1 – 96.7±5.6		72.0±6.4	70.7±14.5
	AB-2	0.5±0.7 – 99.1±1.9		70.6±3.6	70.6±17.5
	AB-3	14.3±5.3 – 99.8±0.4		83.1±11.4	32.9±6.3
	AB-4	0.1±0.0 – 100.0±0.0		90.9±19.5	n/a[*]
	AB-5	52.6±6.7 – 96.3±8.6		63.6±14.2	25.8±6.8
	AB-6	1.6±2.5 – 22.8±7.0	69.1±3.6 – 99.9±0.2	82.1±13.8	58.5±10.5
	P-1	0.7±0.9 – 20.2±11.0	45.6±6.9 – 99.7±0.5	52.3±7.4	n/a[*]
	P-2	3.4±5.7 – 99.1±2.2		81.9±13.0	9.2±5.3
	P-3	7.2±7.5 – 92.9±6.0		18.7±6.0	13.3±3.0
	P-4	0.2±0.2 – 100.0±0.0		74.1±10.4	n/a[*]
	P-5	4. 4±3.9 – 27.2±17.9	65.9±5.2 – 99.8	79.5±13.0	41.8±10.6
Triceps	AB-1	27.8±11.8 – 97.6±1.9		51.8±6.2	22.9±9.6
	AB-2	0.7±0.9 – 17.3±7.2	36.4±7.4 – 97.0±5.2	52.6±4.8	36.7±8.7
	AB-3	32.1±2.5 – 67.3±8.6		52.8±7.1	25.5±6.3
	AB-4	35.7±5.4 – 97.4±1.9		72.0±7.2	27.5±6.3
	AB-5	1.1±1.3 – 11.7±3.1	49.3±6.0 – 99.1±1.6	77.4±19.5	10.6±1.4
	AB-6	1.5±1.6 – 19.9±9.2	68.3±2.5 – 100.0±0.0	69.1±12.5	63.6±9.0
	P-1	11.3±14.4 – 99.9±0.2		51.5±16.6	11.0±3.6
	P-2	3.1±4.4 – 10.5±4.4	40.7±3.7 – 90.8±6.6	58.1±5.8	n/a[*]
	P-3	1.2±1.3 – 15.2±6.8	32.3±10.5 – 99.3±0.5	71.4±12.7	33.9±5.5
	P-4	10.7±7.7 – 22.6±5.0	40.0±4.8 – 96.8±4.9	70.3±16.3	35.5±7.9
	P-5	--	--	84.5±8.4	15.9±3.3

-- Unclear burst

[*] Physiologically unrealizable
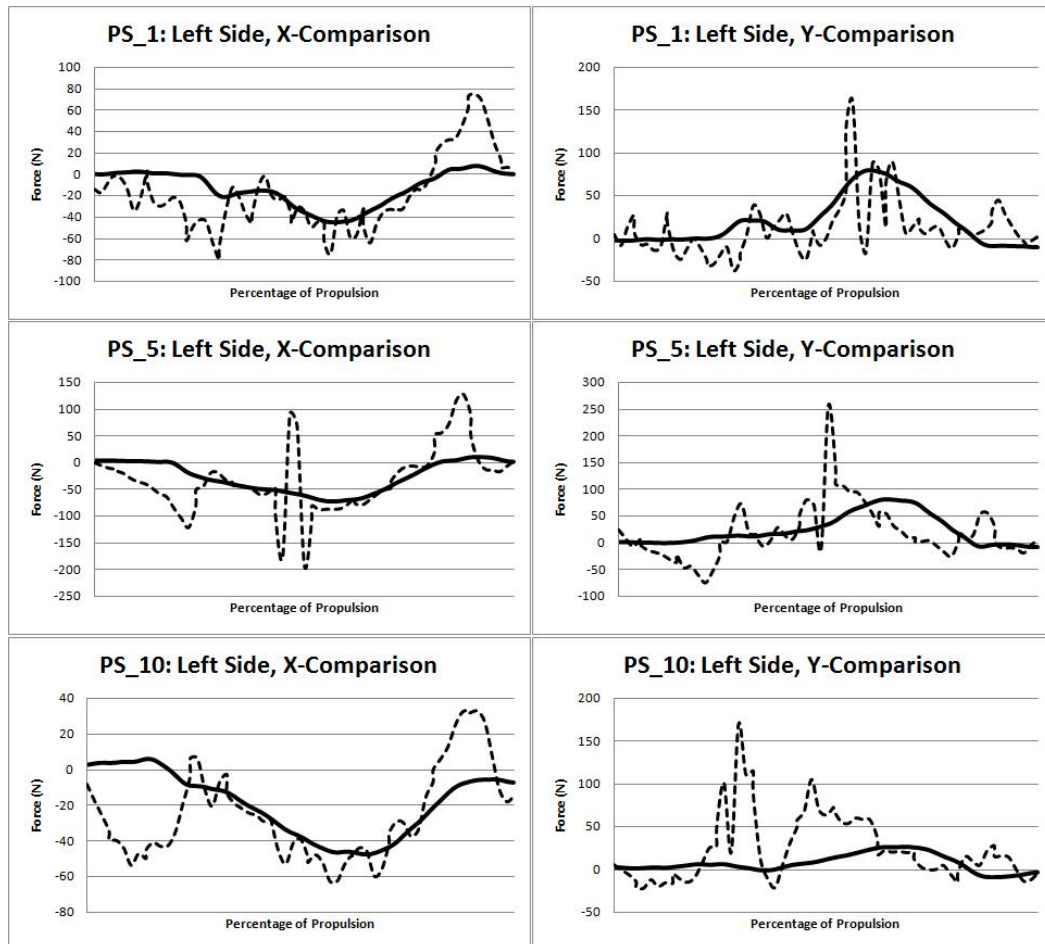
Chapter 4

## B-4-1: Kinetics validation results, right side, PP-2

Solid lines are the original SmartWheel x- (left), and y- (right) outputs. The dotted lines are the computationally calculated x- (left), and y- (right) outputs, as determined based on a kinematics and torque-driven model.
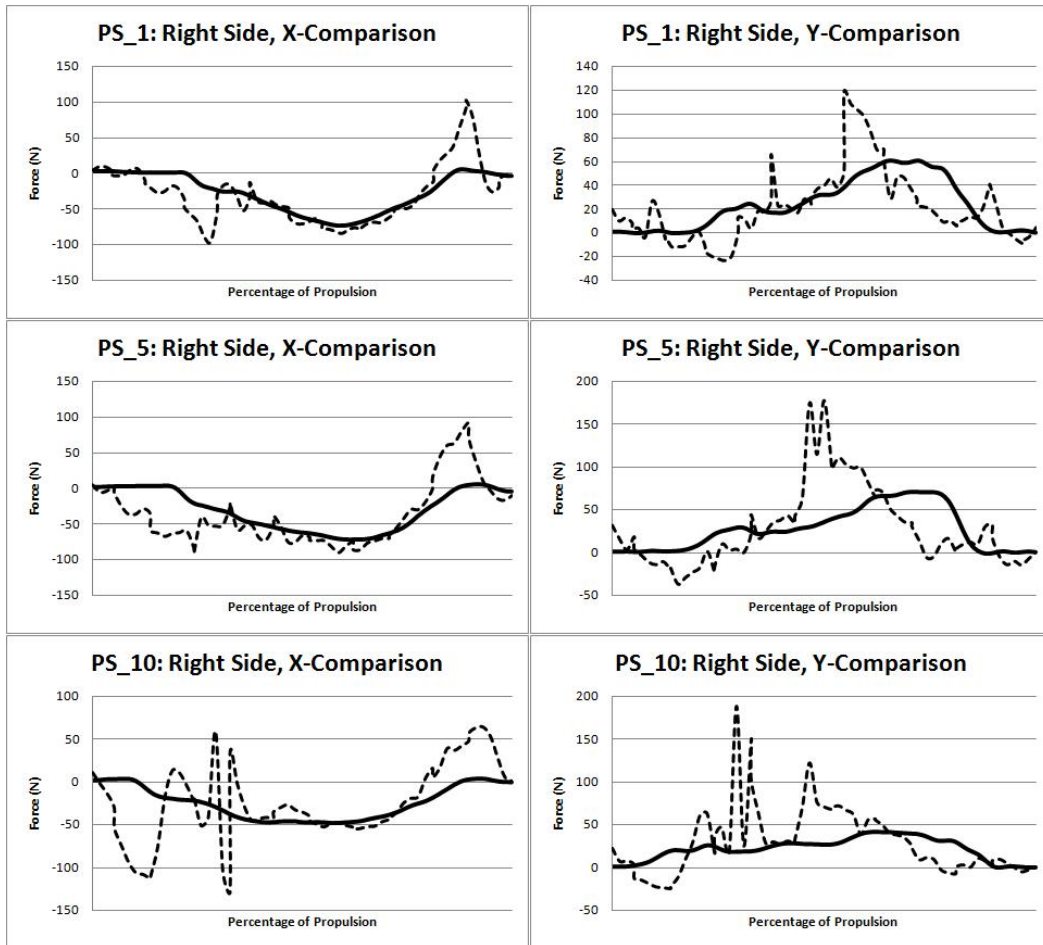
B-4-2: Kinetic validation results, left side, PP-2

Solid lines are the original SmartWheel x- (left), and y- (right) outputs. The dotted lines are the computationally calculated x- (left), and y- (right) outputs, as determined based on a kinematics and torque-driven model.
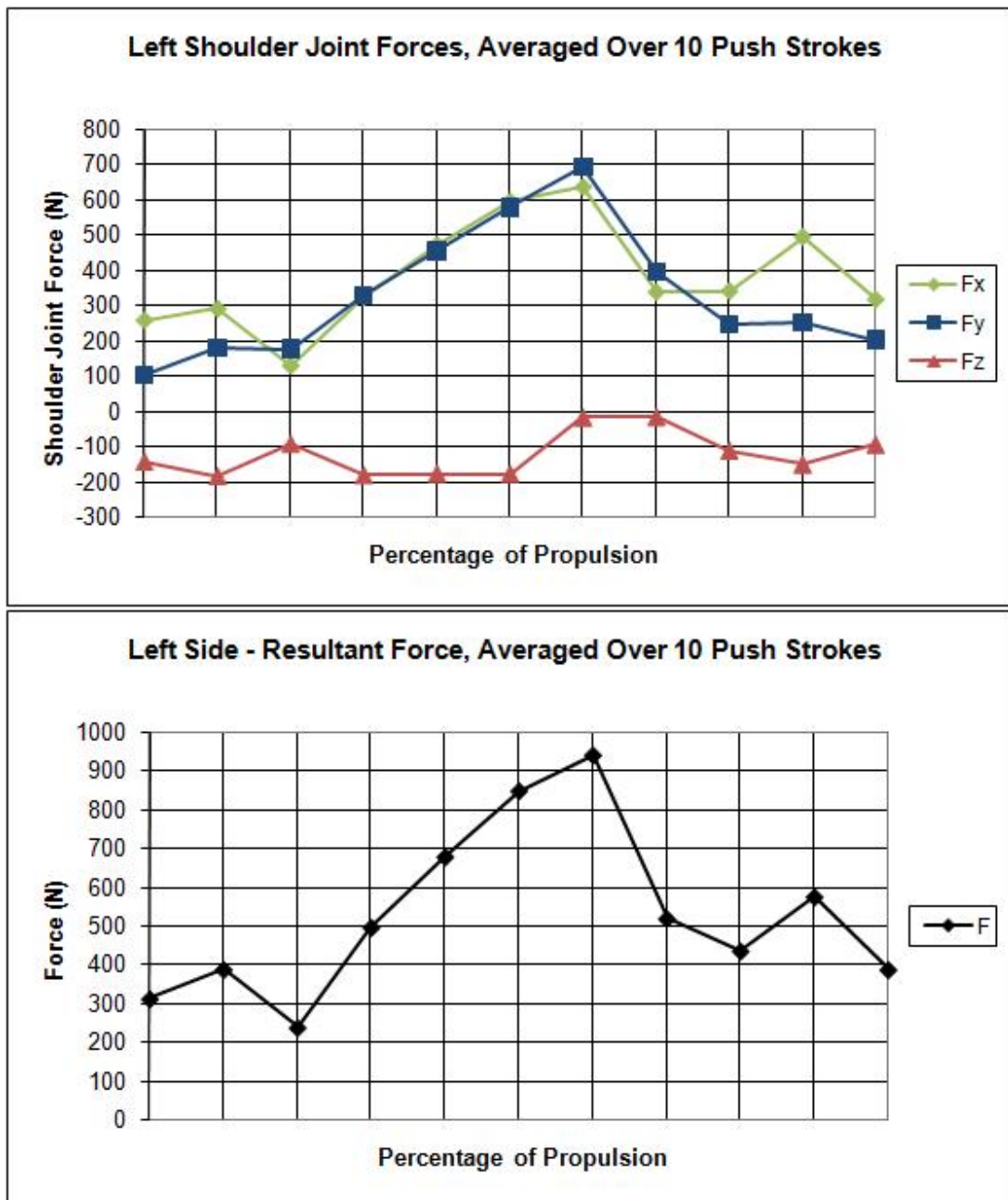
Chapter 5

B-5-1: Right shoulder joint force results, PP-2

Top graph: F_x, F_y, and F_z forces. Bottom graph: Resultant force. The graphs are calculated by normalizing the joint forces throughout propulsion and then graphing the resulting joint forces in 10% increments.
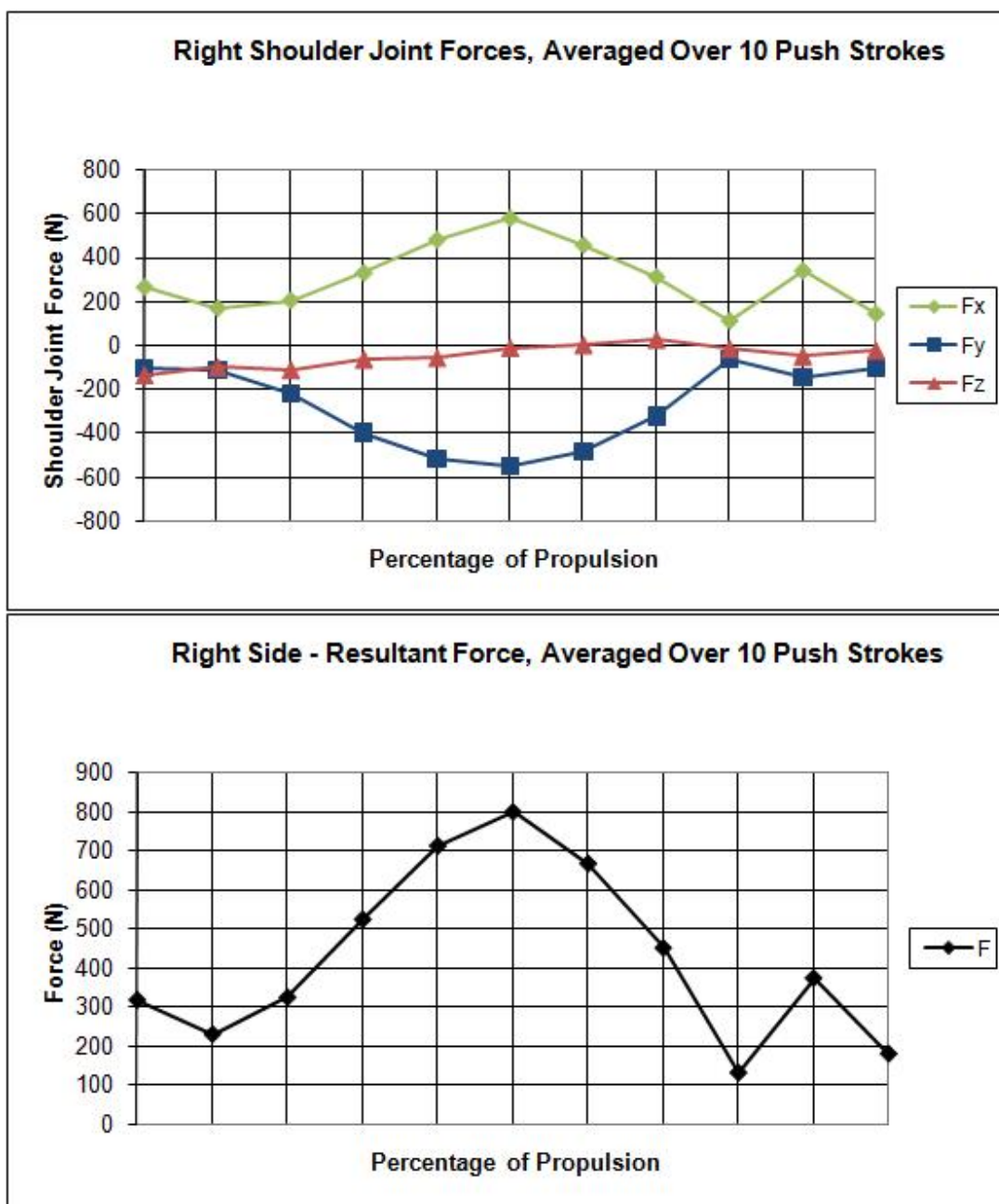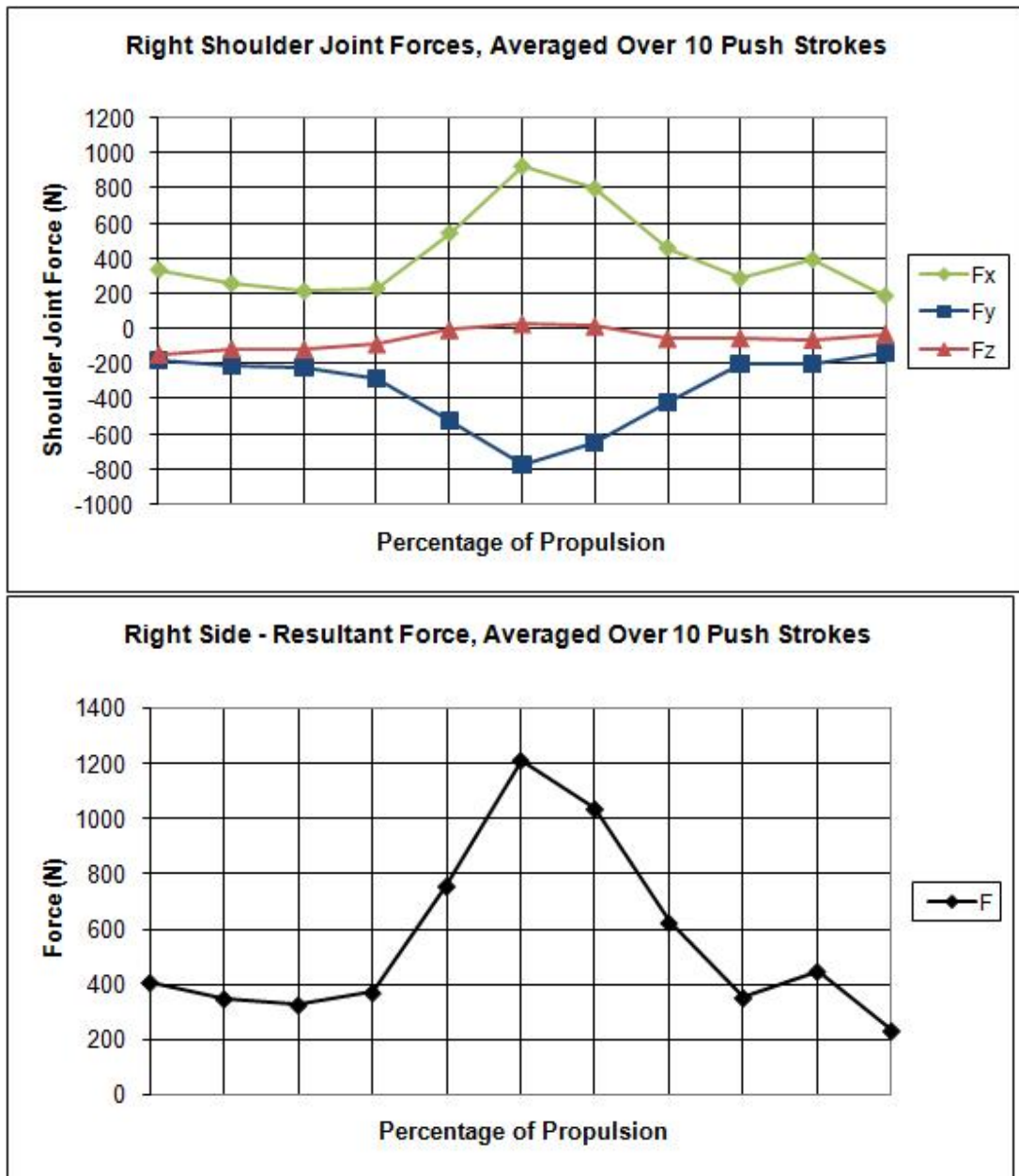
B-5-2: Left shoulder joint force results, PP-2

Top graph: F_x, F_y, and F_z forces. Bottom graph: Resultant force. The graphs are calculated by normalizing the joint forces throughout propulsion and then graphing the resulting joint forces in 10% increments.

B-5-3: Right shoulder joint force results, AB-1

Top graph: F_x, F_y, and F_z forces. Bottom graph: Resultant force. The graphs are calculated by normalizing the joint forces throughout propulsion and then graphing the resulting joint forces in 10% increments.
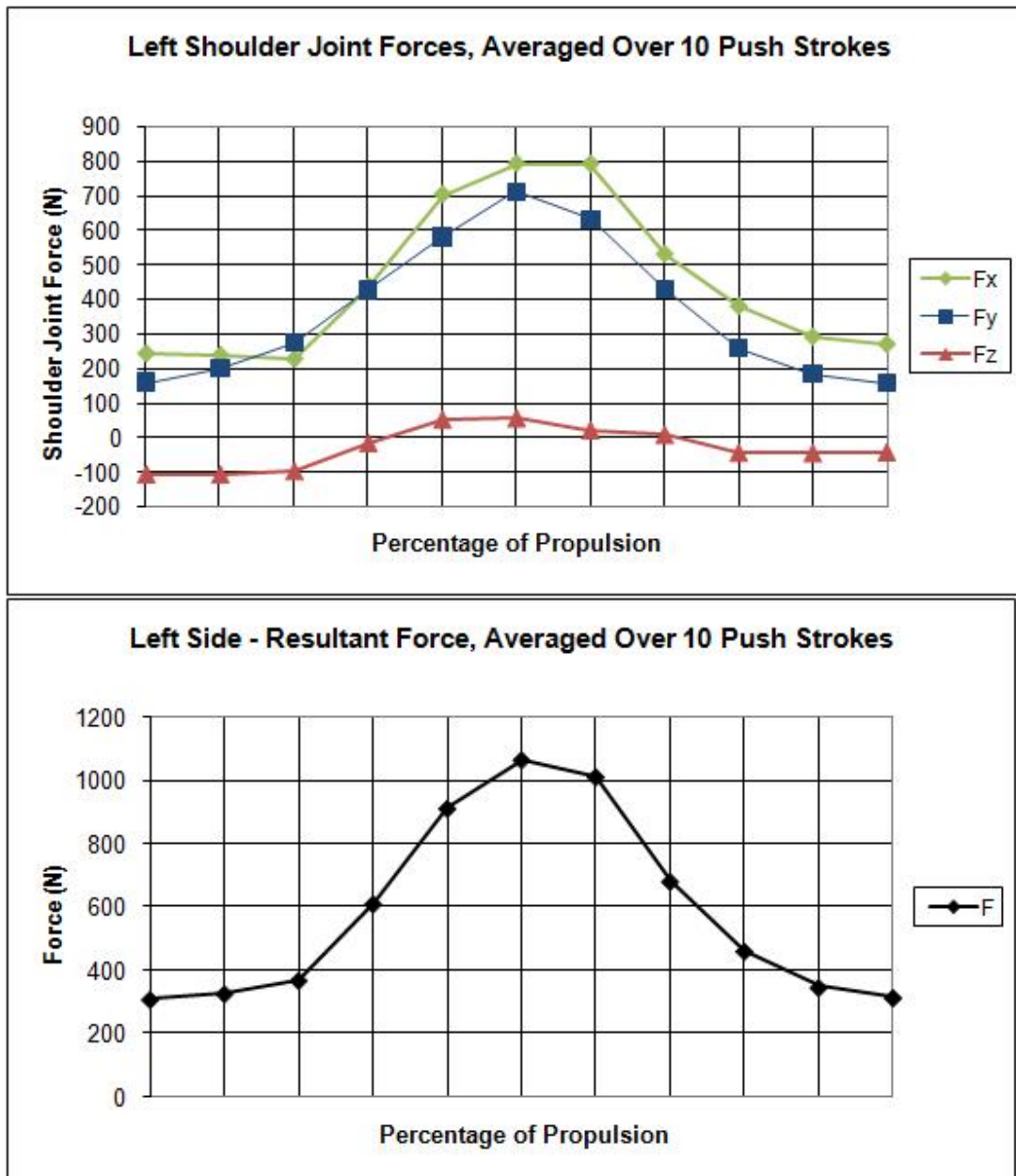
B-5-4: Left shoulder joint force results, AB-1

Top graph: F_x, F_y, and F_z forces. Bottom graph: Resultant force. The graphs are calculated by normalizing the joint forces throughout propulsion and then graphing the resulting joint forces in 10% increments.

VITA

Sarah Rebecca Dubowsky

2003   B.S., Biomedical Engineering, University of Rochester, Rochester, NY

2003-08 Sullivan SR, Langrana NA, and SA Sisto. "Multibody Computational Biomechanical Model of the Upper Body," in the Proceedings of ASME IDETC/CIE 2005, Sept 2005, Long Beach, California.

      Sullivan SR, Langrana NA, and SA Sisto, "A Patient-Specific Upper Body Computational Biomechanical Model," Page 99, in the Proceedings of BMES Conference, Baltimore, MD, October 2005.

      Sullivan SR, Langrana NA, and SA Sisto, "Upper extremity Computational Muscle forces in Comparison with Subject Electromyography," in the Proceedings of the 2006 Bioengineering Conference, Paper No. BIO2006-157469, ASME, Amelia Island, Florida, June 2006.

      Sullivan SR, Langrana NA, and SA Sisto, "Correlating Kinematics, Kinetics, and EMG in Wheelchair Propulsion in Normal and Paraplegia Subjects," Page 290, in the Proceedings of BMES Conference, Chicago, IL, October 2006.

      Dubowsky SR, "Adjusting the Axle Placement in Wheelchair Users to Minimize Shoulder Joint Forces," International World Wide Web Broadcast: AnyBody Modeling System, November 2007.

      Dubowsky SR, Langrana NA, and SA Sisto, "Comparison of Kinematics, Kinetics, and EMG Throughout Wheelchair Propulsion in Able-Bodied and Persons with Paraplegia: An Integrative Approach," Journal of Biomechanical Engineering, in press, February 2008.

      Dubowsky SR, et al., "Validation of a musculo-skeletal model of wheelchair propulsion and its application to minimizing shoulder joint forces," Journal of Biomechanics, submitted 12-28-07.

2008   Ph.D., Biomedical Engineering, Rutgers, The State University of New Jersey, Piscataway, NJ